EFFECTS OF GLUTAMATE ON RETINAL GLIAL CELLS AND CONE PHOTORECEPTORS

Monique Emma Petronella Sarantis

A thesis submitted for the degree of
Doctor of Philosophy
in the
University of London

Department of Physiology
University College London

November 1990

Abstract

Glutamate is a major neurotransmitter in the retina. Glutamate is released by photoreceptors to convey the visual signal to postsynaptic bipolar and horizontal cells, and is released from bipolar cells to act on amacrine and ganglion cells. The actions of glutamate on horizontal, bipolar and ganglion cells are well understood but not much is known about its effect on photoreceptors, or its action on retinal glial cells.

The first part of this thesis deals with experiments in which the whole-cell variant of the patch-clamp technique was used to study the action of glutamate on isolated cone photoreceptors from the tiger salamander retina. Glutamate is shown to bind to a kainate-type receptor and evoke a current carried by chloride ions and blocked by removal of external sodium. The glutamate-evoked current is localized to the synaptic terminal of the cone suggesting that these receptors act as autoreceptors.

Next, the effect of glutamate on retinal glial (Müller) cells isolated from the rabbit retina is described. Glutamate evokes an inward membrane current by activating a high affinity uptake carrier. Uptake is strongly inhibited by depolarization, by removal of extracellular sodium or intracellular potassium, and by raising the extracellular potassium concentration. This suggests that the uptake carrier transports sodium ions into the cell and potassium ions out of the cell. Uptake of glutamate into glial cells may be important in terminating its transmitter action.

Finally, the distribution of Müller cell processes around the photoreceptor output synapse is investigated by injecting tiger salamander Müller cells with horseradish peroxidase for examination in the electron microscope. Although Müller cells do not project between the processes of bipolar and horizontal cells entering the photoreceptor synaptic pedicle, they do wrap around the synaptic terminals of the photoreceptors and come within 1-3μm of the site of glutamate release.

Contents

List of figures

List of tables

Acknowledgements

I would like to thank my supervisor David Attwell for his continual encouragement and support throughout the course of this work and for giving me the opportunity of carrying out the experiments for this thesis.

I thank Peter Mobbs for his help and advice and for giving me the photograph in Figure 6.1.

I also thank my colleagues; Boris Barbour, Helen Brew, Beverley Clark, Alison Cook, Karen Everett, Angus Silver and Marek Szatkowski for useful discussion and companionship and Keith Caddy for help with the electron microscopy techniques.

Chapter 1
Introduction

This thesis describes experiments characterizing a glutamate-activated ion channel in cone photoreceptors of the salamander retina and studying an electrogenic uptake mechanism for glutamate in rabbit retinal glial (Müller) cells. It also describes an electron-microscopic analysis of the anatomical arrangement of Müller cell processes near the photoreceptor output synapse in the salamander retina. This introduction presents the reasons for carrying out these experiments. I first review our current knowledge of the cellular structure of the retina, of some of the electrophysiological properties of the different retinal cell types, and of their synaptic connections. The experiments presented in this thesis are then introduced.

1.1 Organization of the vertebrate retina

In this thesis I report experiments in which glutamate was applied to retinal neurones and glial cells. It is useful, therefore, to review briefly the organization of the cell types in the retina. This review will be split into a description of the neurones present and a description of the glial cells present.

1.1.1 Neuronal cell types in the retina

The earliest information on retinal cell types came from studies by Ramón y Cajal (1893) and Polyak (1941), who used light microscopy to examine Golgi-impregnated cells. From these and later studies six different types of neurones were distinguished: photoreceptors, horizontal cells, bipolar cells, amacrine cells, interplexiform cells (Ehinger, Falck and Laties, 1969) and ganglion cells. In all vertebrate retinae these cells are organized in five layers: three cell body layers and two synaptic layers (Figure 1.1). Furthest towards the back of the eye is the outer cell body (nuclear) layer, containing the cell bodies of photoreceptors. The photoreceptive part of these cells projects out towards the back of the eye. Moving towards the vitreous humour and the front of the eye, the next layer is the outer plexiform layer, where the

Figure 1.1 The position of different cell types in the retina.

This drawing of the major cell types found in the vertebrate retina (modified from Dowling, 1987) is based on observations of cells found in the mudpuppy retina that had been stained by the Golgi method. R, photoreceptors; H, horizontal cell; B, bipolar cells; A, amacrine cell; G, ganglion cell; I, interplexiform cell; M, Müller (glial) cell. The cell body and synaptic layers of the retina are indicated: outer nuclear layer (ONL), outer plexiform layer (OPL), inner nuclear layer (INL), inner plexiform layer (IPL), ganglion cell layer (GCL). In situ the receptors at the top project out towards the back of the eye and the bottom of the drawing borders the vitreous humour.

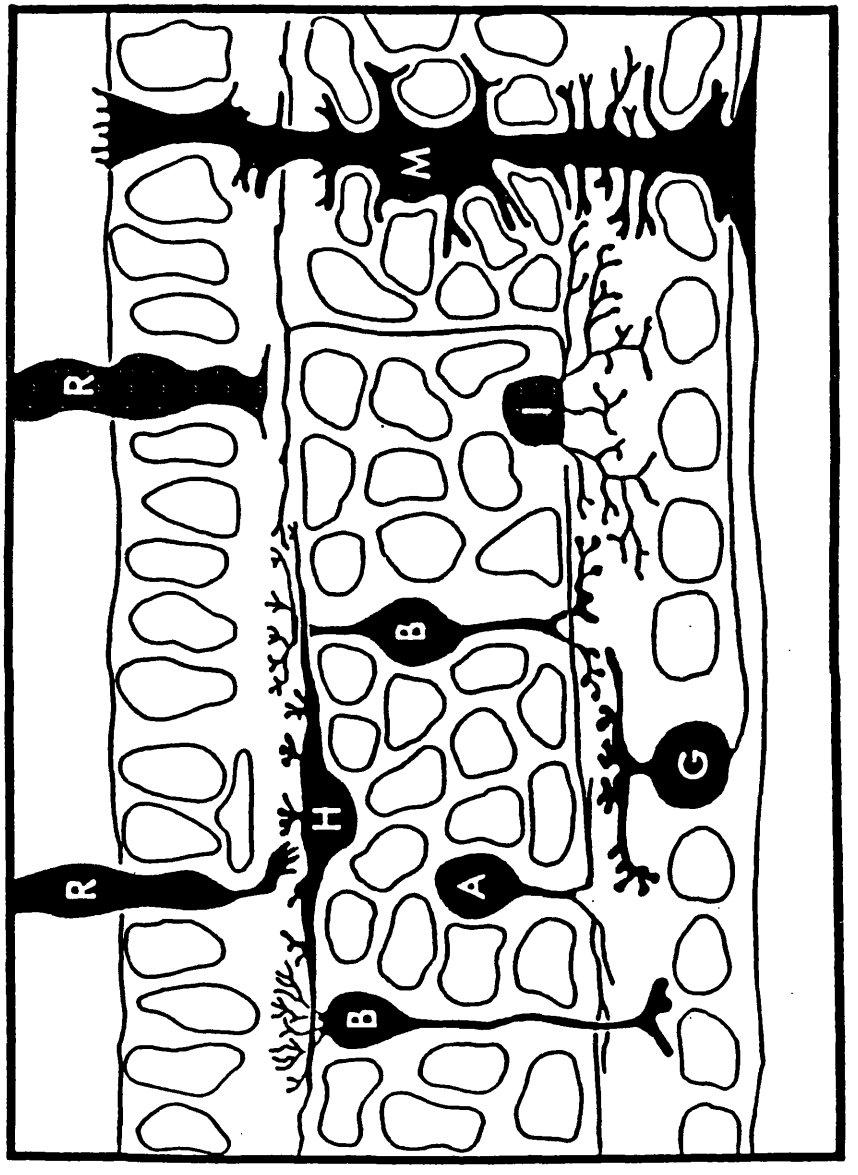
R
M
R
I
H
B
A
B
G
ONL
OPL
INL
IPL
GCL

photoreceptors make synapses onto processes of bipolar and horizontal cells. The cell bodies of the bipolar and horizontal cells are situated in the next layer, the inner nuclear layer. The proximal (inner) part of the inner nuclear layer also contains the cell bodies of amacrine and interplexiform cells. In the inner plexiform layer, processes from bipolar and amacrine cells form synapses with ganglion cells, whose cell bodies are situated in the ganglion cell layer which borders the vitreous humour. Exceptions to this cellular arrangement do occur when cells become "displaced". For example amacrine cell bodies are sometimes found in the ganglion cell layer in the retinae of many species (Vaney et al., 1981).

1.1.2 Glial cells

The term neuroglia was first given to the non-neuronal cells in the nervous system because, as the name suggests, their main function was thought to be provision of structural support (or "nerve glue") for neurones. Macroglial cells in the central nervous system (CNS) of vertebrates are usually classified into astrocytes and oligodendrocytes. Oligodendrocytes produce myelin. Astrocytes are found both in white and grey matter, and can be identified by the filaments they contain made up of a protein called glial fibrillary acidic protein (GFAP).

The predominant type of glial cell in the vertebrate retina is the Müller cell. This cell contains the enzyme glutamine synthetase (Riepe and Norenburg, 1977), which is regarded as a glial cell marker. Müller cells do not produce myelin, so they are not oligodendrocytes, but they only express GFAP after injury which makes it difficult to classify them as astrocytes. Müller cells span the whole width of the retina (Figure 1.1; Chapter 6, Figure 6.1). Glial cells like the Müller cell, that are orientated perpendicularly to neuronal layers, are known as radial glial cells. They are present throughout the developing nervous system of all vertebrates, where they are probably involved in the guidance of neurones as they migrate, but they persist only in certain regions of adult nervous tissue e.g. the Müller cell in the adult vertebrate retina and the Bergmann glial cell in the cerebellum.

Müller cells are involved in the spatial buffering of changes in extracellular potassium ion concentration around neurones

(Newman, 1984) and in the removal of neurotransmitter (such as glutamate) from the extracellular environment (Ehinger, 1977). The inner half of the vertebrate retina contains other types of glial cells: astrocytes, perivascular glia (in retinae containing blood vessels e.g. the rabbit) and microglia.

1.2 Information processing in the retina

To appreciate the relevance of the experiments reported in this thesis for understanding retinal function it is necessary to have some background knowledge of how the retina processes visual information. In this section and sections 1.3-1.5 I review our current knowledge of this topic, and describe the synaptic mechanisms which underlie the information processing carried out.

1.2.1 Phototransduction

Light is converted into an electrical signal in the photoreceptors (rods and cones). In the absence of illumination an inward "dark" current (carried by sodium and calcium ions) flows through the membrane of the photoreceptor outer segment, keeping the cells depolarized. Light, after passing through the whole width of the retina, is absorbed by the visual pigment (rhodopsin) in the outer segments. This then activates an enzyme cascade which leads to a drop in the concentration of cyclic GMP (cGMP) in the cytoplasm of the outer segments. Fesenko, Kolesnikov and Lyubarsky, (1985) showed that cGMP directly gates the "dark" current channels, keeping them open in the dark. A reduction in cGMP levels decreases the number of channels open, reduces the inward current and so the photoreceptors hyperpolarize. As a result, the release of neurotransmitter (believed to be glutamate, section 1.3.2) from photoreceptors is decreased (Cervetto and Piccolini, 1974).

1.2.2 Information transfer in the retina

Information is carried into two directions in the retina. The direct, or vertical pathway for information transfer is from photoreceptors to bipolar cells to ganglion cells. Ganglion cell axons form the optic nerve which projects to the lateral geniculate nucleus (which in turn sends visual information on to the visual cortex). Information is also carried laterally by the horizontal and amacrine cells. Synapses from horizontal cells onto bipolar cells

result in the excitatory centre of the bipolar cell receptive field (due to direct input from photoreceptors) being surrounded by an antagonistic area (due to input from distant photoreceptors via the horizontal cells: Dowling and Werblin, 1969; Werblin and Dowling, 1969). Electrical coupling between horizontal cells increases the size of the receptive field surround. Part of this antagonistic surround is also formed by a feedback synapse from horizontal cells to cones (Baylor, Fuortes and O'Bryan, 1971; Attwell et al., 1983). This centre-surround arrangement produces lateral inhibition, leading to the enhanced detection of spatial changes in light intensity between neighbouring photoreceptors. Amacrine cells pass information laterally, via bipolar cells to ganglion cells. This pathway operates in a similar manner to the horizontal cell pathway, except that it is more sensitive to moving stimuli (Werblin, 1972). A feedback pathway vertically through the retina is created by interplexiform cells that have processes in both the inner and outer plexiform layers. They are believed to provide feedback from mainly amacrine cells in the inner retina to bipolar and horizontal cells in the outer retina where they regulate the amount of lateral inhibition occuring (Dowling and Ehinger, 1975).

The magnitude of the hyperpolarization in photoreceptors in response to light depends on the light intensity. The photoreceptors respond with graded potentials, so that dim light generates a small hyperpolarization and bright light gives a hyperpolarization up to 25mV in amplitude (from the normal dark resting potential of about -40mV). In bipolar cells the graded signal from photoreceptors at one point on the retina has subtracted from it an average of the signal in the surrounding area as a result of the antagonistic surround contributed by horizontal cells. In the ganglion cells, the graded signals from bipolar cells are converted into changes of action potential frequency, for long-distance transmission along the optic nerve to the brain.

1.2.3 ON and OFF pathways

Bipolar cells can be divided into two classes, those that depolarize in response to light in the centre of their receptive field (ON cells) and those that hyperpolarize in response to light in the centre of their receptive field (OFF cells). The existence of

these two classes probably results from the neurotransmitter released by photoreceptors opening non-selective cation channels in hyperpolarizing (OFF) bipolar cells and closing similar channels in depolarizing (ON) bipolar cells (Attwell et al, 1987; see section 1.3.3.1). This organization of visual information into ON and OFF pathways persists at the ganglion cell level: ON bipolars project to ON ganglion cells which depolarize and fire action potentials in response to increased light stimulation in the centre of their receptive field, whereas OFF bipolars project to OFF ganglion cells which fire action potentials when light stimulation is decreased in the centre of their receptive field (Miller and Dacheux, 1976).

1.3 Synaptic transmission in the retina

1.3.1 Synaptic mechanisms in the outer retina

When the retina is stimulated by light most of the distal neurones (photoreceptors, horizontal cells and hyperpolarizing bipolar cells) hyperpolarize. There was early anatomical evidence to suggest that synaptic transmission between vertebrate photoreceptors and second order neurones is chemically mediated since there are vesicles in the photoreceptor terminals where the synaptic contacts with postsynaptic cells are made. These vesicles are believed to contain neurotransmitter (DeRobertis and Franchis, 1956). It is well established that neurones release neurotransmitter upon depolarization, when calcium entry into the cell triggers the fusion of vesicles with the cell membrane (Katz and Miledi, 1967). This led to the idea that photoreceptors release transmitter at a high rate when they are depolarized in the dark, and that light, by hyperpolarizing the cells, suppresses transmitter release. When neurotransmitter release from photoreceptors is blocked by high levels of Mg^{2+} (Katz and Miledi, 1967), horizontal cells hyperpolarize (just as occurs when light hyperpolarizes the photoreceptors) and they lose their response to light (Dowling and Ripps, 1973). Ayoub (1989) has since shown that at least some release of transmitter from photoreceptors is calcium-dependent (but see also section 1.4.2).

1.3.2 The transmitter released by photoreceptors

Miller and Schwartz (1983) have shown that five neurotransmitter candidates are released from isolated toad photoreceptors on depolarization: glutamate, aspartate, putrescine, cadavrine and N-acetylhistidine. Of these, glutamate and aspartate mimick the actions (described below) of the endogenous photoreceptor transmitter on second order neurones in isolated carp and rabbit retinae (Ariel et al., 1984; Bloomfield and Dowling, 1985a). However, in these studies no effects were seen with concentrations below mM concentration which is much higher than what is expected physiologically. Experiments like these on whole retinae can be difficult to interpret because uptake (section 1.4.1) of the transmitter by the cells of the retina greatly reduces the actual concentration of applied transmitter which reaches the cells deep in the tissue.

Glutamate (but not the other transmitter candidates mentioned above as being released from photoreceptors) has been found to induce current changes in isolated and cultured horizontal and bipolar cells (Ishida, Kaneko and Tachibana, 1984; Lasater, Dowling and Ripps, 1984; Attwell et al., 1987). Cultured horizontal cells respond to low (10μM) concentrations of glutamate but not to aspartate, and are strongly depolarized by micromolar concentrations of the glutamate analogues quisqualate and kainate (section 1.6.1) but not by the aspartate analogue N-methyl-D-aspartate (Ariel et al., 1984). All of this evidence is consistent with glutamate being the neurotransmitter released from photoreceptors.

1.3.3 Actions of the major neurotransmitters in the retina

1.3.3.1 Different actions of the photoreceptor transmitter

Recording the responses of horizontal cells, depolarizing bipolar and hyperpolarizing bipolar cells to application of different analogues of glutamate to the retina showed that glutamate activates pharmacologically distinct receptors in each cell type (Slaughter and Miller, 1981; 1983a; 1983b; 1985). This presumably allows the photoreceptor transmitter to generate responses of different time course in the three types of postsynaptic cells, and of different sign in the two types of bipolar cell (see below).

In horizontal cells glutamate opens channels with a reversal

potential near 0mV (Tachibana, 1985). Thus, when light suppresses glutamate release from photoreceptors, the horizontal cells are hyperpolarized (from their normal resting potential of about -30mV).

As stated in section 1.2.3, the visual signal is segregated into ON and OFF pathways at the photoreceptor to bipolar cell synapse. Murakami, Ohtsuka and Shimazaki (1975) have shown that glutamate has different effects on hyperpolarizing and depolarizing bipolar cells, suggesting that just one transmitter is released from photoreceptors which has different effects on the two classes of bipolar cells. Attwell et al. (1987) suggested that this is achieved by the glutamate receptors on the two types of cells being linked to different types of ion channel. They studied the effect of glutamate on isolated bipolar cells from the salamander retina. Glutamate evoked an inward current by opening channels (E_{rev} -10mV) in some, presumed hyperpolarizing bipolar cells (light would suppress glutamate release from photoreceptors in the intact retina evoking an outward current in these cells), and glutamate evoked an outward current by closing channels (with a similar reversal potential) in other, presumed depolarizing bipolar cells (in the intact retina light would evoke an inward current in these cells). It has been suggested that in depolarizing bipolar cells the glutamate-gated channels are kept open by cGMP, and that a glutamate receptor closes the channels by increasing the rate of cGMP hydrolysis through a G-protein mediated mechanism (Nawy and Jahr, 1990).

1.3.3.2 Horizontal cell transmitter

Lateral transmission of information in the outer retina is thought to be mediated by the release of γ-aminobyturic acid (GABA) from horizontal cells which acts on bipolar cells and cone photoreceptors. Partial evidence for this is that GABA is accumulated within frog (Voaden, Marshall and Murani, 1974) and goldfish horizontal cells (Marc et al., 1978), and glutamate-induced release of GABA has been demonstrated in the goldfish retina (Ayoub and Lam, 1984). GABA has been shown to gate postsynaptic $GABA_A$-type chloride channels in isolated turtle cones (Kaneko and Tachibana, 1986) and bipolar cells from the salamander (Attwell et al., 1987). Furthermore, receptors for GABA have been morphologically localized by immunocytochemistry to cone synaptic terminals in chicken and

goldfish retinae (Yazulla et al., 1987). In the salamander retina only about 60% of horizontal cells accumulate GABA, and a similar percentage of hyperpolarizing bipolar cells receive GABA-mediated inhibitory input (Wu, 1986). It seems possible, therefore, that another transmitter (e.g. glycine) may mediate the receptive field inhibitory surround of the other bipolar cells.

When horizontal cells are hyperpolarized by light (see section 1.3.3.1), release of GABA is suppressed. GABA acts on postsynaptic bipolar cells and cones by opening chloride channels (Kaneko and Tachibana, 1986), so the effect on the postsynaptic cells will depend on the resting potential (E_{rest}) and the chloride reversal potential (E_{Cl}) of the cell. If E_{Cl} is below E_{rest}, GABA will evoke an influx of chloride ions, which will hyperpolarize the cell. In this case light, which suppresses GABA release, will depolarize the cell. This is thought to be the mechanism producing the antagonistic surround response of cone photoreceptors (Kaneko and Tachibana, 1986) and hyperpolarizing bipolar cells. The hyperpolarizing surround response of depolarizing bipolar cells is probably generated by them having an E_{Cl} value above E_{rest} so that light (removal of GABA) hyperpolarizes the cell (Miller and Dacheux, 1983).

1.3.3.3 Transmitters in the inner retina

In the inner retina glutamate is believed to be the transmitter released from bipolar cells (Bloomfield and Dowling, 1985b; Slaughter and Miller, 1983c). Glutamate has been shown to act on isolated ganglion cells in the rat (Aizenman, Frosch and Lipton, 1988) and in the tiger salamander retina (Everett, Mobbs and Thompson, 1989). The two types of bipolar cells release the same transmitter (Slaughter and Miller, 1983c).

The antagonistic surround to ganglion cell receptive fields partly reflects the inhibitory surround present in the receptive fields of the bipolar cells they receive input from (i.e. generated in the outer retina by the horizontal cells). In addition, amacrine cells send synapses to ganglion cells and contribute to the properties of the ganglion cell receptive field surround. The transmitters in this mechanism are believed to be GABA and glycine, since amacrine cells have been shown to accumulate these agents and

to release them on depolarization (Ehinger, 1972; Voaden, Marshall and Murani, 1974; Miller et al., 1981). GABA and glycine have both been shown to gate chloride channels in isolated retinal ganglion cells (Ishida and Cohen, 1988; Everett, Mobbs and Thompson, 1989).

Glycine may be the transmitter used by interplexiform cells in some retinae to provide a direct pathway between the outer and inner plexiform layers. Marc and Liu (1984) have shown in radiolabelling experiments that horizontal cells receive synapses from glycine-containing interplexiform cells and glycine is accumulated by interplexiform cells in goldfish (Chin and Lam, 1980). In other retinae dopamine is the probable transmitter released by interplexiform cells. Application of dopamine to the carp retina results in an accumulation of adenosine 3'5'-monophosphate (cyclic AMP) in horizontal cells (Van Buskirk and Dowling, 1981), which reduces the receptive field size of horizontal cells by decreasing the electrical coupling among these cells (Lasater and Dowling, 1985), and thus decreases the strength of lateral inhibition generated in the outer retina.

The above sections describe the actions of the major neurotransmitters in the retina. However, many more neuroactive agents are present in the retina. For instance, it has been reported that in the cat retina, amacrine cells contain more than twenty different transmitter candidates (mostly peptides).

1.4 Termination of the neurotransmitter action of glutamate

From the data reviewed in section 1.3 it is clear that glutamate is a major candidate for the neurotransmitter employed by cells in both the inner and the outer retina. The action of glutamate on its postsynaptic receptors must be terminated either by glutamate diffusing away or by glutamate being taken up into cells, since there are no extracellular enzymes present to convert it into an inactive molecule (analogous to the enzyme acetylcholinesterase which breaks down the vertebrate neuromuscular junction transmitter, acetylcholine). Even if diffusion of glutamate away is more important initially, this is only made possible by glutamate uptake maintaining a low extracellular concentration around the synapses.

In addition to being essential so that synapses can function, a

low extracellular concentration of glutamate is necessary because high extracellular glutamate levels are neurotoxic: too much activation of NMDA-type glutamate channels (section 1.6.1), which are present on ganglion cells in the inner retina, can lead to an excessive influx of calcium into the cell which activates lethal proteases, and neurones may swell due to excessive glutamate-induced ion movement (Rothman and Olney, 1987). Thus uptake of glutamate serves two functions: it helps terminate glutamate's synaptic action and it prevents neuronal death from a raised extracellular glutamate concentration.

A major part of this thesis (Chapters 3 to 5) describes experiments that were carried out to investigate the actions of glutamate on cone photoreceptors of the salamander retina and on isolated Müller cells of the rabbit retina. In principle, both of these cell types could take up glutamate (as it turns out, glutamate acts by activating an electrogenic uptake carrier in Müller cells, but in cones glutamate gates ion channels). In the following sections (1.4.1-1.4.3) I will give background information on the functions and the mechanism of glutamate uptake.

1.4.1 Uptake of glutamate into cells in the outer retina

Synaptically released glutamate may be reaccumulated directly into the nerve terminals which released it or into adjacent glial cells. Studies of uptake of radiolabelled glutamate in the retina have shown that glutamate is taken up preferentially into Müller cells in the frog (Kennedy, Voaden and Marshall, 1974), rat (White and Neal, 1976) and rabbit (Ehinger, 1977). Once in the glial cell, glutamate can be used as a metabolic fuel or be converted into glutamine by the enzyme glutamine synthetase which has been located in Müller cells (Riepe and Norenburg, 1977). Glutamine might then be passed back to neurones and be converted back into glutamate by mitochondrial glutaminase. However, glutaminase activity is inhibited by cytoplasmic glutamate at concentrations above 10μM (McMahon and Nicholls, 1990). It is therefore difficult to see whether this system can be of any importance since the cytoplasmic glutamate concentration is thought to be as high as 10mM (Schousboe, Fosmask and Hertz, 1975; Kvamme et al., 1985).

Synaptically released glutamate can also be removed from the synaptic cleft by uptake into the neurones that released it (e.g. photoreceptors). This would enable them to re-use the transmitter. Although from radiotracing experiments it appears that neurones take up less glutamate than glia, any uptake carriers in the presynaptic membrane will be ideally placed to remove glutamate after it has acted postsynaptically. In some species uptake of glutamate into photoreceptors has been demonstrated e.g. in goldfish (Marc and Lam, 1981), human and rat retinae (Brandon and Lam, 1983).

1.4.2 Reversed uptake as a glutamate release mechanism

Depolarization-induced reversal of the glutamate uptake mechanism can serve as a calcium-independent release mechanism for glutamate (Szatkowski, Barbour and Attwell, 1990). Although release of transmitter from photoreceptors is probably at least partly from vesicles (section 1.3.1), Schwartz (1986) has shown that synaptic transmission continues in the outer retina under conditions expected to block the entry of calcium into presynaptic terminals, indicating that some non-vesicular release of transmitter from photoreceptors may occur. Additional evidence that two modes of transmitter release may occur comes from the observation that vertebrate photoreceptors make two morphological type of chemical synapses, ribbon and basal. Ribbon synapses have an aggregation of cytoplasmic vesicles while basal junctions do not (Kolb, 1970, Lasansky, 1971; 1973). Basal synapses are the only point of contact between photoreceptors and one type of bipolar cell in primate (Kolb, 1970) and turtle (Lasansky, 1971) retinae, and are believed to be chemical rather then electrical since there is no narrowing of the intercellular cleft which is typical of electrical synapses (Brightman and Reese, 1969).

1.4.3 Monitoring uptake of glutamate

Radiotracing experiments have shown that the energy needed to accumulate glutamate into neurones and glial cells is derived from the co-transport of an excess of sodium ions with each glutamate anion on the uptake carrier (Baetge, Bulloch and Stallcup, 1979). Co-transport of (say) two sodium ions with one glutamate anion should lead to glutamate uptake generating an inward membrane

current. The work of Bowman and Kimelberg (1984) and Kettenman and Schachner (1985) suggested that glutamate could depolarize glial cells by activating an electrogenic carrier. Subsequent electrophysiological studies have shown that the uptake of glutamate into Müller cells of the salamander is indeed via an electrogenic carrier mechanism that transports a net positive charge into the cell with each cycle of the carrier (Brew and Attwell, 1987). Glutamate uptake via a similar mechanism has also been shown in type-1 astrocytes from rat cerebellum (Cull-Candy, Howe and Ogden, 1988). The electrogenic nature of the glutamate carrier mechanism allows the study of glutamate uptake in isolated cells with the whole-cell patch-clamp technique: uptake can be monitored as the membrane current it produces. This technique is used extensively in Chapter 5.

1.5 Neurotransmitter-gated channels in glial cells

Experiments described in Chapter 5 of this thesis were carried out to study the effect of glutamate on rabbit Müller cells. In salamander Müller cells glutamate generates an inward current due to an electrogenic mechanism that carries positive charge into the cell (Brew and Attwell, 1987). The function of this uptake is presumably to clear synaptically released glutamate from the extracellular space. Neurotransmitters (including glutamate) also activate channels in a variety of glial cells as they do in neurones. Glutamate acts on a non-NMDA receptor (section 1.6.1) activating a cation-selective channel in cultured cortical astrocytes (Sontheimer et al, 1988) and in cultured cerebellar type-2 astrocytes (Usowicz, Gallo and Cull-Candy, 1989), and GABA gates a chloride-specific channel in cultured cortical astrocytes (Bormann and Kettenman, 1988). Channels are not just present in cultured cells, since GABA activates a chloride channel in freshly dissociated skate Müller cells that seems to be similar to the $GABA_A$ receptor-activated channel in neurones (Malchow, Qian and Ripps, 1989), glutamate gates channels in isolated glial progenitor cells (Barres et al, 1990), and glutamate- and GABA-gated ion channels are present in astrocytes in the isolated rabbit retina (Clark and Mobbs, 1990). The function of the neurotransmitter-gated channels in glial cell is not known, but their existence implies that, when experiments are done (as in

Chapter 5) monitoring glutamate uptake as the current it produces, one must be careful to determine whether any ion channels contribute to the current changes seen.

1.6 Pharmacology of glutamate-activated ion channels and the glutamate uptake system

A large part of the experiments described in this thesis were carried out to study the effect of glutamate on voltage-clamped cells. Glutamate can generate a current in voltage-clamped cells either by gating ion channels or by activating an electrogenic carrier mechanism. One way to distinguish between these two actions is by studying the pharmacological profile of the response evoked by glutamate. In this section I will give background information on the pharmacology of glutamate-activated channels and of the glutamate uptake system. Some of the compounds mentioned were used, in the experiments described in later chapters, to investigate the pharmacological profile of the glutamate-evoked current in cones and Müller cells.

1.6.1 Pharmacology of glutamate-activated channels

In the late 1970's, the responses of CNS neurones to glutamate were defined by electrophysiological analysis of the action of a large number of glutamate analogues. From these studies three receptor subtypes were identified: they were known as the N-methyl-D-aspartate (NMDA), quisqualate and kainate receptor subtypes (Watkins and Evans, 1981).

The NMDA receptor gates a cation channel which is permeable to Ca^{2+}, Na^{+} and K^{+} (Mayer and Westbrook, 1985) and which is blocked by Mg^{2+} in a voltage-dependent manner (Novak *et al.*, 1984). Other blockers of this channel are the non-competitive antagonists phencyclidine (PCP) and MK801 (Wong *et al.*, 1986) and the competitive antagonist 2-amino-5-phosphonovalerate (APV).

Both kainate and quisqualate gate channels that are permeable to Na^{+} and K^{+} ions (Mayer and Westbrook, 1985). The quisqualate receptor has recently been renamed the AMPA receptor. AMPA (alpha-amino-3-hydroxy-5-methyl-4-isoxazolepropionic acid) is an analogue of quisqualate that is more specific, since quisqualate has been found to also act on the "metabotropic receptor" described below.

CNQX (6-cyano-7-nitroquinoxaline-2,3-dione) is the most commonly used antagonist (competitive) for blocking the non-NMDA receptors (Honore, et al., 1988).

Recently, two more glutamate receptor subtypes have been identified. One is the L-AP4 (L-2-amino-4-phosphonobutanoic acid) receptor, activated by this phosphono analogue of glutamate (Monaghan, Bridges and Cotman, 1989). The second is the metabotropic receptor, which is activated by quisqualate. This receptor is linked to phospholipase C via a G protein and activation of the receptor leads to the production of inositol 1,4,5-triphosphate (IP_3) and the release of calcium from intracellular stores (Sugiyama, Ito and Hirono, 1987).

In the retina, horizontal cells, bipolar cells and ganglion cells have kainate-type receptors (Everett, Mobbs and Thompson, 1989; Ishida, Kaneko and Tachibana, 1984; Lasater, Dowling and Ripps, 1984; Miller and Slaughter, 1986; Shiells, Falk and Naghshineh, 1981). AP4 mimics the action of glutamate on depolarizing bipolar cells (Miller and Slaughter, 1986; Shiells, Falk and Naghshineh, 1981). In addition to kainate receptors, ganglion cells also have NMDA receptors (Aizenman, Frosch and Lipton, 1988; Bloomfield and Dowling, 1985b)

1.6.2 Pharmacology of the glutamate uptake system

The analogues used to classify glutamate-gated ion channels, i.e. quisqualate, kainate and NMDA, are not usually taken up into cells (Watkins and Evans, 1981; Johnston, Kennedy and Twitchin, 1979). Aspartate however, which is a neurotransmitter candidate acting on NMDA channels, is taken up (Balcar and Johnston, 1972; Erecinska et al, 1986) by the glutamate uptake carrier (Barbour, Brew and Attwell, 1991).

The electrogenic uptake of glutamate into Müller cells is blocked by the glutamate analogue threo-3-hydroxy-DL-aspartate (THDA), which has been shown to reduce glutamate uptake in radiolabelled experiments in a variety of cells (Balcar and Johnston, 1972). Uptake is not blocked by blockers of glutamate-gated channels such as CNQX and APV (Barbour, Brew and Attwell, 1991).

1.7 Experiments presented in this thesis

1.7.1 Effect of glutamate on photoreceptors

Glutamate is a strong candidate for the neurotransmitter released from photoreceptors, conveying the visual signal to postsynaptic bipolar and horizontal cells, There is however little information on the action of this agent on the photoreceptors themselves. Murakami, Ohtsu and Ohtsuka (1972) report that glutamate has no effect on rods in the gecko retina. Glutamate may, however, be expected to have some action on photoreceptors for two reasons. Firstly, there is histological evidence for a synapse from rods to cones in the salamander retina (Lasansky, 1973) and cones may therefore be expected to have receptors for the transmitter released from rods. Secondly, radiotracing experiments have shown that glutamate is taken up into photoreceptors, and glutamate uptake in the synaptic terminal might generate an inward current as it does in Müller cells (section 1.4.3). Since there may be some non-vesicular release of neurotransmitter from photoreceptors (section 1.4.2), any uptake carrier present could also act as a release mechanism.

I investigated the actions of glutamate on cone photoreceptors of the salamander retina to find out whether they have an electrogenic uptake mechanism similar to that in glial cells or whether glutamate gates ion channels in the cone membrane. The whole-cell variant of the patch-clamp technique was used to monitor the current evoked by glutamate, mainly in freshly isolated cones which are large cells and easy to identify from their appearance. Advantages of this technique are the following: (1) studying isolated cells means that there is no input from neighbouring cells and that the dose of applied drug can be controlled since it is not taken up by other cells; (2) in patch-clamp studies on isolated cells the ionic composition of the extracellular and intracellular solutions can be controlled; (3) glutamate-evoked currents can be studied while the voltage of the cell remains clamped.

Although most of the experiments to examine the glutamate-evoked current in cones were carried out on isolated cells, the retina is an easily accessible part of the CNS, and some experiments were carried out *in situ* in isolated retinae. Experiments on the glutamate-evoked current in cone photoreceptors are described in Chapters 3 and 4.

1.7.2 Effects of glutamate on mammalian glial cells

As described in section 1.4.3 above, in lower vertebrates glutamate is taken up into glial cells via an electrogenic carrier mechanism, but in mammalian astrocytes glutamate has been reported to open cation channels as it does in neurones (section 1.5). It is important to understand the action of glutamate on mammalian glia since uptake of glutamate into these cells is thought to play a major role in keeping the extracellular glutamate concentration below neurotoxic levels in the CNS (section 1.4; Chapter 7, section 7.2.4). To investigate the actions of glutamate on a mammalian glial cell, I applied glutamate to Müller cells isolated from the rabbit retina, while monitoring these cells' membrane current (using the whole-cell variant of the patch-clamp technique). The results are described in Chapter 5. Rabbit Müller cells were chosen for these experiments because glutamate is likely to be the neurotransmitter released from photoreceptors (Bloomfield and Dowling, 1985a) and bipolar cells (Bloomfield and Dowling, 1985), and because rabbit Müller cells are known from radiotracing experiments to have an uptake system for glutamate (Ehinger, 1977).

1.7.3 Anatomical arrangement of glial cell processes at a glutamatergic synapse

The synaptic action of glutamate is probably terminated by glutamate diffusing away from the site of release and by uptake into cells. It has been shown that glutamate is taken up into Müller cells in the salamander retina. However, it is not known precisely how close Müller cell processes, that presumably contain the uptake carriers, come to the site of glutamate release. Consequently, it is difficult to assess the importance of this uptake mechanism in terminating synaptic action. It has been reported in the turtle retina that the decaying phase of the synaptic current during transmission from rods to postsynaptic horizontal cells is 7 times slower than for transmission from cones to horizontal cells (Copenhagen, Ashmore and Schnapf, 1983), and this could, in principle, reflect a greater diffusion distance to nearby Müller cell processes from the rod output synapse then from the cone output synapse.

To investigate these issues I studied the anatomical

arrangement of Müller cells processes near the photoreceptor output synapse in the outer plexiform layer of the salamander retina. Müller cells in isolated retinae were labelled with horseradish peroxidase, so that their processes could be identified in the electron microscope. I studied the distribution of Müller cell processes near ribbon synapses, which are one type of synaptic contact between photoreceptors and postsynaptic horizontal and bipolar cells. I chose this synapse for two reasons: (1) it is a chemical synapse which almost certainly uses glutamate as a transmitter; and (2) it is very easy to identify the transmitter release site at this synapse in the electron microscope because of the distinctive appearance of the synaptic ribbons (see Chapter 6).

The experiments in this thesis were carried out on retinal cells and the results provide information on the actions of glutamate on photoreceptors and on retinal glial cells. However, since glutamate is a major neurotransmitter elsewhere in the CNS, these mechanisms provide useful models for the operation of glutamatergic synapses in other parts of the brain and spinal cord.

Chapter 2
Methods

This chapter is divided into two sections dealing with:

(1) whole-cell patch-clamp experiments, and

(2) injection of cells with horseradish peroxidase (HRP) and processing for electron microscopy.

2.1 Whole-cell patch-clamp experiments

Experiments were performed on retinae from larval tiger salamanders (*Ambystoma tigrinum*), 15-25cm long, and from New Zealand White male rabbits, 2-3.5kg in weight. All experiments were performed at room temperature (18-22°C).

Recordings were made from three preparations: (1) isolated cone photoreceptors from the salamander retina; (2) cone photoreceptors in the intact, isolated salamander retina (both of these preparations were used to study the effect of the neurotransmitter glutamate on cones, the isolated retina preparation was also used to study the light responses in cones); (3) isolated Müller cells from the rabbit retina (this preparation was used to study the electrogenic uptake of glutamate into glial cells).

2.1.1 Cell preparations

2.1.1.1 Preparation of isolated photoreceptors from salamander retina

An eye was excised from a salamander immediately following decapitation. Excess tissue was trimmed from the eyeball under a dissecting microscope. While holding the eye with forceps a cut was made in the sclera, anterior to the ora serrata, using a piece of broken valet blade. The cut was continued round the eye using ophthalmological scissors until the front of the eye could be removed. The lens was pulled out with fine forceps while scissors were used to cut any attachments between the lens and the rear half of the eye. The vitreous humour was removed by capillarity using a piece of microelectrode glass. The eyecup was either used immediately or stored in Ringer's (solution RA, Table 2.1) in a refrigerator (5°C) and used within 30 hours. Storing the eyecup in this way did not affect the results obtained.

Next an isolated eyecup was cut in half, and one half was trimmed with ophthalmological scissors by cutting through the retina, choroid and sclera posterior to the ora serrata. While under Ringer's, the retina was gently separated from the eyecup using fine forceps. Isolated cone photoreceptors were obtained by treating the retina with a proteolytic enzyme, followed by mechanical dissociation of the cells. The method used was a modification of the method of Bader, Macleish and Schwartz (1979). Using a cut-off fire polished Pasteur pipette, an isolated retina half was transferred to 2ml of a solution containing (in mM): NaCl 66; $NaHCO_3$ 25; NaH_2PO_4 10; glucose 10; KCl 3.7; DL-cysteine-HCl (Sigma) 10; Na-pyruvate 1; and 0.03ml (containing around 30 units) papain (Sigma, P3125). The retina was incubated in this solution for 7-8 minutes at room temperature.

After incubation, the retina was rinsed by dropping it three times through 3ml of Ringer's and then gently triturated (drawn in and out of a fire polished Pasteur pipette) in 1ml of Ringer's, until the retina could be seen to break up into a suspension of cells. The cells were plated into a recording chamber (a perspex frame with a central 15x15x3mm hole mounted on a 75x50x1mm glass slide). The recording chamber was then transferred to a microscope with a fixed stage (Ergaval, East Germany), fitted with Hoffman modulation contrast optics (Modulation Optics, Inc., Greenvale, NY).

Cone photoreceptors were identified, with a x40 Zeiss water-immersion lens and x10 eyepieces, by their characteristic shape (Figure 2.1). Whole-cell patch-clamp recordings were made from both half of a double and single cones with synaptic terminals. The cells were allowed to settle for 10-15 minutes before recording. Cells remained healthy looking for 2-3 hours after dissociation. After this time the cells began to round up and the cytoplasm became granular in appearance.

The isolated cell population from the enzyme-treated retina contained other retinal neurones apart from photoreceptors. Bipolar cells (identified by the Landolt club (Lasansky 1973)) and ganglion cells (tentatively identified by the presence of an axon) were recorded from in experiments as described in Chapter 4 (section 4.3.5).

Figure 2.1 A cone photoreceptor from the salamander retina. Photomicrograph of a cone photoreceptor isolated from the salamander retina by trituration after incubation in a papain containing solution (section 2.1.1.1). The photomicrograph was taken using Hoffman modulation contrast optics. The outer segment, inner segment, cell body and synaptic terminal are indicated (magnification x1300: the cell body is approximately 15μm across).

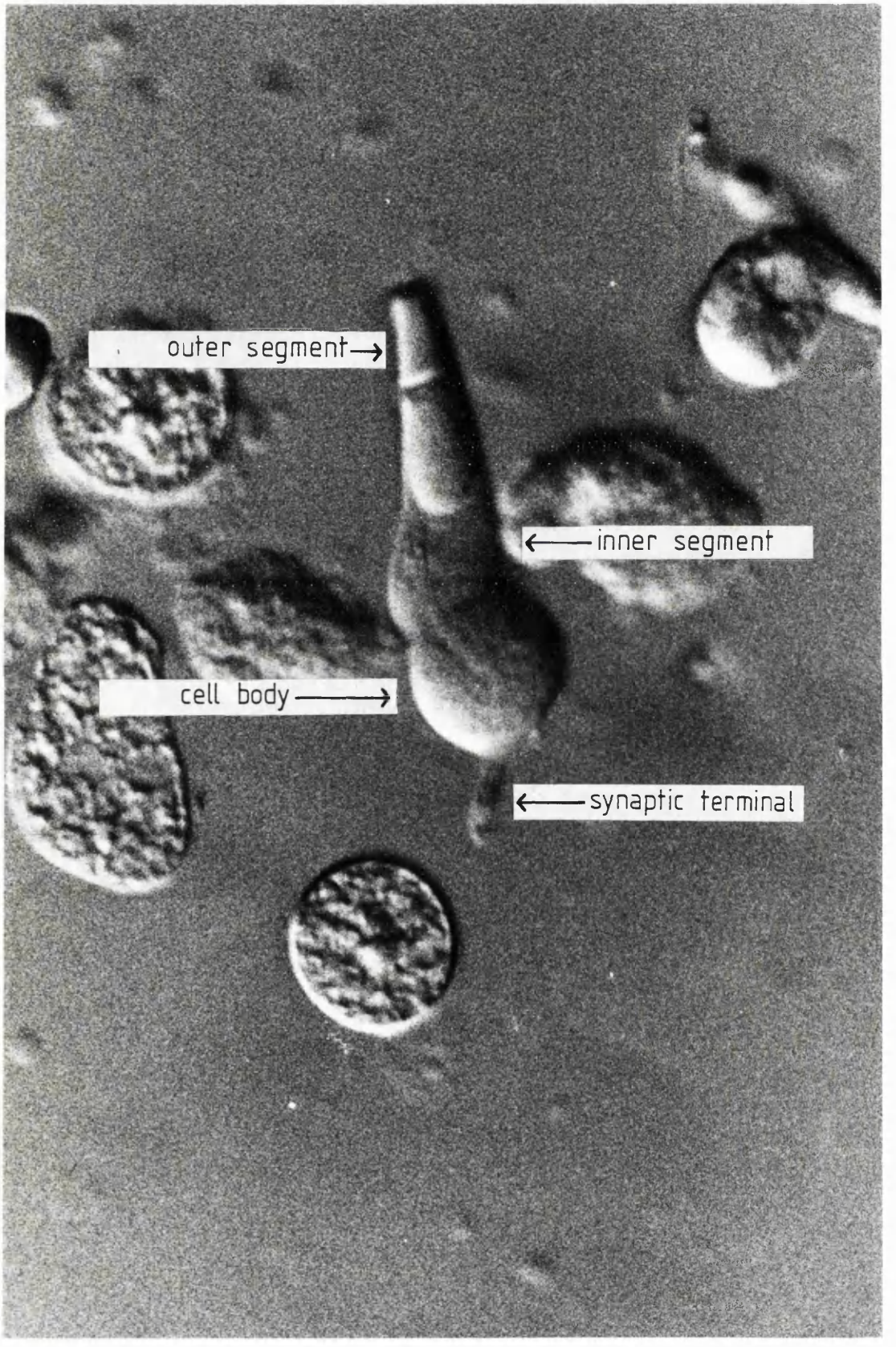
outer segment
inner segment
cell body
synaptic terminal

2.1.1.2 Preparation of an isolated salamander retina mounted photoreceptor side upwards

Under Ringer's (solution RA, Table 2.1), an eyecup, prepared as described in section 2.1.1.1, was cut into four quarters. Each piece was trimmed to remove the parts of the eyecup anterior to the ora serrata. A base for each of the pieces of retina was made in advance by fixing a Millipore filter (diameter: 1cm; pore size: 0.45μm) with Vaseline grease to the bottom of a recording chamber. Using a fragment of razor blade, two to four holes were cut in the filter to precisely fit chips of glass that were slightly smaller than a quarter of a retina. The glass chips were the same thickness as the filter paper and were obtained by crushing a No.1 coverslip. The purpose of these "windows" in the filter paper was to allow illumination of the preparation from below.

Pieces of eyecup were transferred to the recording chamber. Using fine forceps, each piece of eyecup was positioned over one of the glass chips. The edges of the eyecup that extended beyond the glass chip were pressed into the filter paper, with fine forceps, so that the retina adhered to the filter at its edges. The sclera with the choroid and the pigment epithelium attached to it was lifted off to leave pieces of retina flatmounted receptor side upwards, and the recording chamber was flooded with Ringer's.

The recording chamber was transferred to a microscope with a fixed stage, fitted with Hoffman modulation contrast optics. Sufficient light could be passed through the "windows" and the tissue to be able to distinguish individual cells when observed from above with a x40 Zeiss water-immersion lens and x10 eyepieces.

For patch-clamp experiments, it was nearly always necessary to treat the flatmounted retina with enzymes to remove viscous material that surrounded the photoreceptors, which made it difficult to form a high resistance seal between the patch pipette and the cell membrane. The nature of this substance is unknown, but it could be removed by bathing the preparation for 10 minutes in Ringer's to which the following enzymes had been added: collagenase, 2mg/ml (Cooper, L5000476); hyaluronidase, 1.2mg/ml (Sigma, H2376); and trypsin inhibitor, 0.3mg/ml (Sigma, T9253). In patch-clamp experiments, cells studied in enzyme-treated retinae had glutamate- and light responses similar to cells in untreated retinae.

Cone photoreceptors could be identified when viewed from above by their characteristic shape and small size of their outer segments. To record light responses, monochromatic light stimuli (70μm diameter on the retina), were applied to the preparation via the microscope objective, after being passed through a shutter, neutral density filter (for adjusting the intensity) and interference filters (to select a wavelength band). Stimuli were introduced into the microscope light path through a beam combining prism.

During experiments in which light responses were recorded from cones, the following precautions were taken to avoid light adaptation of the retina. Animals were dark-adapted for at least two hours before an experiment. Experiments were performed in a dark room. Apart from removal of the eye from the animal (under dim red light), all viewing of the preparation during the dissection was with an infra-red image converter (F.J.W. Industries). During these experiments, the preparation was viewed on a T.V. screen connected to an infra-red sensitive silicon diode camera (Hitachi, HV17SD) attached to the microscope.

2.1.1.3 Preparation of isolated Müller cells from rabbit retina

The eye was excised from a rabbit immediately following injection of an overdose of sodium pentobarbitone (Sagatal, 4ml, 60mg/ml) into the ear vein. Excess tissue was trimmed from the eyeball. While holding the eye with forceps, a cut was made in the sclera posterior to the cornea, using a piece of broken valet blade. The cut was continued round the eye until the front of the eye could be removed. The lens was pulled out with fine forceps, and the vitreous humour came out together with the lens. The eyecup was immersed in Ringer's (solution RC, Table 2.4) at room temperature and the retina used on the same day.

While under Ringer's a small piece of retina (2x2mm) was cut out of the region of the visual streak (identified by the presence of blood vessels) with ophthalmological scissors. Using a cut-off fire polished Pasteur pipette, it was transferred to 2ml of a solution containing (in mM): NaCl 120; $NaHCO_3$ 25; glucose 15; NaH_2PO_4 10; D,L-cysteine-HCl 10; Na-pyruvate 1; 0.01-0.015ml (containing 10 to 15 units) papain; and NaOH 2, to pH 7.3. The

retina was incubated in this solution for 10-30 minutes at 34°C. The conditions described above gave a good yield of healthy looking Müller cells, with a clear (non granular) cytoplasm and nucleus.

After incubation, the retina was rinsed by dropping it three times through 3ml of Ringer's and then it was gently triturated in 1ml of Ringer's, until the retina could be seen to break up into a suspension of cells. The cells were then transferred to a recording chamber on a microscope with a fixed stage, and the cells were allowed to settle for 15 minutes before recording. Müller cells could be identified from their characteristic appearance (Figure 2.2) with a x40 Zeiss water-immersion lens and x16 eyepieces. Cells remained healthy for several hours after dissociation, after which time they began to lose their elongated shape, and the cell membranes became more fragile which often resulted in cell death when trying to whole-cell patch-clamp.

2.1.2 Solutions

2.1.2.1 Superfusion

The superfusion solutions used outside cells in whole-cell patch-clamp experiments are given in Tables 2.1, 2.2 and 2.4. Tables 2.1 and 2.2 list solutions used in experiments on salamander photoreceptors. Table 2.4 lists solutions used in experiments on Müller cells from rabbit retinae.

Some experiments required exposing an isolated cell to a uniform concentration of an agent (as when determining a dose-response curve for glutamate), to several pharmacological agents in succession, or to solutions of different ionic composition. For this type of experiment a bath-perfusion system was used. Solutions were fed into the recording chamber through plastic tubing by gravity flow. Excess solution was removed by a pump sucking through a small tube. To speed up the turnover time of solution around a cell in experiments on isolated cells, the cell being studied was lifted off the bottom of the bath, after going to whole-cell recording mode, and moved close to the solution inlets before starting the recording.

Most experiments described in Chapters 3 to 5 were carried out to study the action of L-glutamate on cones and Müller cells. The bulk of the experiments were carried out in Ringer's containing 6mM

Figure 2.2 A Müller cell from the rabbit retina.
Photomicrograph of a Müller cell isolated from the rabbit retina by trituration after enzyme treatment (section 2.1.1.3). The photomicrograph was taken using Hoffman modulation contrast optics. The apical processes (that would project out between photoreceptors *in vivo*), cell body and endfoot (which would face the vitreous humour *in vivo*) are indicated (magnification x1100: the cell is approximately 100μm long).

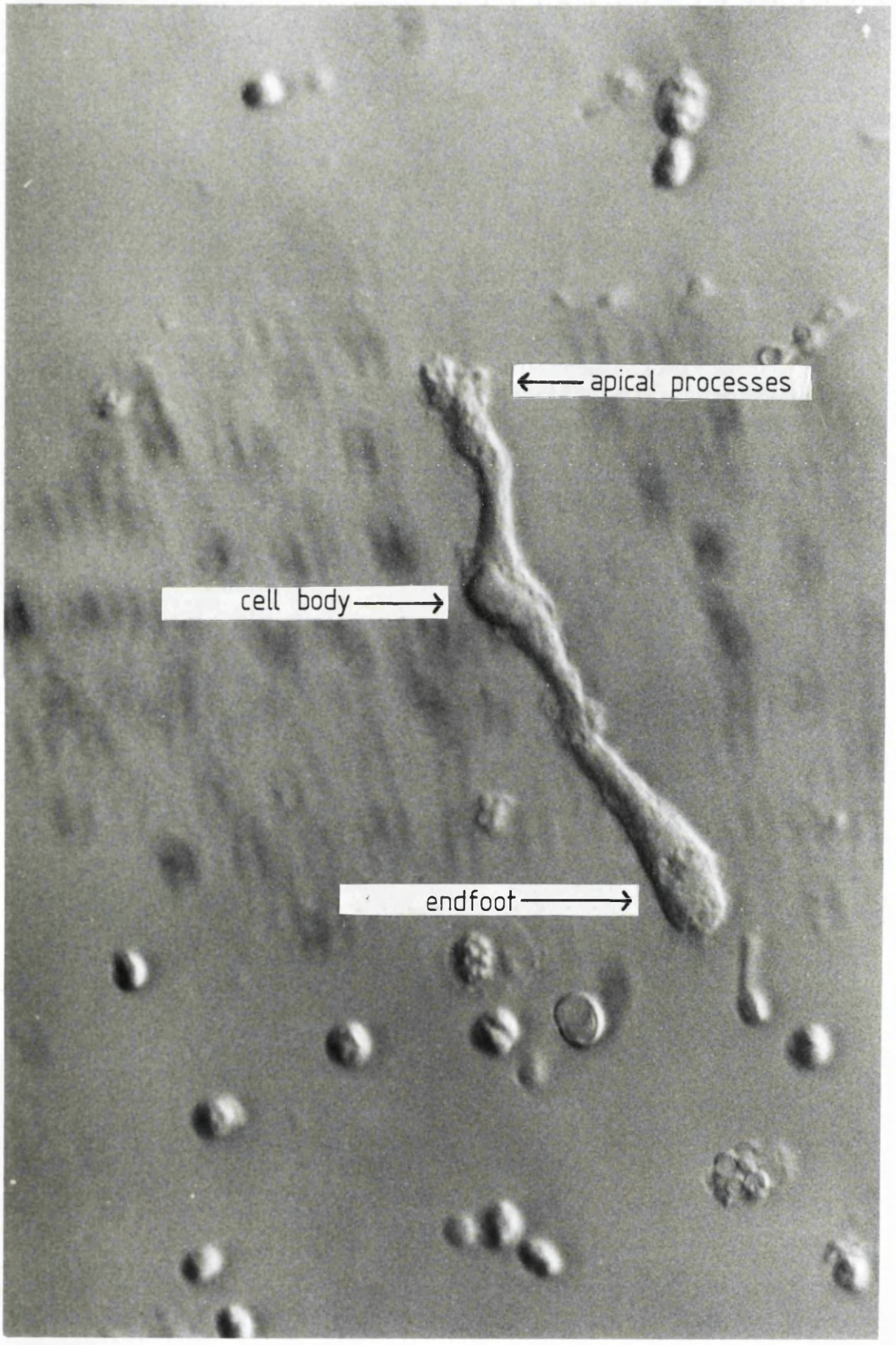
apical processes
cell body
endfoot

Table 2.1 External solutions: salamander cone photoreceptors

Solution RA is the standard Ringer's used, based on a recipe by Bader, Macleish and Schwartz (1979). Solution RB is standard Ringer's with 6mM barium added to it to block the resting potassium conductance of the cells (Newman, 1985). Solution C22, with approximately 22mM chloride, was used to test the chloride-dependence of the glutamate-induced current in isolated cones. Concentrations are in mM.

	RA **standard Ringer's**	**RB** **barium Ringer's**	**C22** **low external chloride**
NaCl	104.5	104.5	-
KCl	2.5	2.5	2.5
$CaCl_2$	3	3	3
$MgCl_2$	0.5	0.5	0.5
Glucose	15	15	15
HEPES	5	5	5
$BaCl_2$	-	6	6
Na-gluconate	-	-	104.5
NaOH	2	2	2

The pH of the solutions was 7.25.

In experiments on the intact retina, all external solutions contained 10μm bicuculline.

In solution C22, sodium chloride was replaced by sodium gluconate to give a final chloride concentration of 22mM.

Table 2.2 External solutions: salamander cone photoreceptors

Solutions Na60-NA2 in this table were used to study the sodium-dependence of the glutamate-evoked current in isolated cones. Solutions Na2, LCa and Na2/LCa were used to study the effect of low external calcium and sodium. Concentrations are in mM.

	Na60-Na2 low external sodium	**LCa low external calcium**	**Na2/LCa low external sodium and calcium**
NaCl	n	104.5	-
KCl	2.5	2.5	2.5
$CaCl_2$	3	0.1	0.1
$MgCl_2$	0.5	0.5	0.5
Glucose	15	15	15
HEPES	5	5	5
$BaCl_2$	6	-	-
Choline-Cl	104.5-n	-	104.5
Na_2EGTA	-	0.5	0.5
NaOH	2	2	2

The pH of the solutions was 7.25.

For solutions Na60-Na2, sodium was replaced with choline to give final sodium concentrations of 60, 25 and 2mM (i.e. n = 58, 23 and 0 respectively).

The free calcium concentration in solutions LCa and LCa/Na2 was 3 x 10^{-8}M.

Table 2.3 Internal solutions: salamander cone photoreceptors

Patch pipettes were filled with the solutions listed in the table below. Solutions C101, C30 and C9 were used to study the chloride-dependence of the glutamate-induced current in isolated cones; solution C16 was used for experiments in the intact retina. Concentrations are in mM unless otherwise indicated. Junction potentials are indicated, measured as described by Fenwick et al., 1982.

	C101	C30	C9	C16
$[Cl^-]$	101	30	9	16
KCl	80	9	-	-
K-acetate	15	86	95	100
K_2EGTA	5	5	5	5
NaCl	5	5	5	-
Na_2ATP	5	5	5	5
$CaCl_2$	1	1	1	1
$MgCl_2$	7	7	1	7
Mg-(acetate)$_2$	-	-	6	-
HEPES	5	5	5	5
Na_3GTP	-	-	-	1
cGMP	-	-	-	5μM
KOH	15	15	15	15
Junction potential (mV)	-3	-6	-7	-7

The pH of the internal solutions was 7.0.

The free internal calcium concentration was 1.3×10^{-7}M for all the above solutions.

In C30-C9 chloride was replaced by acetate to give chloride concentrations of 30, 16 and 9mM.

Table 2.4 External solutions: rabbit Müller cells

Solution RC is the standard Ringer's used. Solution RD is standard Ringer's with 6mM barium added to it to block the cells' resting potassium conductance. Solutions Na70-Na2 were used to study the sodium-dependence, and solutions K0-K70 the potassium-dependence of electrogenic uptake of glutamate.

	RC standard Ringer's	**RD** barium Ringer's	**Na70-Na2.5** low external sodium	**K0-K70** high external potassium
NaCl	140	140	n	70
KCl	2.5	2.5	2.5	x
Choline-Cl	-	-	140-n	70-x
$CaCl_2$	3	3	3	3
$MgCl_2$	0.5	0.5	0.5	0.5
Glucose	15	15	15	15
HEPES	5	5	5	5
$BaCl_2$	-	6	6	6
NaOH	2-2.5	2-2.5	2-2.5	2-2.5

The pH of the solutions was 7.4.

For solutions Na70-Na2, sodium was replaced by choline (n = 68, 33, 16, 7, 6, 0) to give final sodium concentrations of 70, 35, 18, 9, 8 and 2mM.

For solutions K0-K70 potassium was replaced by choline to give potassium concentrations of 70, 35, 20, 10, 2.5 and 0mM.

Table 2.5 Internal solutions: rabbit Müller cells

Patch pipettes were filled with solutions listed in the table below. Solution Q was the normal solution used to perfuse the inside of the cells. KQ140-KQ0 were used to study the effect of low internal potassium on the electrogenic uptake of glutamate.

	Q standard internal	KQ140-KQ0 low potassium internal
KCl	120	140-n
Choline-Cl	-	n
NaCl	5	-
K_2EGTA	5	-
Na_2EGTA	-	5
Na_2ATP	5	-
MgATP	-	5
$CaCl_2$	1	1
$MgCl_2$	7	2
HEPES	5	5
KOH	14	-
NaOH	-	14
Junction potential (mV)	-3	-3

The pH of the internal solutions was 7.2.

The free calcium concentration in the above solutions was 5.9×10^{-8}mM.

In solutions KQ140-KQ0 potassium was replaced by choline to give final potassium concentrations of 140 (control), 15 and 0mM.

barium (see Chapter 3, section 3.2 and Chapter 5, section 5.2). The concentration of free glutamate in the superfusion solutions will be reduced from its nominal value by binding to divalent cations. In the presence of Mg^{2+}, Ca^{2+} and Ba^{2+} the fraction of amino acid unbound is given by:

$$[\text{free amino acid}]/[\text{total amino acid}] = \frac{1}{(1+K_{Mg}[Mg]+K_{Ca}[Ca]+K_{Ba}[Ba])} \quad (1)$$

where K_{Mg} ($79.43M^{-1}$), K_{Ca} ($26.91M^{-1}$) and K_{Ba} ($19.05M^{-1}$) are the stability constants for divalent cations binding to glutamate (Martell and Smith, 1974). With $[Ca^{2+}]$=3mM and $[Mg^{2+}]$=0.5mM this fraction has the value of 89% in the absence of barium, and 81% in the presence of 6mM barium. Thus, the glutamate concentration in the external solutions is 9% less in solutions with barium compared to solutions containing no barium. For simplicity, the nominal concentrations of bath-applied glutamate have been quoted throughout this thesis. Barium has little effect on the glutamate-evoked current in cones (Chapter 3, Figure 3.1) or Müller cells (Chapter 5, Figure 5.1).

2.1.2.2 Iontophoresis

In experiments on isolated cells, pharmacological agents were often applied by iontophoresis. Iontophoretic electrodes (resistance around 30MΩ) were pulled on a Livingstone-type microelectrode puller (Narishige), from borosilicate glass with a microfilament insertion (Clark Electromedical Instruments, No. GC150TF10). Electrodes were connected via a platinum wire to the head stage of a recording amplifier equipped with a current pump system for iontophoresis.

Glutamate (sodium-L-glutamic acid, Sigma, G1626), glycine (Sigma, G7126) and GABA (γ-aminobutyric acid, Sigma, A2129) were dissolved in distilled water at the following concentrations and pH values: glutamate 1M, pH adjusted to 8 with NaOH; glycine 0.5M, pH 3 with HCl; GABA 0.5M, pH 3 with HCl. At pH 8 glutamate exists mainly as a negatively charged ion and was ejected with 40nA negative current. In experiments described in this thesis only the L isomer of glutamate was used and this will be referred to as glutamate hereafter. Both glycine and GABA were iontophoresed with a positive current (40nA). Between ejection pulses a backing current (+30nA for

glutamate and -30nA for glycine and GABA) prevented leakage of pharmacological agent out of the pipette. Iontophoresis and bath-perfusion of neurotransmitter candidates gave similar results.

Kainate was sometimes applied by pressure ejection from a pipette filled with Ringer's containing 10-100μM kainate (kainic acid, Sigma, K0250) in Ringer's. Between puffs the kainate-filled electrode was moved away from the cell.

2.1.2.3 Intracellular media

The various solutions used to fill patch pipettes for whole-cell recordings are given in Table 2.3 for experiments on cone photoreceptors, and in Table 2.5 for experiments on Müller cells. Included in those tables are the free calcium concentrations for the patch pipette solutions, calculated using the equilibrium constants for calcium binding to EGTA given by Martell and Smith (1974), and allowing for magnesium binding and the pH-dependence of the constants.

During whole-cell recording, small ions in the patch pipette solution diffuse into the cell within a few minutes. By using different pipette solutions, cells with different internal concentrations of ions such as potassium and chloride could therefore be studied.

2.1.3 Recording from cells

2.1.3.1 Whole-cell patch-clamp recording

The whole-cell variant of the patch-clamp technique (Hamill *et al.*, 1981) was used to study the effect of glutamate on cone photoreceptors (Chapter 3 and 4), light responses in cones in the intact retina (Chapter 3) and the electrogenic uptake of glutamate into Müller cells (Chapter 5). Patch pipettes were pulled on a BBCH puller (Mecanex, Geneva) from borosilicate glass with a microfilament insertion (Clark Electromedical Instruments, No.GC150TF10) and coated with Sylgard resin (Dow Corning) to reduce capacitive coupling between the pipette contents and the extracellular medium (Hamill *et al.*, 1981). Their resistance in Ringer's was about 15MΩ for clamping photoreceptors and about 4MΩ for clamping Müller cells. On some occasions thick-walled glass was used (Clark, No.GC150F10) which was not coated with Sylgard.

To obtain a whole-cell recording, a patch pipette was brought close to the cell membrane, and gentle suction was applied to the pipette resulting in the formation of a high resistance seal (in the GΩ range) between the patch pipette and the cell membrane. After forming a high resistance seal, a further pulse of suction produced a low resistance pathway into the cell. The cell could then be voltage-clamped, with the current being measured as the voltage drop across the 500MΩ resistance of a current to voltage converter (List Electronics, Darmstadt, F.R.G., L/M EPC-7). The indifferent electrode was an Ag/AgCl pellet placed in the recording chamber, except when the chloride concentration in the superfusion solution was altered, in which case a 4M NaCl agar bridge connected the bath to the Ag/AgCl pellet to avoid changes in electrode potential.

The series resistance in the pathway from the patch pipette to the cell was measured from the current response to a voltage-clamp step (section 2.1.4.2 and Figure 2.3). The series resistance was typically 18MΩ for photoreceptors and 5MΩ for Müller cells (these values are different because of the different size electrodes used). The series resistance sometimes changed during the course of an experiment and was therefore monitored frequently. The voltage error (series resistance x total current flowing) produced by the series resistance could be corrected for by subtraction from the nominal voltage-clamp potential. In most experiments the voltage error was less than 1mV and considered to be negligible.

Since the patch pipette and the bath contained different solutions, a junction potential exists at the tip of the pipette when it is in the solution prior to forming a seal. This was corrected for as described by Fenwick, Marty and Neher (1982). Junction potentials were measured by comparing the zero current voltage obtained when the pipette and the bath contained intracellular medium, to that obtained when the bath contained the extracellular medium used while forming a seal. During this procedure a 4M NaCl agar bridge connected the bath to the reference electrode to avoid changes in reference electrode potential. Junction potentials measured for various intracellular media relative to extracellular solutions are given in Tables 2.3 and 2.5.

2.1.3.2 Voltage-clamp quality

The non-spherical shape of photoreceptors and Müller cells raised the question of how uniform the potential was in these cells during voltage-clamp experiments.

(a) Voltage-clamp quality in isolated Müller cells

In order to address the question of voltage uniformity in isolated Müller cells, I treated the cell as an infinite uniform cable and assumed that the conductance was evenly distributed throughout the cell. With these assumptions (which are discussed below) the relation between the potential and distance from the voltage-clamping electrode is given by the equation:

$$V_x/V_o = e^{-x/\lambda} \qquad (2)$$

in which: V_x is the potential at a distance (x) from the electrode where the potential is V_o and λ is the electrical space constant and is the distance over which the potential declines to a fraction 1/e = 36.8% of its original amplitude V_o.

The value of λ is given by:

$$= (a.R_m/2R_i)^{1/2} \qquad (3)$$

in which: a = cell radius (m)

R_i = the specific cytoplasmic resistance of the cell (assumed to be 2 Ωm)

R_m = the specific membrane resistance of the cell = membrane resistance x membrane area (Ωm^2)

The membrane resistance of rabbit Müller cells is around 550MΩ when most of the potassium conductance is blocked by barium (as in most of the experiments carried out: Chapter 5, section 5.2). If the cell is assumed to be a cable (10μm in diameter and 100μm in length), with a membrane area ($2\pi aL$, L being the length of the cable) of 3141μm^2, the length constant according to equation 3 is

1469μm. Müller cells were always patch-clamped at the cell body which is situated roughly in the middle of the cell. Using equation 1, the voltage at the apical and basal end of the cell (50μm away) will be 3% less than in the cell body.

These figures for voltage non-uniformity in Müller cells are overestimated for the following reasons: (1) because I assumed an infinitely long cable, and hence an exponential decay of voltage, while in practice the cell is sealed at both ends; (2) the value taken for the membrane resistance (550MΩ) was actually a typical value for the input resistance of the cell, which represents the parallel combination of the membrane resistance and the seal resistance, i.e. $1/R_{input} = 1/R_{membrane} + 1/R_{seal}$. Since the seal resistance is not infinitely greater than the membrane resistance, the true membrane resistance must be larger then the input resistance, and so the length constant must be somewhat larger then that calculated above.

Thus, unless there is substantial non-uniformity of membrane conductance, the voltage-clamped rabbit Müller cell should essentially be uniform in potential.

(b) Voltage-clamp quality in isolated cones

As described in Chapter 3, the glutamate-evoked current in cones was isolated to the synaptic terminal. The maximum current that was recorded in a cone was 800pA. This consisted of a kainate-evoked current of 600pA and other currents (not gated by kainate) of 200pA, at -100mV. All glutamate-induced currents were less than half this size. For a "worst case" analysis of voltage uniformity I assumed that all the conductance was in the tip of the synaptic terminal. The synaptic terminal is about 2μm in diameter and 10μm long. Cones were always patch-clamped at the cell body which is 10μm away from the tip of the terminal. The total cytoplasmic resistance between the cell body and the synaptic terminal is R_C.

$$R_C = R_i \times L/A \qquad (4)$$

in which: R_i = the specific cytoplasmic resistance of the cell (2 Ωm)

L = the length of the terminal (10μm)

A = the cross-sectional area (πa^2, with a=1μm)

R_c is 6.4MΩ. A 800pA current across this resistor will drop 5mV, which is less than 10% of the command potential applied (60mV) to displace the cell from its resting potential (-40mV) to -100mV. For glutamate-evoked (rather then kainate-evoked) currents this figure will be at most 5%, since the maximum evoked current recorded in cones was 400pA, but in most cases much less.

The above calculation shows that the voltage-clamped isolated cones are practically voltage-uniform. I have only considered the voltage-uniformity in the cone synaptic terminal. It has been shown that rods and cones are voltage-uniform across the rest of the cell at potentials below -35mV (Attwell and Wilson, 1980; Attwell, Werblin and Wilson, 1982).

2.1.4 Data acquisition and analysis

All experimental records were stored on magnetic tape on a RACAL store 4DS tape recorder, or on video tape. For analysis, current traces could be fed into a computer (PDP 11/73) via an analogue-to-digital converter (Cambridge Electronic Design, 502, 12-bit), and numbered in blocks and stored for analysis if necessary. Data were plotted using a Hewlett Packard plotter (model 7470A).

2.1.4.1 Noise analysis

Noise in the membrane current (in voltage-clamp) is produced by random opening and closing of ion channels in the cell membrane. When a neurotransmitter is applied to a cell at a non-saturating dose, channels activated by the ligand will open and close, and the noise in the current trace will increase. (At a saturating dose the ligand-activated channels will be permanently open and the noise will not increase). Analysing the amount of noise in a current induced by a pharmacological agent can therefore give information about whether this current is as a result of ions flowing through channels, or whether an electrogenic carrier mechanism (which generates much less noise) has been activated. Noise analysis can also be used to obtain information about single channel currents, without the need to record from single channels. The amount of noise at different frequencies can also be analysed to give information on

the number of different states a channel can exist in. The computer programs used for noise analysis were provided by Prof. David Colquhoun and modified by Dr. Marc Tessier-Lavigne.

For the analysis of current noise, samples of data (10-160 seconds long) were fed into the computer after being filtered. On one channel the signal was sampled after low-pass filtering (usually 1000Hz) (8-pole Butterworth, Bar and Stroud EF5-01 filter), to make sure that there are no components of the signal at frequencies higher than half the computer sampling frequency (2048Hz), which may give problems due to aliasing (high frequency components appear to have a lower frequency due to sampling too infrequently). Before sampling on a second channel, the low-pass filtered signal was also high-pass filtered (EF5-02 filter). This removed the component of current change induced by the drug, but not the components of current noise at frequencies above the cut-off of the filter (usually 2Hz). This allowed greater amplification of the signal for noise analysis.

After sampling the signal was edited, and undesirable stretches of data could be removed. During editing the record was broken up into subsamples of periods equal to 1/(resolution frequency). Choosing the resolution frequency was a compromise because: information about noise at frequencies below the resolution frequency is lost, but a higher resolution frequency means that there are more data samples to average over, which gives a smoother power spectrum (see below).

For each subsample the mean current flowing was calculated from the data that were low-pass filtered, while the low and high-pass filtered data were used to calculate the variance of the current noise fluctuations about the mean current. The variance for each data segment could be plotted as a function of time, or as a function of the mean current flowing during the corresponding data segment. If the variance as a function of mean current is a straight line, the open probability of the channel is low (Colquhoun and Hawkes, 1977). Assuming that there is only one type of channel gated by the transmitter, the slope of the line is the single channel current.

The value for single channel current, i, was corrected for loss of variance due to low and high-pass filtering, and from this

corrected value the single channel conductance, g, could be calculated:

$$g = i/(V-V_{rev}) \qquad (5)$$

in which: V = holding potential

V_{rev} = the reversal potential of the current through the channel

High-pass filtered stretches of data from steady state currents before and during drug application were used to obtain power spectra (using Fourier transforms to dissect the current fluctuations into sine waves of different frequency) to determine the amount of power at each frequency. Subtracting the power spectra obtained before and during drug application, gave a net spectrum of the change in noise produced by a drug. Analyzing the amount of noise at different frequencies can give information on the number of different states a channel can ex ist, by fitting the net power spectrum with Lorentzian components of the form (Colquhoun and Hawkes, 1977):

$$G(f) = G(0)/(1 + (f/f_c)^2) \qquad (6)$$

in which: G(f) = noise variance at frequency f

f_c = the half power frequency at which G(f) falls to half of G(0)

G(0) = noise variance at f = 0

2.1.4.2 Measurement of capacitance and series resistance when whole-cell patch-clamping

The membrane capacitance (C), and the series resistance at the mouth of the patch pipette (R_p), were measured from the current response to a 10mV voltage-clamp step from a holding potential near to the zero current potential. At this potential there is little contribution of voltage-gated currents. The cell can be treated as the parallel combination of a capacitor and a resistor, R_{in}, where R_{in} is the parallel combination of the cell membrane resistance, R_m, and the resistance of the seal between the electrode and the cell, R_{seal}, (Figure 2.3). The time course of the change in current in

Figure 2.3 Analysis of cell capacitance, C, and pipette resistance, R_p.

A. Current flow in response to a 10mV depolarization (bottom trace) from an isolated rabbit Müller cell at holding potential of -40mV. The inset shows the current used for analysis of the capacity transient. R_{in} represents the parallel combination of the cell resistance and the resistance of the seal between the patch pipette and the cell. The resting potential of the cell, which could be represented in this circuit by a battery, is omitted for simplicity. The current does not rise instantaneously at t=0 as predicted by equation (7), because of filtering by the tape recorder.

B. Semi-logarithmic plot of the decay of current in A to its steady value (I_∞). For this cell the series resistance was 5MΩ, the capacitance was 100pF and the cell input resistance was 112MΩ.

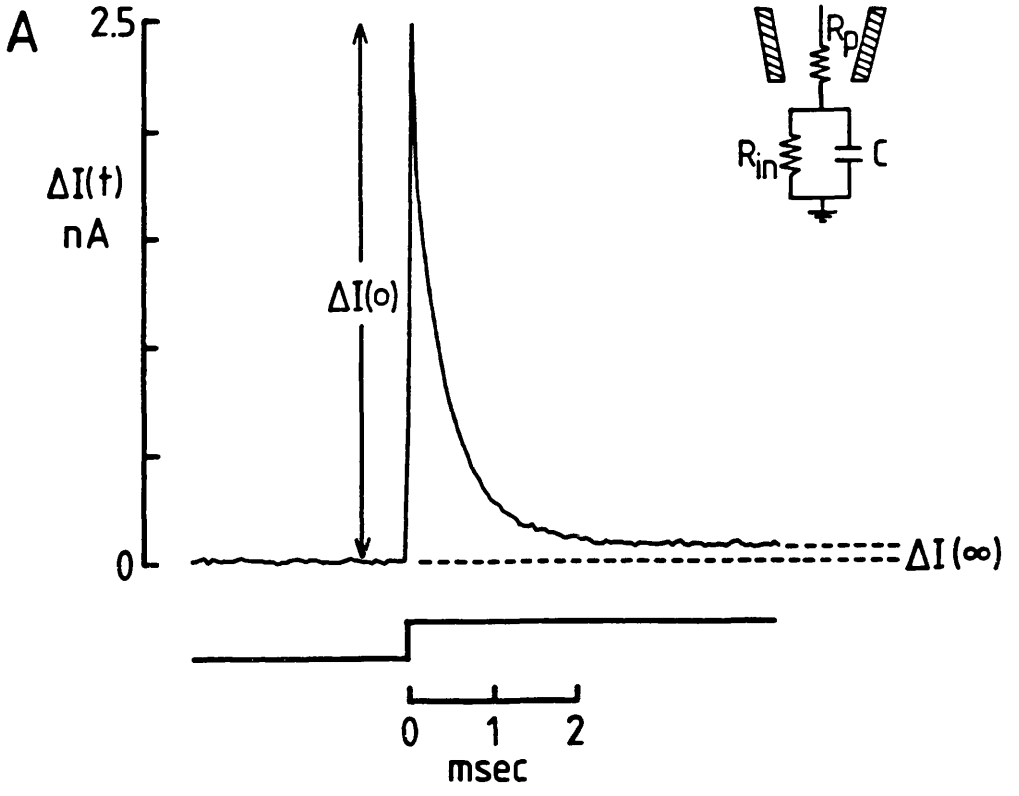
A
2.5
ΔI(t)
nA
0
ΔI(o)
ΔI(∞)
R_p
R_{in}
C
0
1
2
msec

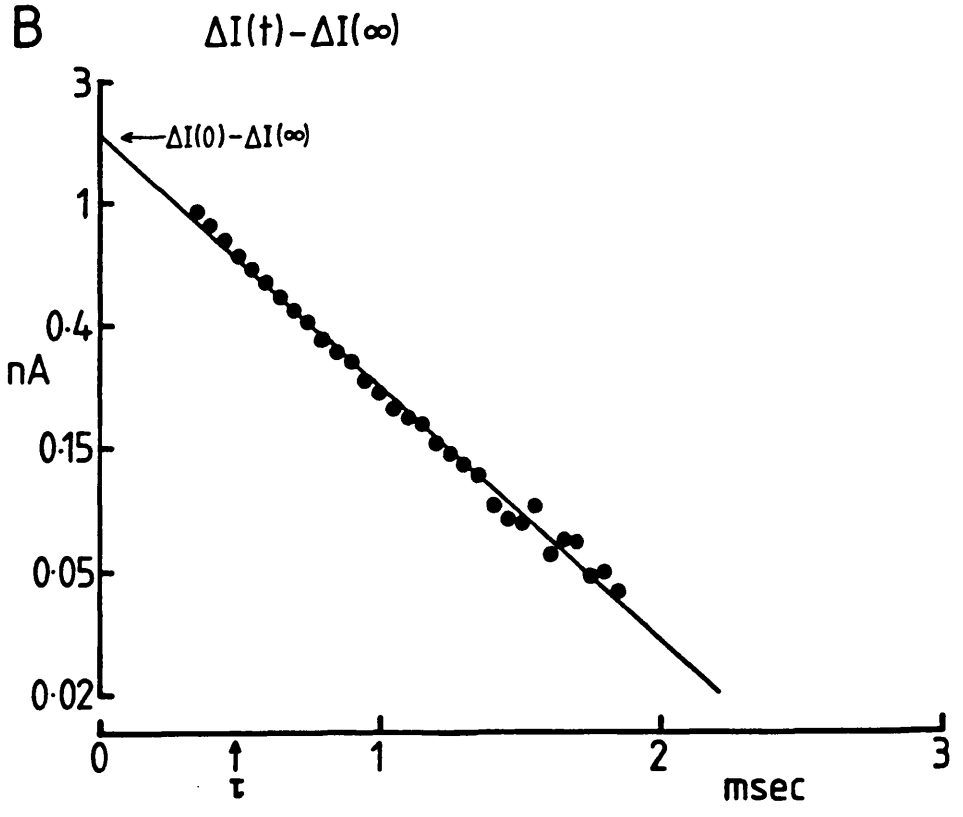
B
ΔI(t)-ΔI(∞)
3
1
0·4
nA
0·15
0·05
0·02
←ΔI(0)-ΔI(∞)
0
τ
1
2
3
msec

response to a voltage-clamp step is predicted (Tessier-Lavigne et al., 1988) to have the waveform:

$$\Delta I_{(t)} = V/(R_{in} + R_p) \times (1 + (R_{in}/R_p)e^{-t/T}) \quad (7)$$

where t = time after application of the voltage-clamp step
V = amplitude of the step (10mV)
T = the decay time constant of the transient

$$T = CR_{in}R_p/(R_{in} + R_p) \quad (8)$$

Thus, the current amplitude at t = 0 (obtained by semi-logarithmic extrapolation) is:

$\Delta I(0) = V / R_p$ allowing the calculation of R_p

The steady state current is:

$\Delta I(\infty) = V/(R_{in} + R_p)$ allowing the calculation of R_{in}.

The membrane capacitance can then be calculated from the time constant of the current relaxation as:

$$C = T(R_{in} + R_p)/R_{in}R_p \quad (9)$$

The computer programs used to analyse capacity transients were written by Dr. Peter Mobbs. Figure 2.3 shows an example of a capacity transient used for calculating R_{in}, R_p, C and T. The semi-logarithmic plot of the decay of the transient was approximately linear (Figure 2.3) for all cells studied, consistent with the treatment of the cell as a lumped resistor and capacitor in parallel. For isolated salamander cones, the time constant of the decay of the transient (T) in cones was generally around 0.25ms, but varied from 0.12 to 0.61ms, in cells with capacitances varying from 13 to 30pF and R_{in} varying from 100 to 900MΩ. In cones in the intact retina, with no glutamate being released (in the light), and in the presence of bicuculline to block the effect of GABA released onto cones from horizontal cells, the values were: T=1.3 ±0.5 (s.d.) ms,

mean of 7 cells; C=118 ±23pF; and R_{in}=136 ±69MΩ. These values differ from those in isolated cells (higher T, higher C and lower R_{in}), because cones in the intact retina have more intact outer segments (which contribute most of the cones capacitance), and because there is weak electrical coupling between cones and rods in the intact retina (decreasing R_{in}), and possibly because the enzyme used for cell isolation digested some channels out of the membrane. For rabbit Müller cells T was around 0.65ms, varying from 0.16 to 1.1ms, in cells with capacitance varying from 40 to 100 pF, and R_{in} varying from 100 to 1100MΩ. Average frequencies of filtering of the current by the combination of R_p and the cell capacitance (C) are around 350Hz for isolated rabbit Müller cells and around 740Hz for isolated salamander cones.

2.2 Injection of Müller cells with HRP and processing for electron microscopy

2.2.1 Preparation of an isolated retina mounted receptor side downwards

This preparation was used to provide anatomical information concerning the relationship between Müller cell processes and synaptic terminals of photoreceptors. In order to identify the Müller cell processes that wrap around the photoreceptors, Müller cells were injected with HRP. Experiments were carried out on retinae from larval tiger salamanders (Ambystoma tigrinum).

The first step involved obtaining an isolated eyecup as described in section 2.1.1.1. Only retinae from freshly killed animals were used. An isolated retina preparation was made as described in section 2.1.1.2, except that in this case the retina was mounted with the photoreceptor side downwards (to allow injection of a Müller cell with HRP from the vitreal end of the cell without damaging the photoreceptor end, the anatomy of which was to be investigated in detail). To achieve this the retina was carefully removed, under Ringer's (solution RA, Table 2.1), after the eyecup was cut into quarters. The pieces of retina were transferred to the recording chamber with a cut-off fire-polished Pasteur pipette. The pieces of retina were positioned over the glass windows (section 2.1.1.2) with the photoreceptors facing downwards, and the overlapping tissue was pressed into the filter paper to keep the

tissue in place.

The recording chamber was transferred to a microscope with a fixed stage, fitted with Hoffman modulation contrast optics. Sufficient light could be passed through the glass windows and the flatmounted retina to distinguish the vitreal surface. Müller cell endfeet form a nearly continuous layer over which ganglion cell axons lie, running towards the optic nerve. Focussing deeper it was possible to check that the retina was intact, including the photoreceptor layer, in the area were a Müller cell was going to be injected.

2.2.2 Microinjection of Müller cells with HRP

Microelectrodes were pulled on a Livingstone-type horizontal microelectrode puller (Narishige) from borosilicate glass with a microfilament insertion (Clark Electromedical Instruments, No. GC150TF10). For intracellular recording and injection, electrodes were filled with 1µl 5% HRP (peroxidase from horseradish Sigma, P-8375) in 0.1M tris/0.2M KCl pH 7.6 (Snow, Rose and Brown, 1976), and backfilled with 3M potassium acetate. Electrodes usually had resistances in the range 200-300MΩ in Ringer's.

Electrodes were connected via a Ag/AgCl wire to the head stage of a recording amplifier equipped with a current pump system. To microinject a Müller cell, an electrode was positioned so as to just touch the cell's endfoot, and with a gentle tap on the headstage the electrode was inserted into the cell (the identity of which was confirmed by its membrane potential, between -80 and -90mV). HRP was injected into the cell by passing 1-2nA depolarizing current pulses (50% duty cycle) for 1-3 minutes. The amplitude of the injection current and the membrane potential were monitored on an oscilloscope. If the membrane potential, measured between current pulses, became more depolarized than -75mV, or the electrode was not passing the current properly, injection of HRP was stopped. The HRP was later found to be distributed throughout the whole of the Müller cells (as observed in the electron microscope). The mechanism by which this occurs is not known but it is probably by diffusion, although an active transport mechanism may also exist. Spread of HRP from the injection site in the endfoot to the photoreceptor end of the cell (100µM away) was necessary to allow me to investigate the

anatomy of the Müller cell processes around the photoreceptor synapse. Müller cells are electrically coupled, but since HRP does not travel through gap junctions, only one Müller cell in each injection site was filled with HRP. 1 or 2 Müller cells were injected in each quarter of retina during the course of 1 hour.

2.2.3 Fixation of tissue and HRP histochemistry

Following injection, the recording chamber containing the retina was flooded with primary fixative (1% paraformaldehyde and 2.5% glutaraldehyde with 3% sucrose in 0.066M sodium phosphate (Sörensen) buffer at pH 7.4. Paraformaldehyde was freshly prepared the previous day by dissolving paraformaldehyde in distilled water at 60°C and stirring, followed by adding a few drops of 1N NaOH until the solution cleared. During fixation the tissue was eased off the bottom of the dish to improve the penetration of the fixative. The retina was fixed at room temperature for 30 minutes and then placed in fresh fixative in a refrigerator (5°C) for another 85 minutes. After fixation the tissue was washed in two 10 minute washes in the buffered sucrose mixture, followed by a 10 minute wash in 0.1M cacodylate buffer pH 7.4.

(Tissue which was only going to be examined under a light microscope was fixed in 2.5% glutaraldehyde in buffer. In some experiments, in which the aim was to look at the morphology of retinal tissue which did not contain an HRP injected cell in the electron microscope, the fixative used was 2.5% glutaraldehyde/1% OsO_4 in buffer. In these cases the tissue was not post-fixed in OsO_4 (section 2.2.4)).

HRP was visualized using a histochemical procedure based on oxidizing Hanker-Yates reagent (p-phenylenediamine-pyrocatechol (PPD-PC)), which results in a brownish-black reaction product. The pieces of retina were treated as follows: preincubated in 0.15% Hanker-Yates reagent (Sigma, No. H7507) in cacodylate buffer for 10 minutes; washed in cacodylate buffer for 5 minutes; incubated in 0.15% Hanker-Yates reagent in cacodylate buffer, with 0.05% hydrogen peroxide added immediately before use, for 5 minutes; washed in cacodylate buffer for two times 5 minutes. At this stage the Müller cells containing HRP could be clearly identified in the pieces of retina under a dissection microscope (magnification x10).

2.2.4 Processing for electron microscopical analysis

Following histochemical staining, the tissue was processed for EM as follows. Each piece of retina was processed individually in stoppered vials on a tissue rotator for stages a-g.

a) Post-fixation in 1% OsO_4 in cacodylate buffer for 85 minutes.
b) Wash in cacodylate buffer; two changes of 10 minutes each.
c) Wash in distilled water; two changes of 5 minutes each.
d) Dehydration in a graded series of ethanol (50%, 70%, 90%, 100% x 2) for 10 minutes each.
e) Propylene oxide; two changes of 5 minutes.
f) Infiltration with propylene oxide / resin mixture (1:1) overnight.
g) Fresh resin (Epon 812); two changes of 4 hours.
h) Orientation of tissue in resin in block moulds and polymerization at 60°C overnight.

The epon blocks were cut into 30µm sections on a American Optical microtome with a steel knife. The sections were mounted in liquid epon and examined under a Leitz microscope with a x40 lens and x10 eyepieces. A sketch was made of the sections that contained the Hanker-Yates reagent reaction product, marking the place of the injected Müller cell, or a photograph was taken (Ektachrome 400 film). These sections were reembedded in fresh epon in embedding capsules (TAAB), and polymerized again at 60°C overnight.

2.2.5 Sectioning and staining

Epon blocks were trimmed and 1µm sections were cut on a (Reichert Ultracut or Reichert OMU3) microtome with a glass knife (LKB Knifemaker) until fragments of stained Müller cell process were present in the sections. Serial sections (around 60-90nm) were then cut with a diamond knife. Sections were floated on double distilled water and flattened with chloroform vapour. The sections were picked up onto slot grids (Agar Aids, Athene 6220T7) that were coated with formvar, covered with evaporated carbon (Edwards vacuum coater, Model E12E4) and stained with 1.5% uranylacetate in distilled water for 30 minutes and Reynolds lead stain for 7 minutes. Sections were viewed in a transmission electron microscope (Jeol 100CX).

Chapter 3
Glutamate-induced current in cone photoreceptors

3.1 Introduction

This chapter describes experiments showing that application of glutamate evoked a current in cone photoreceptors, and characterizing some of the properties of the glutamate-induced current. Experiments were performed on isolated cone photoreceptors and cones in isolated, intact retinae. The results of the experiments described in this chapter are dealt with under the following headings:

(1) Voltage-dependence of the glutamate-induced current in isolated cones. (2) Dependence of the glutamate-induced current on external glutamate concentration. (3) The effect of glutamate analogues. (4) Noise analysis of glutamate- and kainate-induced currents. (5) The effect of a blocker of glutamate uptake. (6) Spatial localization of the glutamate-induced current. (7) The glutamate-induced current in cones in the intact retina. (8) Light response in cones in the intact retina.

The next chapter (Chapter 4) deals with the ionic basis of the glutamate-induced current in isolated cone photoreceptors. The implications of the results are described in the Discussion (Chapter 7).

3.2 Methods

All experiments described in this chapter were performed on cones from the tiger salamander retina. The experiments described in sections 3.3.1 to 3.3.6 were carried out on single and double cones that were isolated by enzymatic dissociation of the retina (Chapter 2, section 2.1.1.1). Experiments in section 3.3.7 and 3.3.8 were performed on cones in isolated, intact retinae that were flatmounted photoreceptor side upwards (Chapter 2, section 2.1.1.2). The currents induced by glutamate (or light, section 3.3.8) were studied using the whole-cell variant of the patch-clamp technique. In all the figures inward current is shown downwards. Patch pipettes contained solution Cl01 (Table 2.3) for experiments on isolated cones, and solution Cl6 (Table 2.3) for experiments on the intact retina. Glutamate was applied by iontophoresis or by bath-perfusion.

The external solutions were Ringer's or Ringer's containing 6 mM barium (solution RA and RB, Table 2.1 respectively). Adding barium greatly reduced current noise fluctuations without affecting the glutamate-induced current. Figure 3.1 shows the glutamate-evoked current in a isolated cone voltaged-clamped at -53mV, bathed first in normal Ringer's (A) followed by bathing in Ringer's containing 6 mM barium (B). The reduction in current noise produced by barium made it much easier to detect glutamate-induced currents, especially when these currents were small around and above the reversal potential. Barium is known to block potassium channels in glial cells (Newman, 1985) which may account for some of the reduction in current noise. However, adding barium may also modulate the seal resistance which could account for reduction in current noise, and for an outward shift in the current baseline sometimes observed at -40mV. When patch-clamping cones in the intact retina, the Ringer's solution contained 10μM bicuculline.

3.3 Results

3.3.1 Voltage-dependence of the glutamate-induced current in isolated cones

Application of glutamate increased the membrane conductance of isolated cones. With 101mM chloride in the patch pipette (solution Cl01, Table 2.3), glutamate evoked an inward current at the cone dark potential (-40mV). When glutamate was applied by iontophoresis, which produced a near maximum response (section 3.3.6), the current evoked at -40mV was typically 10-20pA, but sometimes as large as 60pA. In Figure 3.2A are the responses to glutamate, applied by iontophoresis to a voltage-clamped cone, held at potentials that are shown by each trace. At -34mV (near the cell dark potential) glutamate induced an inward current of 50pA. This current was larger when the cell was held at more negative potentials. Above -34mV the inward current became smaller and reversed at 0mV. Outward currents were larger when the cell was held at more positive potentials.

In Figure 3.2B the peak glutamate-induced currents from the cell in A are plotted as a function of membrane potential. The dependence of the current on voltage shows inward rectification around the reversal potential. The data in Figure 3.2 were from half of a double cone. Similar results were obtained from single cones.

Figure 3.1 Barium has little effect on the glutamate-induced current in isolated cones.

A. Glutamate-induced current in half of an isolated double cone, voltage-clamped at -53mV, by iontophoresis of glutamate. The patch pipette contained solution C101 (Table 2.3) and the external solution was Ringer's (solution RA, Table 2.1). Timing of iontophoresis is shown by the bottom trace.

B. Glutamate-induced current in the same cell as in A, at the same voltage, but now the external solution was Ringer's containing 6mM barium (solution RB, Table 2.1).

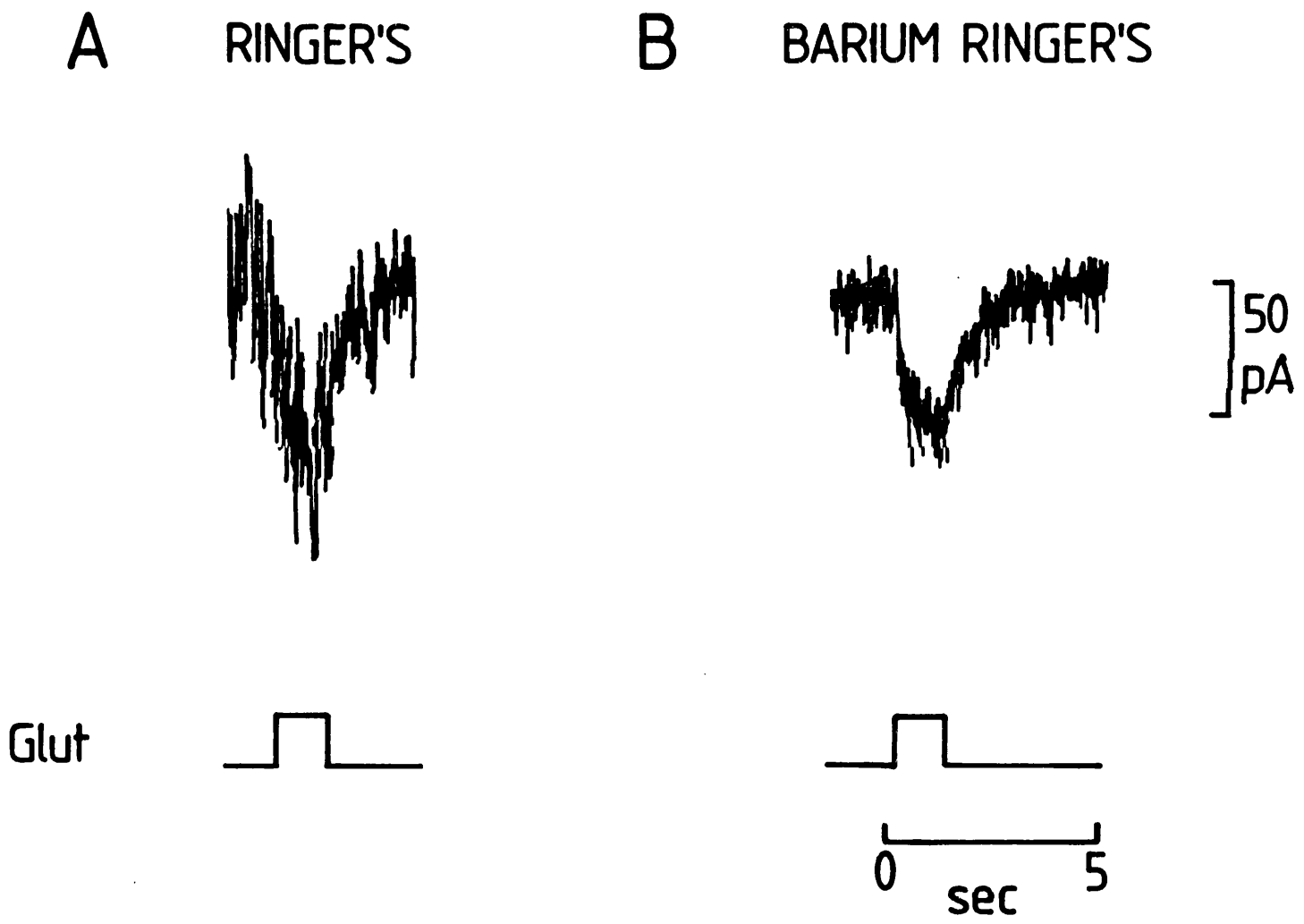
A
RINGER'S
B
BARIUM RINGER'S
50
pA
Glut
0
sec
5

Figure 3.2 Voltage-dependence of the glutamate-induced current in cones.

A. Changes in membrane current of an isolated, voltage-clamped half of a double cone in response to iontophoresis of glutamate (membrane potential shown alongside each trace). Timing of iontophoresis is shown by the square trace below the current traces. The patch pipette contained solution C101 (Table 2.3). The extracellular solution was Ringer's containing 6mM barium (solution RB, Table 2.1).

B. Peak glutamate-induced currents (ordinate) as a function of membrane potential (abcissa) for the experiment in A plus data at other potentials recorded from the same cell.

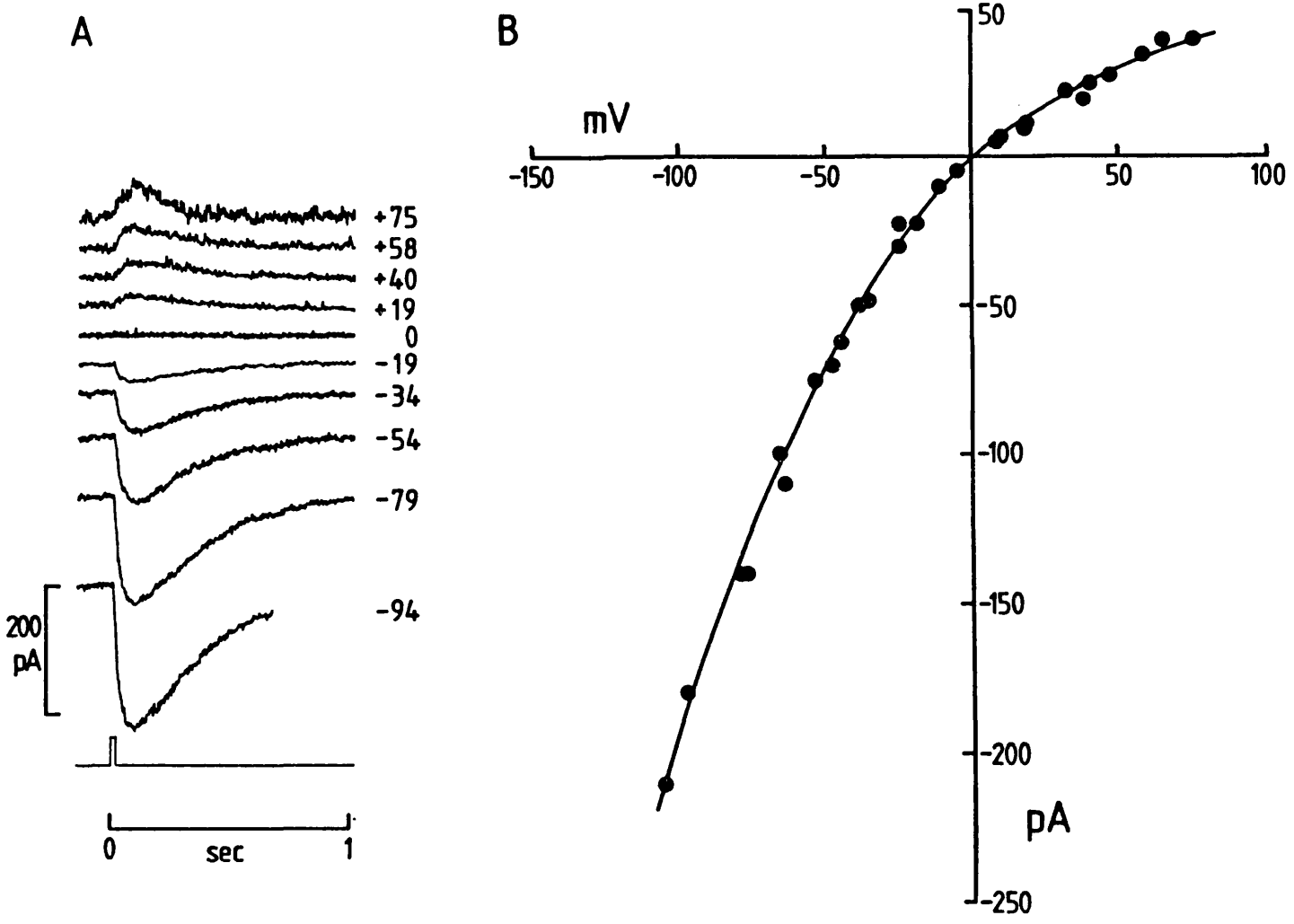
A
+75
+58
+40
+19
0
-19
-34
-54
-79
-94
200
pA
0
sec
1
B
mV
50
-150
-100
-50
50
100
-50
-100
-150
-200
pA
-250

3.3.2 Dependence of the glutamate-induced current on external glutamate concentration

Part A of Figure 3.3 shows the current flowing across the membrane of a cone held at -63mV, during the sequential application, by bath-perfusion, of solutions containing different concentrations of glutamate. A significant current was activated by 1μM glutamate (-37pA) and the currents became larger with higher glutamate concentrations up to 100μM (-77pA). Part B of Figure 3.3 shows the normalized dose-response curve from the data in A. The curve through the points is a Michaelis-Menten relation having the form:

$$I/I_{max} = [\text{glutamate}]/([\text{glutamate}] + K_m) \qquad (10)$$

The K_m was obtained from a Lineweaver-Burke plot, in which 1/I was plotted against 1/[glutamate] and where $-1/K_m$ is the intercept on the 1/[glutamate] axis. For the data in A the K_m calculated in this way was 1.0μM. The approximate fit of the Michaelis-Menten relation to the data in Figure 3.3B suggests that the current may depend on the binding of a single glutamate molecule for its activation (although more data at submicromolar glutamate doses are needed to convincingly rule out the possibility that the curve has a sigmoid onset, reflecting the binding of more than one glutamate anion). The low value of K_m indicates that glutamate binds to its receptor with a high apparent affinity.

In order to investigate whether the membrane potential affected the dose-response curve, glutamate-induced currents from a single cell were plotted against external glutamate concentration (Figure 3.4A) for different holding potentials (given to the right of each trace). The curves through the points were drawn by eye, and their shape looks similar at different holding potentials. Figure 3.4B shows the same data, after the currents were normalized to the maximal response at each voltage. The curve through the points is a Michaelis-Menten relation with a K_m of 1.4μM (as obtained from a Lineweaver-Burke plot of the data for -42mV).

In Figure 3.4C the K_m, obtained from Lineweaver-Burke plots for the data at different potentials (Figure 3.4A), is plotted against voltage. The K_m was 1.0, 1.4 and 1.6μM at -62, -42 and +28mV repectively, suggesting a slight reduction of affinity at positive

Figure 3.3 Dose-response of glutamate-induced currents in cones.

A. The currents induced in an isolated single cone voltage-clamped at -63mV, by sequential superfusion with barium Ringer's (solution RB, Table 2.1) containing different concentrations of glutamate (shown by the bar below the current trace). Solution Cl01 was used to fill the patch pipette.

B. The normalized dose-response curve from the data in A. The currents at each dose were normalized to the current in 100μM. The curve through the points is a Michaelis-Menten relation with a K_m = 1.0μM (as obtained from a Lineweaver-Burke plot).

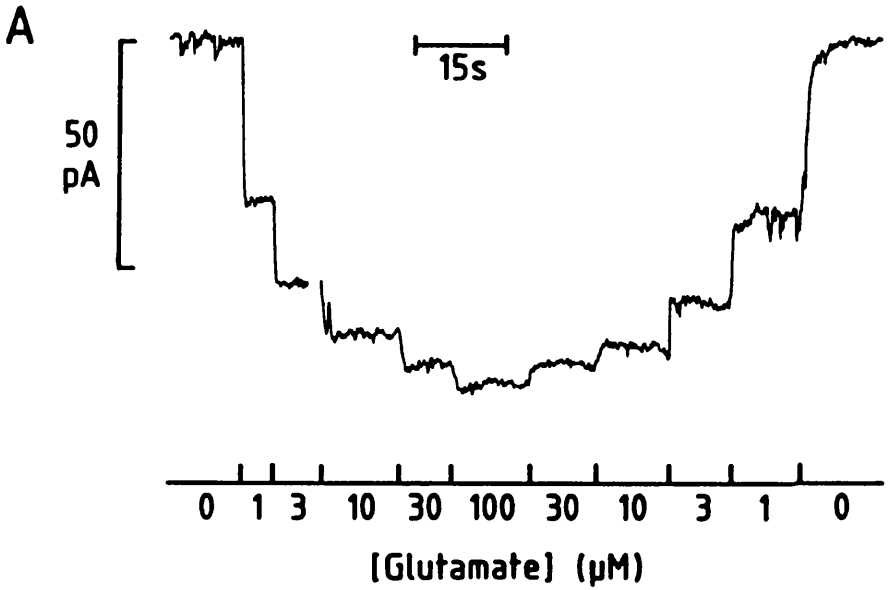
A
15s
50
pA
0 1 3 10 30 100 30 10 3 1 0
[Glutamate] (μM)

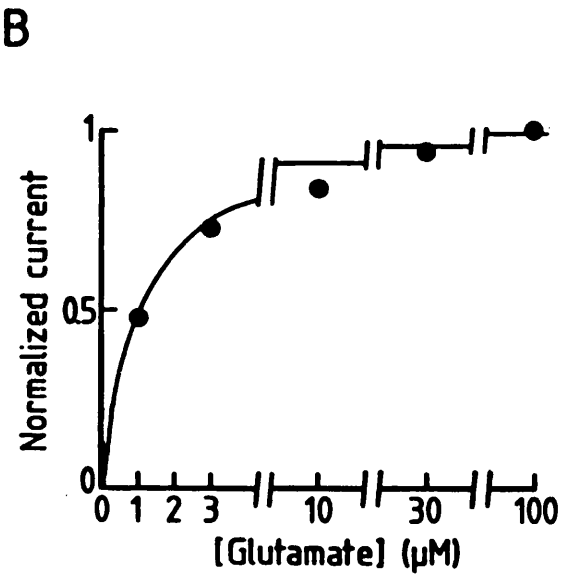
B
Normalized current
1
0.5
0
0 1 2 3 10 30 100
[Glutamate] (μM)

Figure 3.4 Voltage-dependence of the glutamate dose-response curve in cones.

A. Data, such as in Figure 3.3A, from an isolated single cone held at -62, -42 and +28mV. At each potential a range of glutamate concentrations in barium Ringer's was applied to the cell, and the resulting currents were plotted against glutamate concentration. At -62 and -42mV the currents were inward, at +28mV the currents were outward. The curves through the points were fitted by eye.

B. Normalized dose-response curve obtained from the data in A. The currents evoked by 100μM glutamate were -63pA at -42mV, -93pA at -62mV and +24pA at +28mV. The curve through the points is a Michaelis-Menten relation with K_m = 1.4μM (as obtained from a Lineweaver-Burke plot of the data for -42mV).

C. Values of K_m for the data in A, calculated from Lineweaver-Burke plots, plotted against the holding potential.

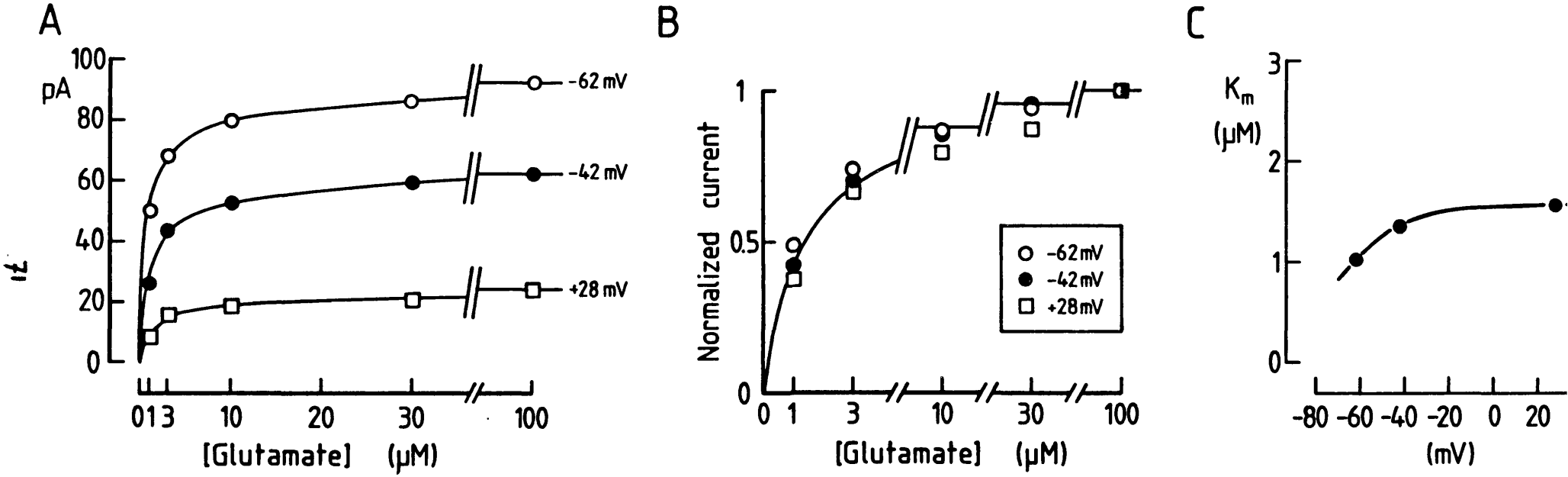
A
pA
100
80
60
40
20
0
-62 mV
-42 mV
+28 mV
0 1 3 10 20 30 100
[Glutamate] (μM)
B
Normalized current
1
0.5
0
-62 mV
-42 mV
+28 mV
0 1 3 10 30 100
[Glutamate] (μM)
C
K_m
(μM)
3
2
1
0
-80 -60 -40 -20 0 20
(mV)

potentials. In two other cones, Lineweaver-Burke plots gave K_m values of 2.6 and 5.5μM at -43mV.

3.3.3 The effect of glutamate analogues

In order to determine the pharmacological properties of the glutamate-induced current, analogues which act relatively specifically on the various subtypes of glutamate channels were applied to isolated cones by bath-perfusion. N-methyl-D-aspartate (NMDA) and quisqualate were applied at concentrations of 10, 30 and 100μM to cells that were voltage-clamped at -43 to -53mV. NMDA and quisqualate did not produce a response at any of the concentrations applied, in cells that did respond to glutamate (n=7 cells). Kainate produced responses that were larger than those produced by glutamate in the same cell and at the same holding potential. At -53mV, the currents evoked by 30μM glutamate and kainate had relative magnitudes 0.45:1 (mean data from 2 cells). Figure 3.5 shows currents evoked by 30μM glutamate, kainate, NMDA and quisqualate in a cone voltage-clamped at -53mV. The glutamate-induced inward current is 17pA while kainate produces a 37pA response.

Kainate-induced currents in cones had the same current-voltage relation as those induced by glutamate. Figure 3.6 shows data for a cone to which 10μM kainate was applied by pressure ejection. At -40mV kainate produced a 100pA inward current, the current reversed at -8mV and showed inward rectification around the reversal potential. Similar current-voltage relations were obtained with 1 μM kainate applied by pressure ejection. When applied by pressure ejection at -40mV, 1μM kainate induced currents of 18 ±9.7 (s.d.) pA in 6 cells, and 10μM kainate 53 ±53 pA in 5 cells.

3.3.4 Noise analysis of glutamate- and kainate-induced currents

The clear reversal potential shown by the current evoked by glutamate and kainate implies that at least some of the current is produced by ion channels being opened. In this section I will assume for simplicity that all the current is generated by ion channels and none by electrogenic glutamate uptake (section 3.3.5 and Chapter 7, section 7.1.2). By analysing the noise in the current induced by a drug, it was possible to gain information on the properties of the channels involved. Data were fed from tape into the computer for

Figure 3.5 Currents induced by glutamate and its analogues in cones.

The currents induced by 30μM concentrations of glutamate (Glu), kainate (KA), N-methyl-D-aspartate (NMDA) and quisqualate (Quis). Recordings were made from half of an isolated double cone, voltage-clamped at -53mV. Drugs were added to Ringer's (solution RA, Table 2.1) and applied by bath-perfusion. Timing of drug application is shown by the bars. The patch pipette contained solution C101 (Table 2.3).

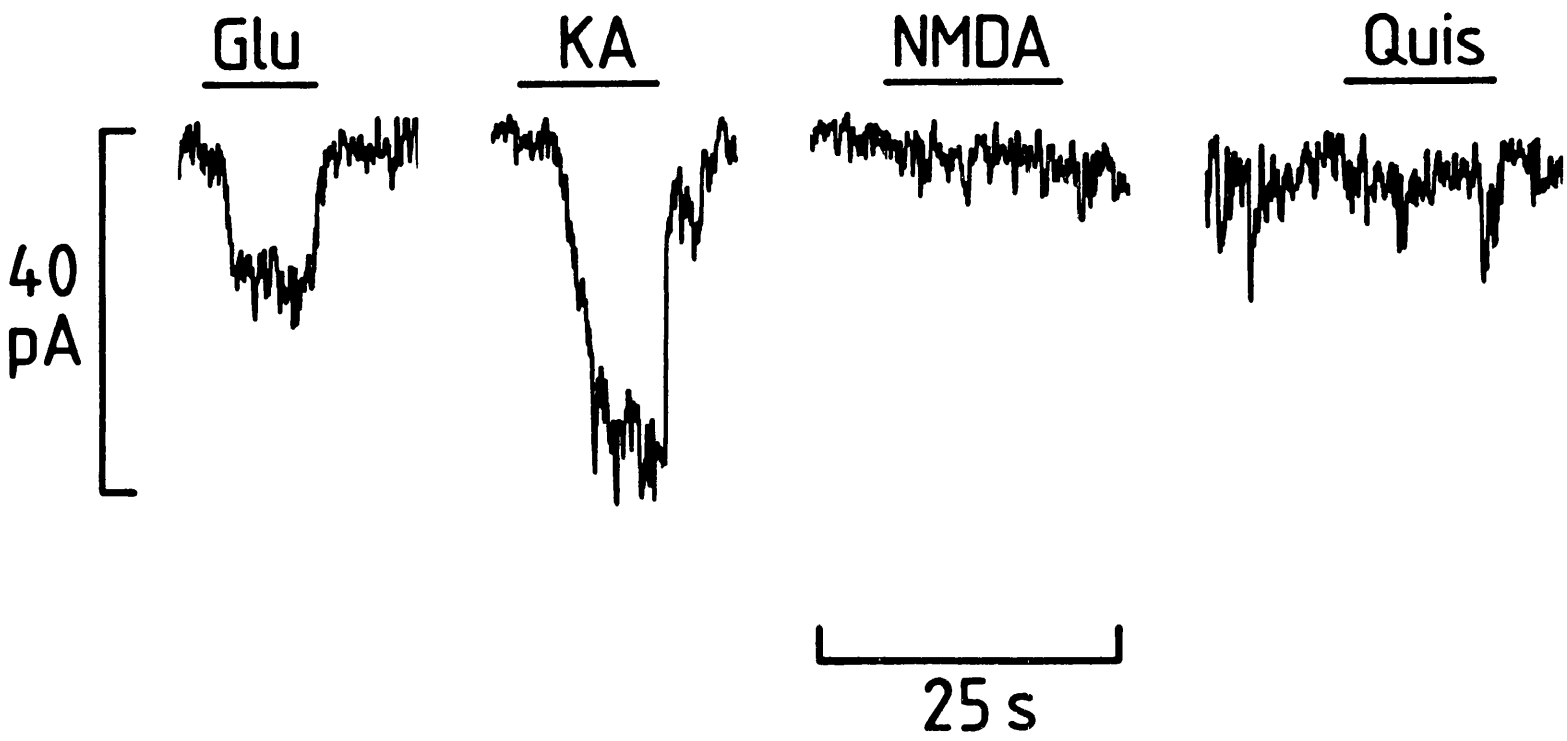
Glu
KA
NMDA
Quis
40
pA
25 s

Figure 3.6 Voltage-dependence of the kainate-induced current in cones.

Currents were induced by pressure ejection of 10μM kainate in half of an isolated double cone. Peak currents (ordinate) are plotted against membrane potential (abcissa). The patch pipette contained solution Cl01 (Table 2.3), and the external solution was Ringer's containing 6mM barium (solution RB, Table 2.1).

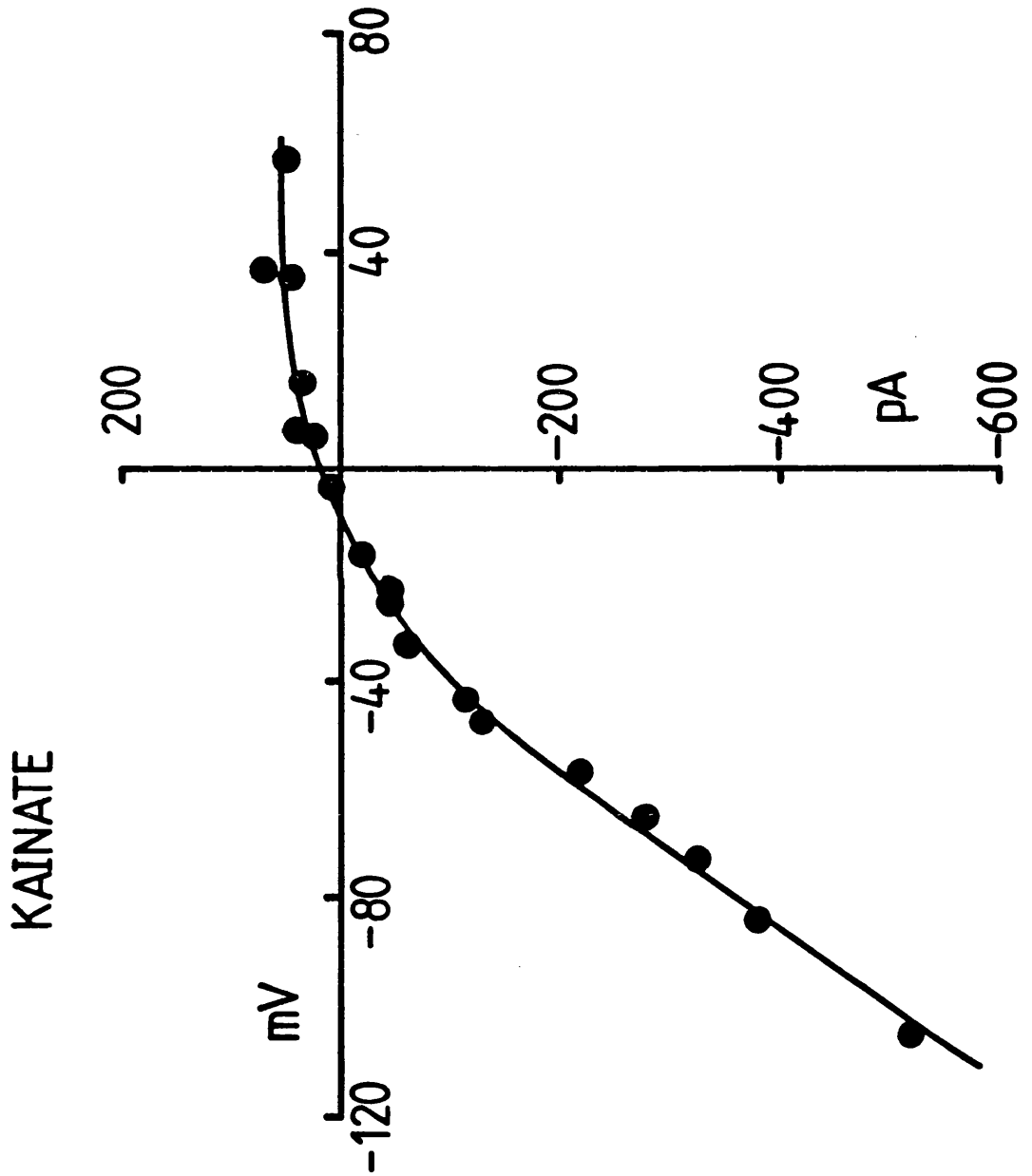
KAINATE
mV
80
40
-40
-80
-120
200
-200
-400
-600
pA

noise analysis after being low-pass filtered at 1000Hz and high-pass filtered at 2Hz (Chapter 2, section 2.1.4.1). Figure 3.7A shows a current induced by kainate, low-pass filtered in the top trace and high- and low-pass filtered in the bottom trace. As the current increased, so did the noise, presumably due to a kainate-induced increase of opening and closing of ion channels. In Figure 3.7B, the variance of the kainate-induced current fluctuations is shown as a function of time. It is clear that the variance is greatest at the time when the kainate-induced current is at a peak.

In Figure 3.7C the variance of the kainate-induced current is shown as a function of the mean kainate-induced current flowing, during the period when the current was changing. The variance is proportional to the mean current flowing, implying that the probability of the channel opening is low (Colquhoun and Hawkes, 1977). In this situation, if it is assumed that there is only one type of kainate-gated channel present, with only one open state, the current flowing through a single channel opened by kainate can be obtained as the ratio of the variance to the mean current. The slope of the linear regression line in Figure 3.7C is 0.14pA. After correction for variance lost below 2Hz and above 1000Hz (the high and low pass filter frequencies) as described in Chapter 2, section 2.1.4.1, this becomes 0.19pA, implying a single channel conductance of 4pS for a reversal potential of -8mV and a holding potential of -56mV. To produce the current change of 220pA in Figure 3.7A, approximately 1158 channels must be open at any time, and since the probability of opening is low, there must be far more channels than this actually in the cell membrane. In 2 other cells studied, the single channel conductance calculated in this way was 3.1 and 4.2pS. For a glutamate-induced conductance increase in 3 cells, the single channel conductances calculated in this way were 0.5, 1.3 and 2.5pS: the reason for this variability is not known.

Figure 3.8A shows the power spectrum of the membrane fluctuations obtained before kainate was applied and during the plateau of the kainate response in Figure 3.7A. The difference between these two spectra, the net spectrum, is shown in Figure 3.8B. The net spectrum cannot be fitted with a single Lorentzian; instead a sum of two Lorentzian components (with different half power frequencies) was necessary. All the glutamate- and kainate

Figure 3.7 Noise analysis of a kainate-induced conductance increase in a cone.

A. Current induced in half of an isolated double cone voltage-clamped at -56mV (data from the same cell as Figure 3.6), by pressure ejection (indicated by the arrow) of 10μM kainate. Top trace: low-pass filtered (8 pole) at 1000Hz. Bottom trace: a higher gain current record of the top trace but now also high-pass filtered (8 pole) at 2Hz. The patch pipette contained solution Cl01 (Table 2.3) and the external solution was barium Ringer's (solution RB, Table 2.1).

B. Variance of the kainate-induced current in the range 2-1000Hz, as a function of time (in 1 second bins). The variance is greatest at peak inward current.

C. Variance of the kainate-induced current in the range 2-1000Hz (ordinate), as a function of the mean kainate-induced current (abcissa). The line through the points was calculated by linear regression and has a slope of 0.14pA.

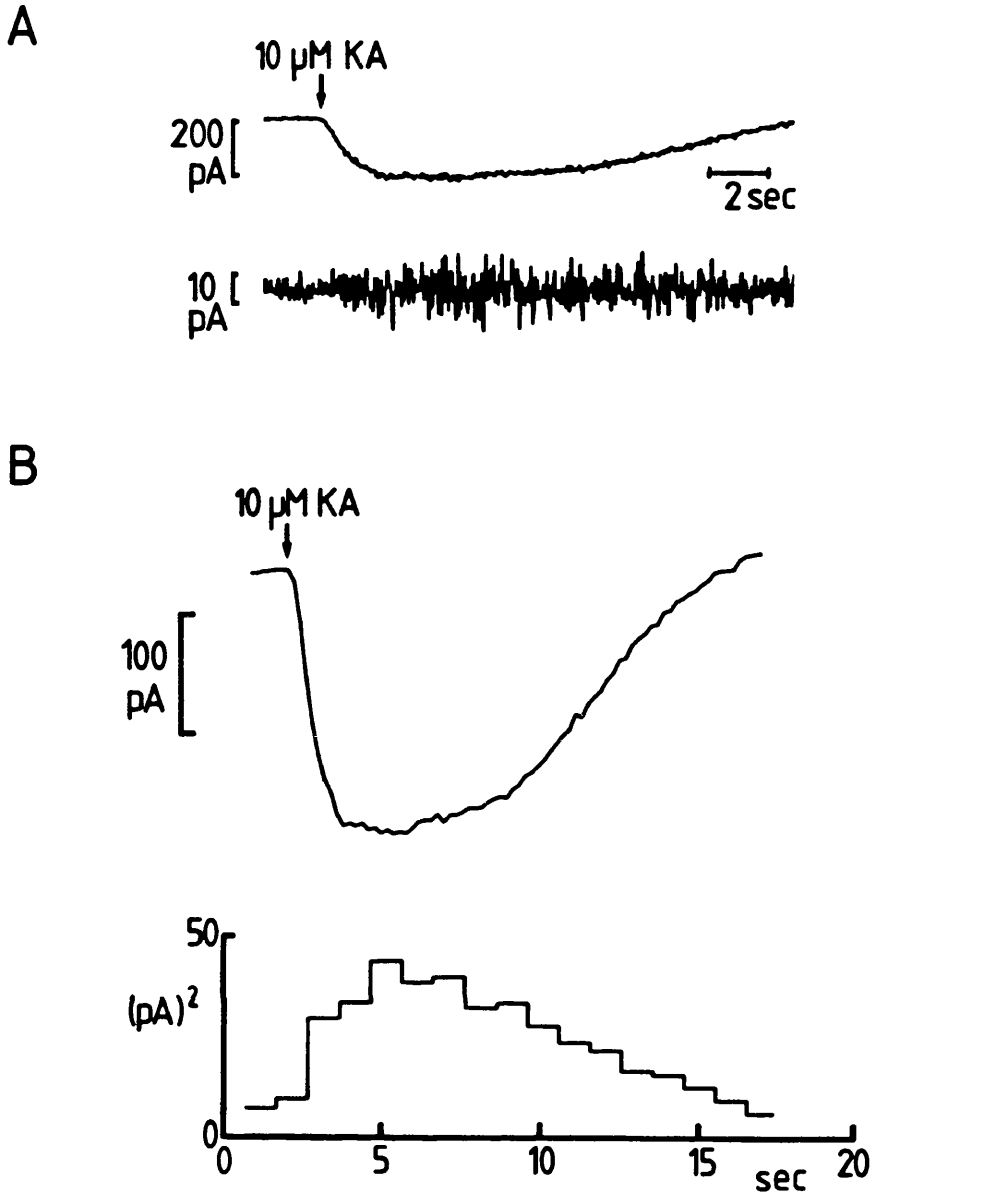
A
10 μM KA
200 pA
2 sec
10 pA
B
10 μM KA
100 pA
50
(pA)²
0
0
5
10
15
sec
20
C
70
(pA)²
60
50
40
30
20
10
0
-100
-200
pA
-300

Figure 3.8 Power spectra of kainate-induced current in cones.

A. Spectrum of the current noise before (dots) and during kainate application (squares).

B. Difference between the spectra in A. Filtering due to the series resistance in this cell would give a Lorentzian roll off at high frequencies with a half power frequency of 940Hz. The solid line is the sum of the 2 Lorentzian components shown as dashed lines. The lower frequency component has $G(o) = 1.78\ (pA)^2$; f_c = 10Hz. The high frequency component has $G(o) = 0.014\ (pA)^2$; f_c = 794Hz.

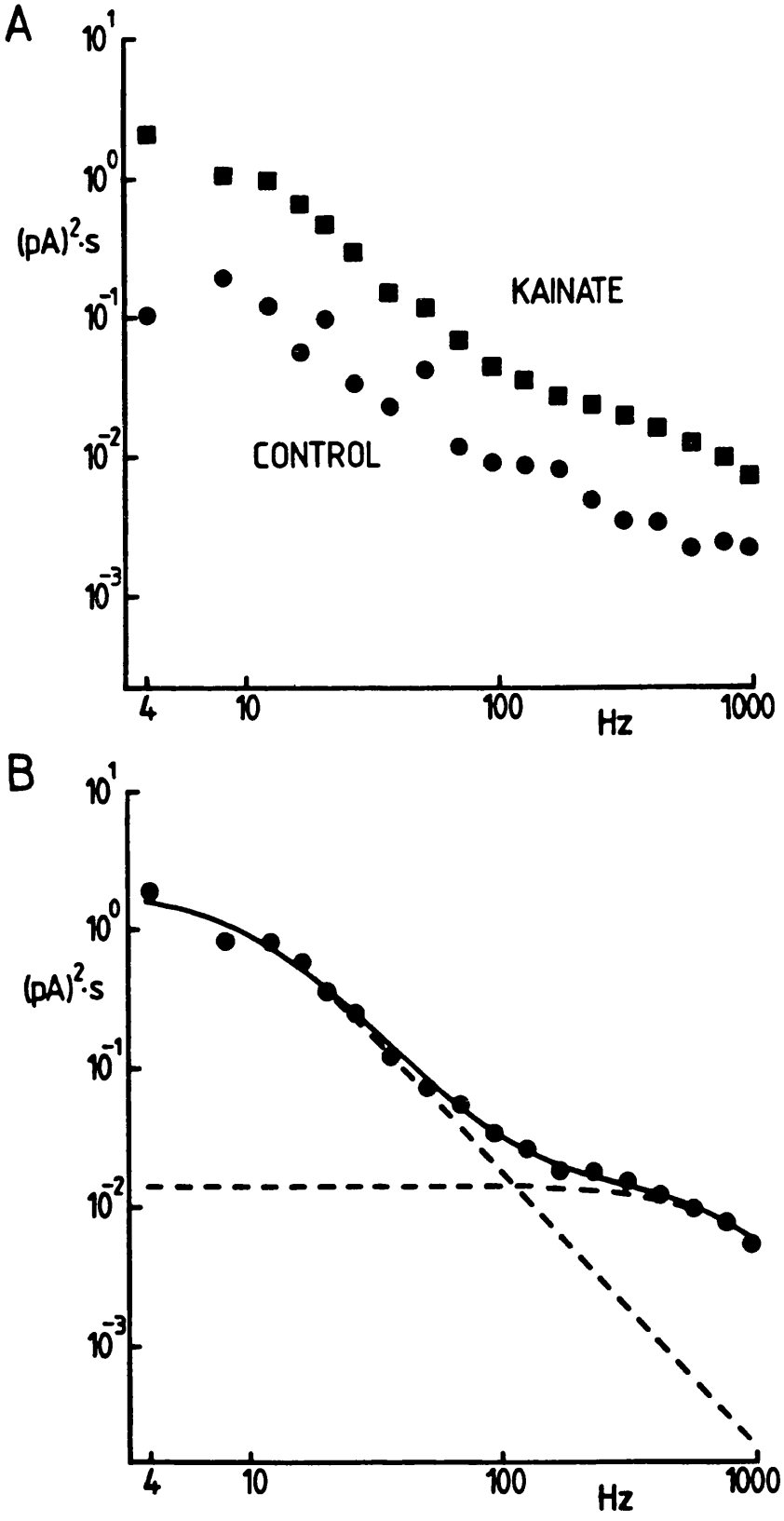
A
10^1
10^0
$(pA)^2 \cdot s$
10^{-1}
10^{-2}
10^{-3}
KAINATE
CONTROL
4
10
100
1000
Hz
B
10^1
10^0
$(pA)^2 \cdot s$
10^{-1}
10^{-2}
10^{-3}
4
10
100
1000
Hz

induced currents which were analysed for noise (n=6 cells), gave net spectra that needed the sum of two Lorentzians to fit the data. The two Lorentzians used to fit the data in Figure 3.8B are shown as dashed lines in the figure, with their sums shown as the continuous curve through the points.

If there is only one type of kainate-gated channel in these cells, a spectrum fitted by the sum of two Lorentzians is consistent with a kinetic scheme for channel opening in which there are 3 states (Colquhoun and Hawkes, 1977), for example:

$$\underset{\text{closed}}{T + R} \underset{k_2}{\overset{k_1}{\rightleftharpoons}} \underset{\text{CLOSED}}{TR} \underset{a}{\overset{b}{\rightleftharpoons}} \underset{\text{OPEN}}{TR} \qquad (11)$$

In this scheme, T represents the transmitter glutamate (or kainate), and R represents the receptor complex which is initially closed and can only open when it has bound transmitter. The parameters k_1, k_2, b and a are the rate constants for transmitter binding and dissociation, and for channel opening and closing.

3.3.5 The effect of a blocker of glutamate uptake

It has been shown in retinal glial cells (Chapter 5; Brew and Attwell, 1987) that the electrogenic uptake of glutamate into voltage-clamped cells generates an inward current. In principle, part of the glutamate-induced current in cones could be due to a similar uptake mechanism. I applied threo-3-hydroxy-DL-aspartate (THDA), a blocker of glutamate uptake (Balcar and Johnston, 1972), to voltage-clamped cells in which an inward current was induced by iontophoresis of glutamate. In each experiment, at voltages ranging from -52 to -84mV, 30μM THDA greatly reduced the glutamate-induced current (n=3 cells). This inhibition was reversed within seconds when the THDA was washed off (Figure 3.9). Unfortunately, this strong blocking effect of THDA on the glutamate-induced current only indicates that this blocker is not specific for acting on glutamate uptake, since a large part of the current must be due to glutamate acting on ion channels (as discussed in sections 3.3.3 and 3.3.4 and Chapter 7, section 7.1.2).

Figure 3.9 Threo-3-hydroxy-DL-aspartate reduces the glutamate-induced current in cones.

Glutamate was applied by iontophoresis (shown in the bottom trace) to half of a double cone, voltage-clamped at -72mV. Application of 30μM threo-3-hydroxy-DL-aspartate (THDA) by bath-perfusion (shown by the bar), reversibly blocked the glutamate-induced current. The patch pipette contained solution Cl01 (Table 2.3) and the external solution was Ringer's (solution RA, Table 2.1).

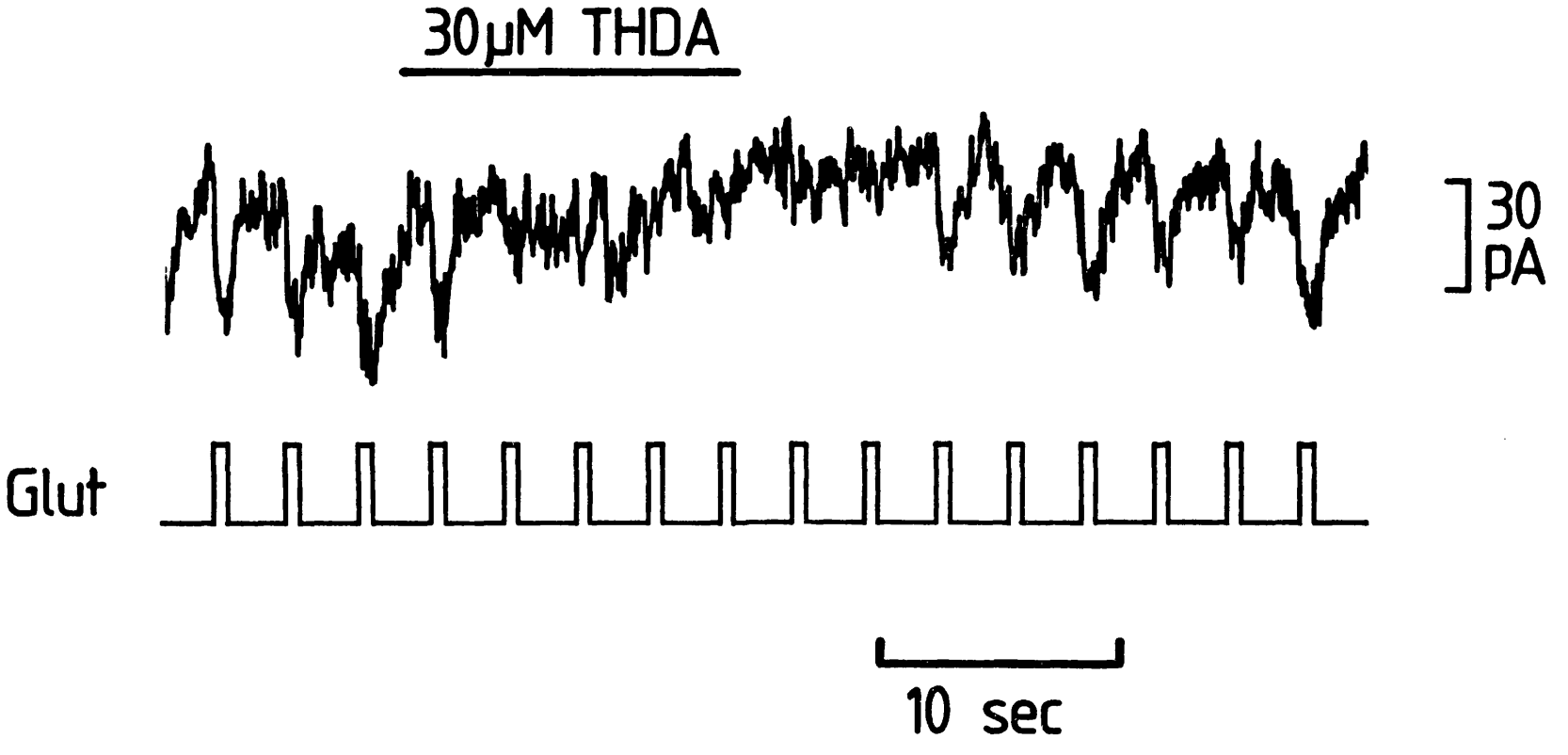
30µM THDA
30 pA
Glut
10 sec

3.3.6 Spatial localization of the glutamate-induced current

The spatial localization of the glutamate-activated current was mapped by iontophoresing glutamate onto voltage-clamped, isolated cones. The iontophoretic pipette was positioned about 5μm away from the cell membrane, at various positions around the cell. Figure 3.10B is a diagram of a cone patch-clamped at the cell body, with the different positions of the patch pipette indicated. In Figure 3.10A are the glutamate-induced currents for each of the positions of the iontophoretic pipette in B. The current was largest and fastest (50ms) in onset when glutamate was applied near the synaptic terminal. At other locations the response was smaller, and notably slower in onset, presumably due to the time needed for glutamate to diffuse to the synaptic terminal. This suggests that the response was generated in the synaptic terminal. Consistent with this is the fact that cones which had lost their synaptic terminals in the cell isolation procedure did not respond to glutamate. Mapping experiments gave similar results in other cones (n=6 cells).

The arrows by the traces in Figure 3.10A show an estimate, for each position of the iontophoretic electrode, of the time ($t = x^2/2D$) at which the glutamate concentration at the synaptic terminal would have reached 32% of the maximum value it would reach if glutamate injection were prolonged. This value was calculated as follows. The concentration, C, of glutamate at time t and at distance x from the site of application, is given by (Crank, 1976):

$$C(x,t) = (q/(4\pi Dx)) \cdot \mathrm{erfc}(x/\{2(Dt)^{1/2}\}) \qquad (12)$$

where: D is the diffusion coefficient for glutamate
q is the rate of release of glutamate from the electrode

The maximum value of C for fixed x is (by setting t=infinity):

$$C_{max} = (q/(4\pi Dx)) \cdot \mathrm{erfc}(0)$$
$$= q/(4\pi Dx)$$

Therefore, $C(x,t) = (C_{max}) \cdot \mathrm{erfc}(x/(2(Dt)^{1/2}))$

At $t=x^2/(2D)$,

$$C = C_{max} \cdot \mathrm{erfc}(1/(2^{1/2}))$$
$$= C_{max} \cdot (0.32)$$

Figure 3.10 Spatial localization of the glutamate-induced current in cones to the synaptic terminal.

A. Responses to glutamate applied by iontophoresis, 5μm away from the cell membrane of half of an isolated double cone voltage-clamped at -72mV, at the positions shown in B. Timing of iontophoresis is shown below the current traces. External solution was Ringer's (solution RA, Table 2.1) and the patch pipette solution was Cl01 (see Table 2.3). The arrows by the traces show an estimate, for each position of the iontophoretic electrode, of the time at which the glutamate concentration at the synaptic terminal would have reached 32% of its maximum value.

B. Diagram of a cone voltage-clamped at the cell body with the positions of the iontophoretic pipette indicated.

C. Normalized plot of the location of the glutamate response, obtained by measuring the currents in A, 50ms after the start of iontophoresis (vertical dashed line in A).

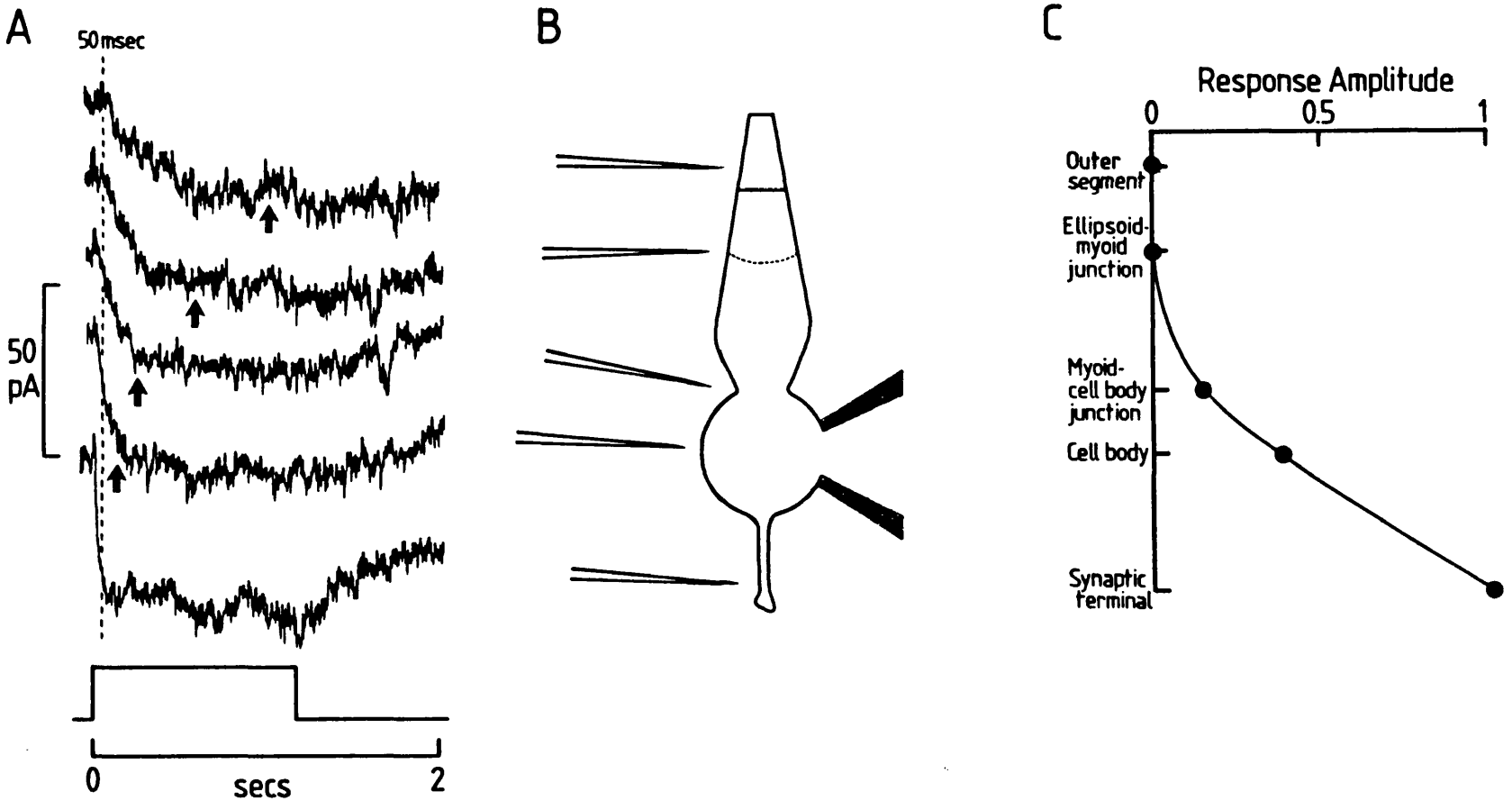
A
50 msec
50 pA
0
secs
2
B
C
Response Amplitude
0
0.5
1
Outer segment
Ellipsoid-myoid junction
Myoid-cell body junction
Cell body
Synaptic terminal

Even with the electrode positioned at the cone outer segment, the glutamate induced current eventually reaches two thirds of the amplitude of that produced by iontophoresis at the synaptic terminal (Figure 3.10A). This probably results from the high concentration of glutamate produced by iontophoresis. From earlier experiments on glial cells (Brew and Attwell, 1987), we estimate the steady-state glutamate concentration generated by continued iontophoresis, at a distance of 50μm (the cone length) from the iontophoretic electrode, to be about 10μM, a concentration which generated an almost maximum response in the cone (Figure 3.3). Figure 3.10C is the normalized plot of the localization of the glutamate response, obtained by measuring the current in A, 50ms after the start of iontophoresis (vertical dashed line in Figure 3.10A). In this time glutamate will have diffused only about 10μm from the iontophoretic electrode (about the length of the synaptic terminal). This plot again indicates that glutamate acts on the cone synaptic terminal.

3.3.7 The glutamate-induced current in cones in the intact retina

Experiments in which the glutamate-induced current was studied in cones in the isolated, intact retina, were performed on light adapted cells in order to suppress the release of glutamate from photoreceptors, which is maximal in the dark (Cervetto and Piccolino, 1974). The preparation was perfused with Ringer's containing bicuculline to block the effect of GABA. Glutamate induces the release of GABA from horizontal cells (Ayoub and Lam, 1984), and GABA is known to gate channels in cone photoreceptors (Kaneko and Tachibana, 1986). Control experiments on isolated cells showed that 10μM bicuculline does not affect the glutamate-induced current in cones (Chapter 4, section 4.3.5).

Glutamate was applied to voltage-clamped cones by bath-perfusion, and it took 30-60 seconds for a response to be evoked due to the time needed for the glutamate to reach the cells. High concentrations of glutamate (5mM) were used to avoid the possibility that uptake into Müller cells might greatly reduce the effective concentration reached at the cone synaptic terminal. With 16mM chloride in the patch pipette, glutamate induced a current in cones which was inward below the cone dark potential, reversed at -38 ±2 (s.d.) (n=6), and was outward at more positive potentials (n=8

cells) (Figure 3.11). The significance of this reversal potential, which is more negative then that seen in isolated cells studied with 101mM chloride in the patch pipette (Figure 3.2), is considered further in the next chapter.

3.3.8 Light response in cones in the intact retina

To assess the physiological significance of the glutamate-evoked current in cones it is necessary to know the magnitude of the current evoked by light in cones. The ion channels mediating the conversion of light into an electrical signal in the cone are open in the dark, carrying an inward current into the receptor. When light is absorbed by the visual pigment in the outer segment this leads to a chain of events (Chapter 1, section 1.2.1), resulting in the light sensitive channels being closed, suppressing the inward current that flows in the dark. In the voltage-clamped cell this results in an outward current being recorded.

In Figure 3.12A are the responses of a voltage-clamped cone to flashes of light (wavelength 700nm) of increasing intensities. (represented as the log to base 10 of the neutral density filter inserted in the light beam: $-\log_{10}(\text{intensity})=4$ represents the dimmest flash ($7.57\text{x}10^2$ photons/μm^2/sec), and $-\log_{10}(\text{intensity})=1.0$, the brightest flash ($7.57\text{x}10^5$ photons/μm^2/sec). The magnitude of the photocurrent increases as the light intensity increased (n=8 cells), to a maximum of about 30pA. In Figure 3.12B the normalized photocurrent (ordinate) is plotted against light intensity.

Figure 3.11 Voltage-dependence of the glutamate-induced current in the isolated, intact retina.

Current evoked by bath-perfusion of 5mM glutamate to a single cone in an isolated, intact retina, plotted as a function of voltage. Points on the line were obtained by subtracting the current flowing at each voltage during a voltage ramp with no glutamate present, from points at the same voltage in the presence of glutamate.

The line through the points was obtained by linear regression, and has a X-axis intercept (reversal potential) of -36mV. The external solution was Ringer's (solution RA, Table 2.1) containing 10μM bicuculline, and the patch pipette contained solution C16 (Table 2.3).

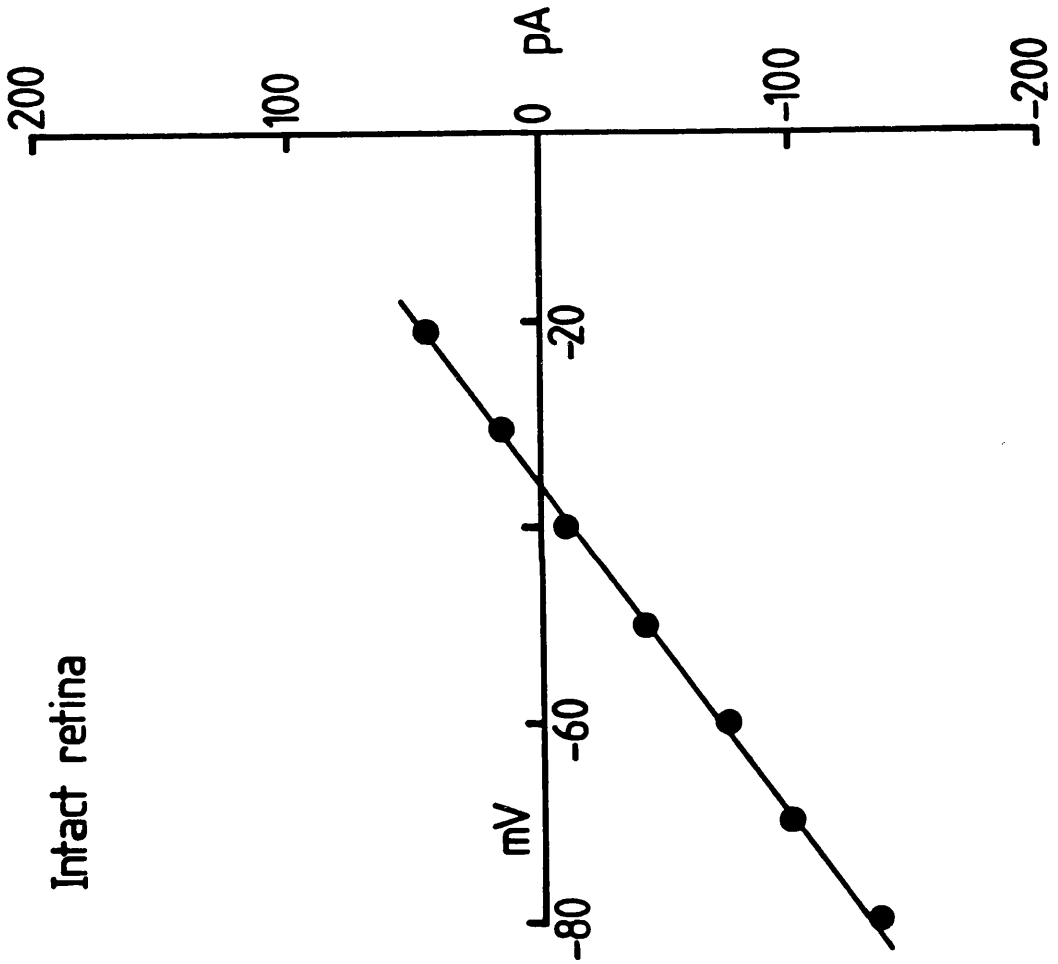
200
100
0 pA
-100
-200
-20
-60
mV
-80
Intact retina

Figure 3.12 Light responses in a dark adapted cone in the intact retina.

A. Red light (wavelenght 700nm) of various intensities was applied to a cone voltage-clamped to -60mV. The patch pipette contained solution C16 (Table 2.3) and the superfusion solution was Ringer's (solution RA, Table 2.1) containing 10μM bicuculline. Numbers corresponding to the light flashes (bottom trace), are on a $\log_{10}$ scale, where 1.0 represents the brightest flash (7.57×10^5 photons/μm^2/sec). When the light intensity is increased from 4.0 to 1.0 (7.57×10^2 to 7.57×10^5 photons/μm^2/sec), the size of the photocurrent is increased. The peak current evoked in the cone, with the brightest flash used was 32pA.

B. Normalized photocurrent (I_{light}/Peak I_{light}) (ordinate) is plotted against $-\log_{10}$ (light intensity) for the cone in A.

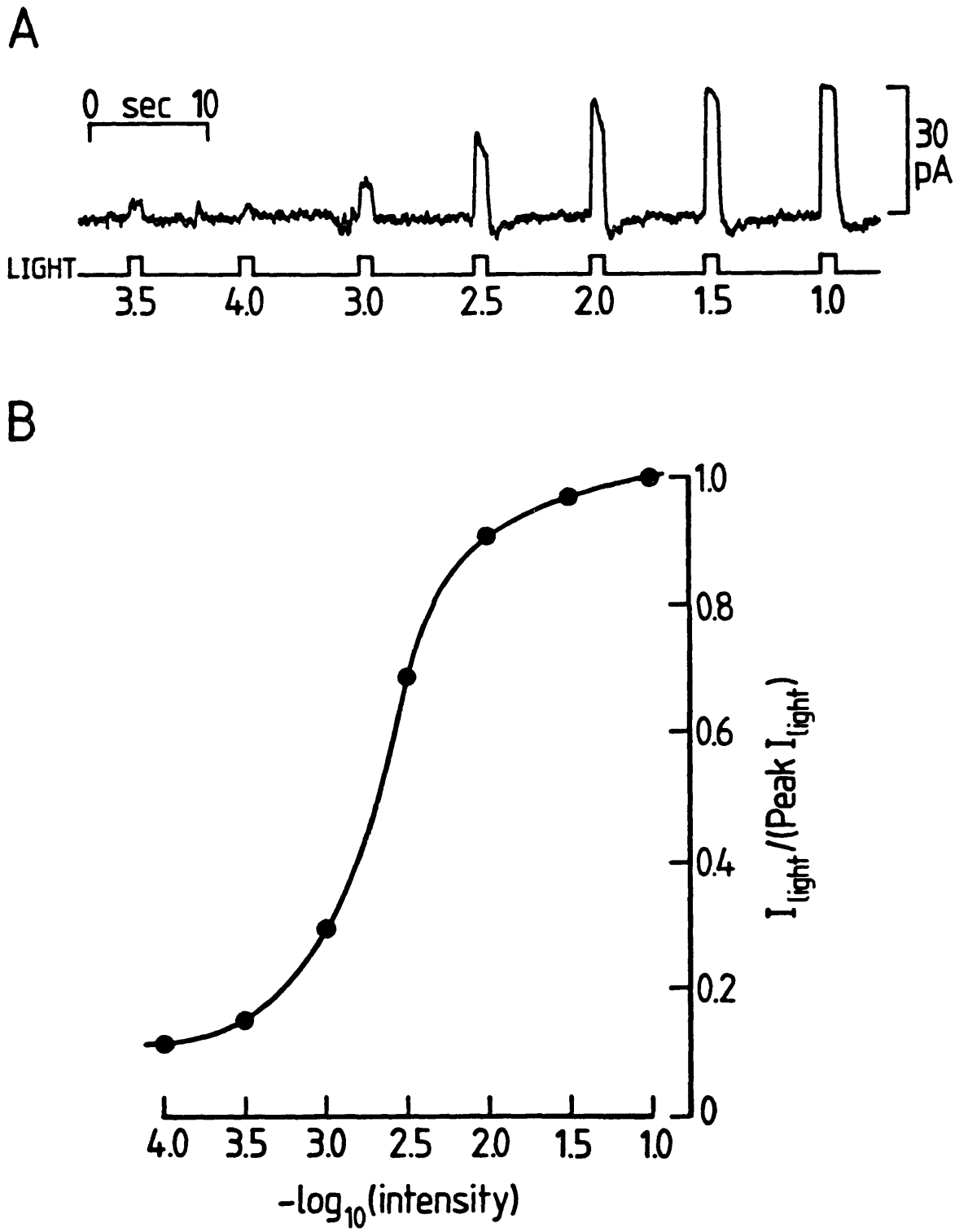
A
0 sec 10
30
pA
LIGHT
3.5
4.0
3.0
2.5
2.0
1.5
1.0
B
1.0
0.8
0.6
0.4
0.2
0
$I_{light}/(Peak\ I_{light})$
4.0
3.5
3.0
2.5
2.0
1.5
1.0
$-\log_{10}(intensity)$

Chapter 4

Ionic basis of the glutamate-induced current in cone photoreceptors

4.1 Introduction

Application of glutamate evokes a current in cone photoreceptors (Chapter 3). The clear reversal potential shown by the current evoked by glutamate (section 3.3.1), the fact that a similar response is evoked by kainate, a glutamate analogue that gates channels (section 3.3.3), and the noise increase associated with the conductance increase (section 3.3.4), imply that at least part of the conductance increase is produced by glutamate opening ion channels. This chapter describes experiments characterizing the ions that carry the current. The results are dealt with under the following headings:

(1) Sodium-dependence of the glutamate-induced current. (2) Dependence of the glutamate-induced current on internal chloride concentration. (3) Dependence of the glutamate-induced current on external chloride concentration. (4) Dependence of the glutamate-induced current on other anions. (5) The glutamate-induced increase in chloride conductance in cones is different from that evoked by GABA. (6) The effect of sodium removal on the glutamate-induced current when the external calcium concentration is low.

4.2 Methods

All experiments described in this chapter were performed on cone photoreceptors and other retinal neurones (section 4.3.5) isolated by enzymatic dissociation of retinae from the tiger salamander (Chapter 2, section 2.1.1.1). The currents induced by glutamate were studied using the whole-cell variant of the patch-clamp technique. Pharmacological agents were applied by bath-perfusion or by iontophoresis. Intracellular solutions with different ionic compositions were studied by using patch pipette solutions of different composition to study different cells (Fenwick, Marty and Neher, 1982). The pipette solutions are described in Table 2.3. Extracellularly, Ringer's solutions with different ionic compositions (Tables 2.1 and 2.2) were perfused onto the cells.

4.3 Results

4.3.1 Sodium-dependence of the glutamate-induced current

It has been reported that glutamate gates relatively non-specific cation channels, permeable to both sodium and potassium (and calcium in the case of NMDA-type channels) (Hablitz and Langmoen, 1982; Mayer and Westbrook, 1985). In order to investigate whether glutamate opened a similar sort of channel in isolated cones, experiments were performed in which sodium in the superfusion solution was replaced by choline.

Figure 4.1 shows the result of one such experiment. Glutamate was repeatedly applied by iontophoresis (top trace) to an isolated cone bathed in Ringer's containing 6mM barium (solution RB, Table 2.1). The cell was held at -53mV and glutamate evoked a current in this cell of around 75pA. While continuing to apply glutamate, the superfusion solution containing 107mM sodium was replaced by a solution containing 2mM sodium (sodium replaced by choline: solution Na2 with n=0, Table 2.2).

The inward current evoked by glutamate was greatly reduced when the extracellular sodium concentration was lowered (similar results were obtained in 15 cells). Removal of nearly all external sodium did not result in glutamate evoking an outward current at -53mV, as might be expected if glutamate opened channels permeable to sodium and potassium ions. The reduction in glutamate-induced current when external sodium was low was observed when cells were held at a range of voltages (-80 to +55mV). The outward shift of the baseline current on removal of sodium (Figure 4.1) may be due to influx of sodium ions through non-specific cation channels or membrane carriers like Na/Ca exchange that is suppressed when sodium is removed resulting in an outward current.

To investigate the effects of less drastic $[Na^+]_o$ reductions, I carried out similar experiments in which the normal Ringer's solution (containing 107mM sodium) was replaced by a solution containing 60 or 25mM sodium (sodium replaced by choline). Figure 4.2A shows the currents evoked by iontophoretically applied glutamate in a cone bathed in Ringer's containing 107mM sodium, held at various potentials. The glutamate-evoked current reversed around 0mV and had a magnitude of around 25pA at -46mV. In Figure 4.2B are

Figure 4.1 The glutamate-induced current in cones is sodium-dependent.

Glutamate was repeatedly applied by iontophoresis (top trace) to an isolated double cone voltage-clamped at -53mV. The patch pipette contained solution Cl01 (Table 2.3). After 12 seconds, the superfusion solution containing 107mM sodium (solution RB, Table 2.1) was replaced by a solution containing 2mM sodium (bottom trace) (sodium replaced by choline) (solution Na2, n=0, Table 2.2). The inward current evoked by glutamate (middle trace) was greatly reduced by reducing the external sodium concentration. The glutamate-induced current regained its original size after reapplying Ringer's containing 107mM sodium.

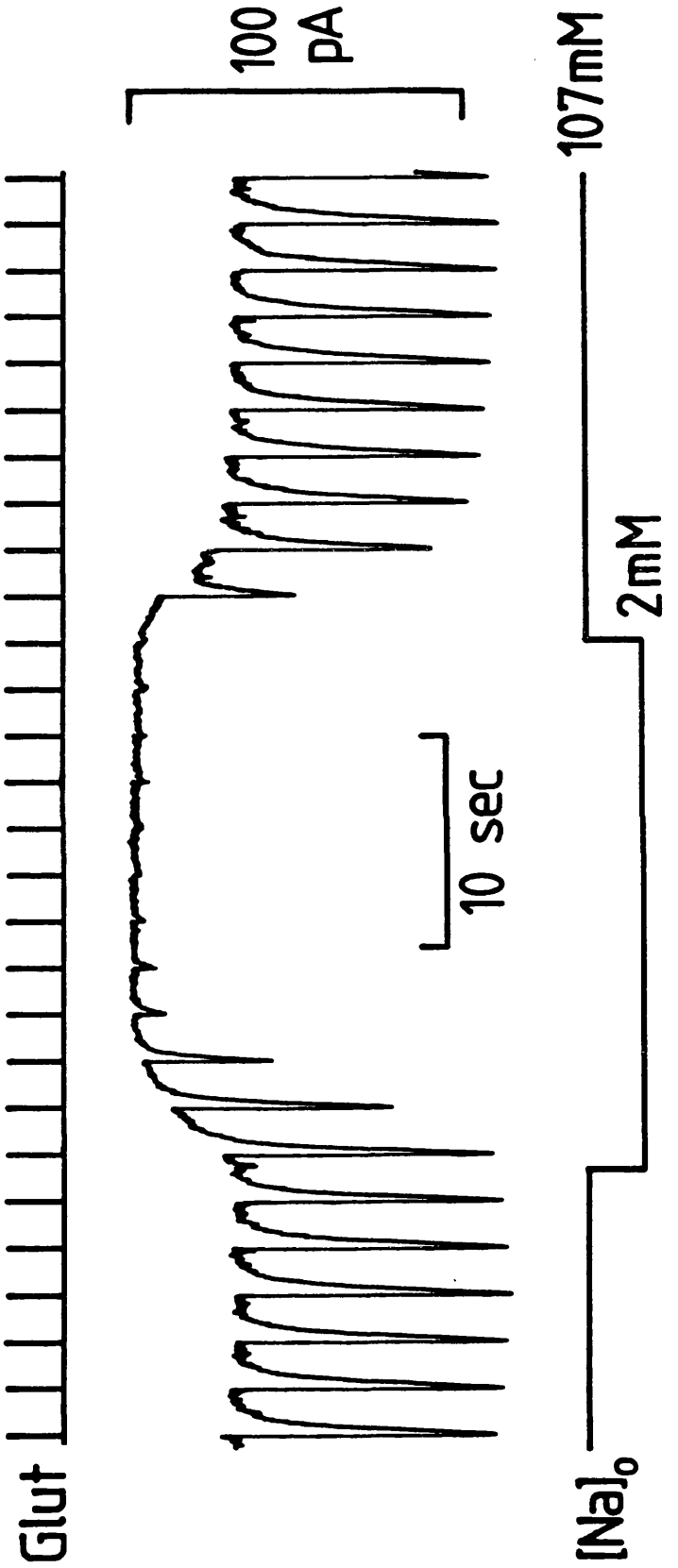
Glut
100
pA
10 sec
107mM
2mM
[Na]o

Figure 4.2 Sodium- and voltage-dependence of the glutamate-induced current in cones.

A and **B.** Changes in membrane current of an isolated, voltage-clamped double cone in response to iontophoresis of glutamate at potentials shown alongside each current trace. Timing of iontophoresis is shown by the square pulse at the bottom. The patch pipette solution was solution Cl01 (with 101mM chloride; Table 2.3). In **A** the extracellular solution was barium Ringer's containing 107mM sodium (solution RB, Table 2.1). In **B** the extracellular solution was barium Ringer's containing 25mM sodium (sodium replaced by choline) (solution Na25 with n=23, Table 2.2).

C. Peak glutamate-induced currents (ordinate) as a function of membrane potential (abcissa) for the experiments in A (closed circles) and B (open cicles). The glutamate-induced currents are reduced in 25mM sodium, but there is no shift in the reversal potential of the response.

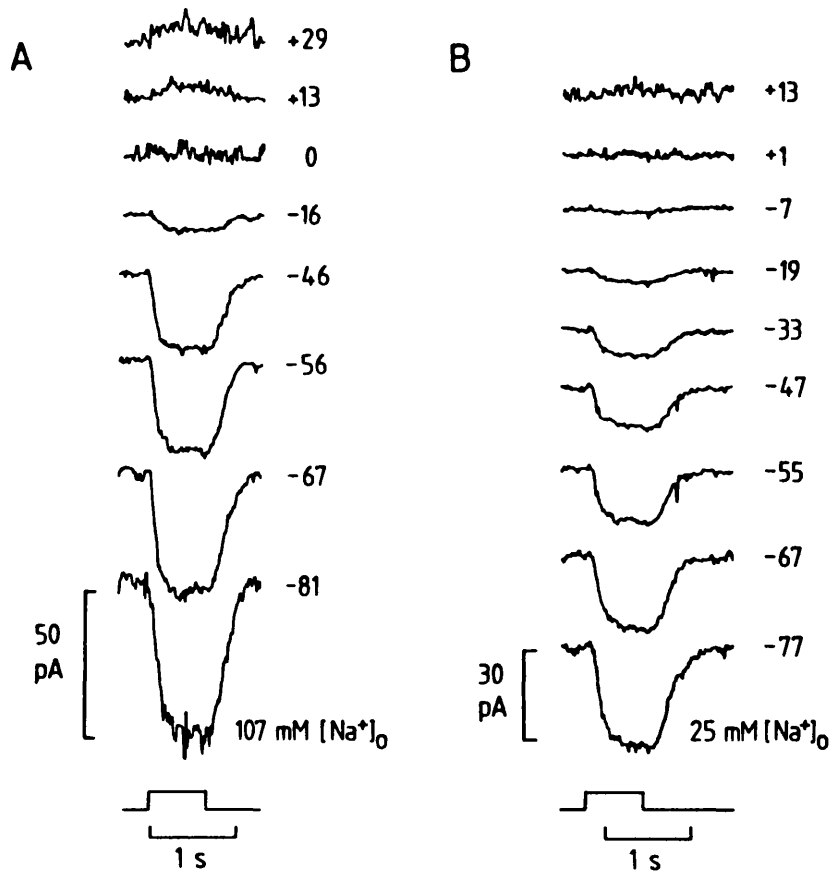
A
+29
+13
0
-16
-46
-56
-67
-81
50
pA
107 mM [Na+]o
1 s
B
+13
+1
-7
-19
-33
-47
-55
-67
-77
30
pA
25 mM [Na+]o
1 s
C
mV
-90
-60
-30
30
10
-10
-20
-30
-40
-50
-60
pA
25 mM [Na+]o
107 mM [Na+]o

the currents induced in the same cell when superfused with Ringer's solution containing 25mM sodium (solution Na25 with n=23, Table 2.2). The glutamate-induced currents are smaller (15pA at -47mV), but the reversal potential of the response is still around 0mV.

From the Goldman-Hodgkin-Katz equation, E_{rev}= $-(RT/F).\ln\{((PNa/PK)[Na^+]_i+[K^+]_i)/((PNa/PK)[Na^+]_o+[K^+]_o)\}$, a permeability ratio of PNa/PK = 1.25 gives a reversal potential of -0.5mV with normal Ringer's (107mM) externally and solution Cl01 in the patch pipette, which is near the observed reversal potential of the glutamate-induced current. With 25mM sodium in the external solution a reversal potential of -35.6mV would be predicted. However, a shift in reversal potential was not observed in this experiment or in any other in which 107mM sodium Ringer's was substituted by 25 or 60mM sodium Ringer's (n=11 cells): low external sodium simply reduced the glutamate-evoked current at both negative and positive potentials (-80 to +55mV).

The experiments described above suggest that sodium ions do not pass through the glutamate activated channel. A possible mechanism of the suppressive effect of sodium removal will be considered below (section 4.3.6).

4.3.2 Dependence of the glutamate-induced current on internal chloride concentration

Although glutamate usually gates non-specific cation channels in vertebrate neurones, glutamate-evoked chloride currents have been reported in invertebrate neurones (Szczepaniak and Cottrell, 1973) and muscle cells (Cull-Candy, 1976). In order to investigate whether the glutamate-induced current in cones could be carried by chloride ions, I first carried out experiments in which the concentration of chloride in the patch pipette and hence in the intracellular solution was changed (replacing chloride by acetate). The results of these experiments are described in this section. Secondly, I changed the concentration of chloride ions in the extracellular solution and the results of those experiments are described in section 4.3.3 below.

The experiments described in this section were carried out in Ringer's containing 6mM barium, the extracellular chloride concentration was 126mM chloride (solution RB, Table 2.1). With

101mM chloride in the patch pipette, glutamate evoked a current which reversed around 0mV (Figure 3.2, Chapter 3; Figure 4.2C (closed circles), this Chapter).

Figure 4.3A and B show the results of an experiment in which the patch pipette solution contained 30mM chloride (solution C30, Table 2.3, 71mM chloride replaced by acetate). In A are the currents induced in a cone by iontophoretically applied glutamate at voltages as indicated next to each current trace. In B the peak currents evoked in this cell by glutamate are plotted against voltage. The reversal potential of the response is -33mV. With 30mM chloride in the patch pipette, the mean reversal potential of the glutamate-induced current was -28 $\pm$2 (s.d.) mV (n=6 cells).

Figure 4.3C and D show the results of an experiment similar to that described above but with the patch pipette containing 9mM chloride (solution C9, Table 2.3). As can be seen in Figure 4.3D, the reversal potential of the glutamate-induced current is now -45mV. The mean reversal potential of the response with 9mM chloride in the patch pipette was -48 $\pm$2 (s.d.) mV (n=4 cells).

These results indicate that at least part of the glutamate-induced current in cones is carried by chloride ions. However, not all the current is carried by chloride, since the reversal potentials obtained in these experiments are more depolarized than what would have been predicted for a chloride-specific channnel as discussed below in section 4.3.4.

4.3.3 Dependence of the glutamate-induced current on external chloride concentration

To investigate further the conductance of chloride ions through the glutamate-activated channel in cones, experiments were carried out in which the external chloride concentration was changed. All experiments described in this section were carried out with the patch pipette solution containing 9mM chloride (solution C9, Table 2.3), so that the chloride reversal potential fell in the negative potential range. (With 101mM $[Cl^-]_i$ the reversal potential with low $[Cl^-]_o$ would have been at positive potentials, and hence difficult to study). Glutamate was repeatedly applied by iontophoresis to isolated cones while the superfusion solution was changed from Ringer's containing 126mM chloride (solution RB, Table 2.1) to

Figure 4.3 Dependence of the glutamate-induced current on internal chloride concentration.

A. Glutamate-induced currents in a double cone voltage-clamped to the potential shown beside each current trace. Timing of glutamate iontophoresis is shown in the bottom trace. The patch pipette solution contained 30mM chloride (solution C30, Table 2.3). The external solution was Ringer's containing 6mM barium (solution RB, Table 2.1); this solution contains 126mM chloride.

B. Peak glutamate-induced currents (ordinate) as a fuction of membrane potential (abcissa) for the experiment in A. The reversal potential of the response is -33mV.

C. A similar experiment as described in A but now the patch pipette contained 9mM chloride (solution C9, Table 2.3).

D. Peak glutamate-induced currents as a function of membrane potential for the experiment in C. The reversal potential of the response is -45mV.

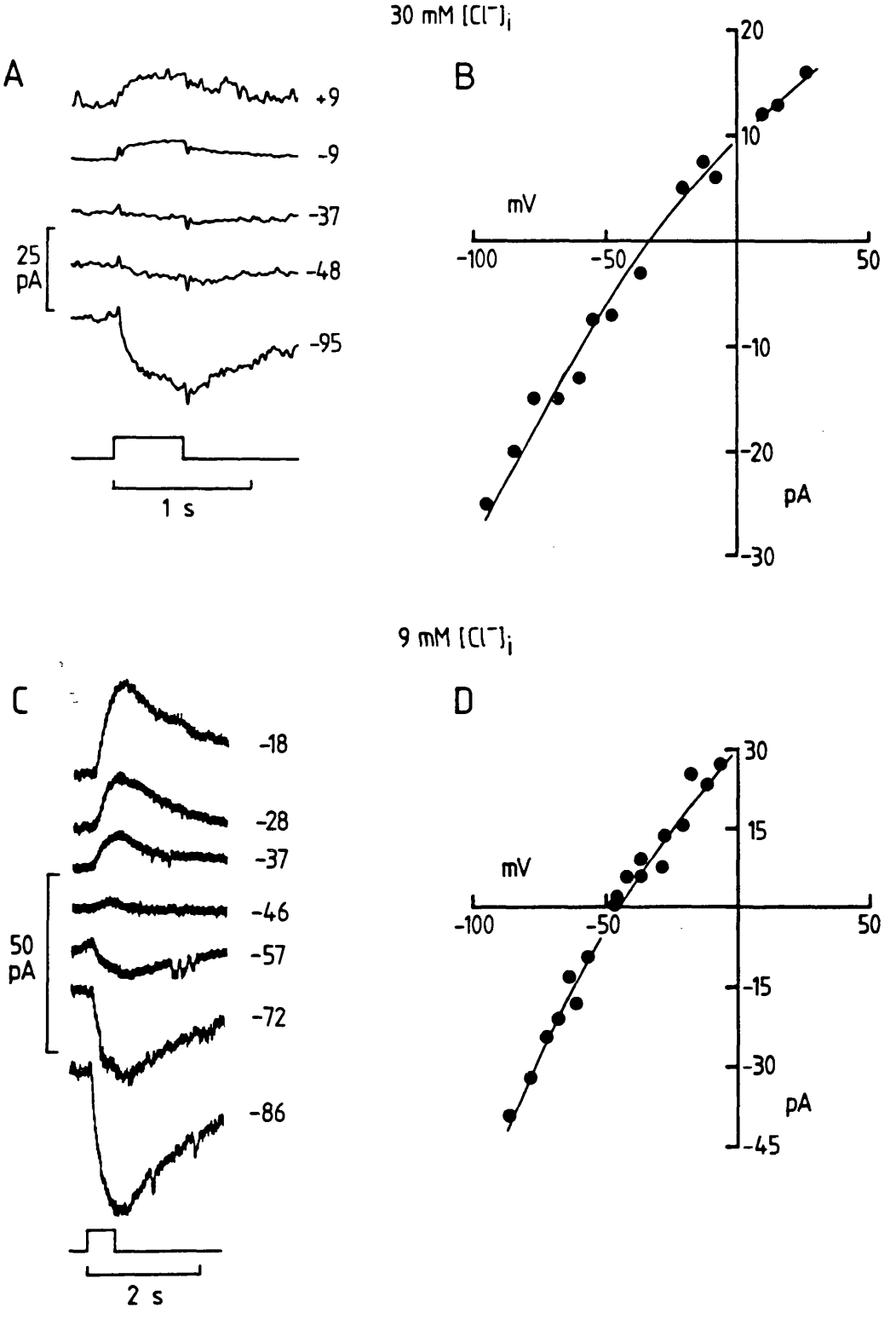
30 mM [Cl⁻]ᵢ
A
+9
-9
-37
-48
-95
25 pA
1 s
B
20
10
mV
-100
-50
50
-10
-20
pA
-30
9 mM [Cl⁻]ᵢ
C
-18
-28
-37
-46
-57
-72
-86
50 pA
2 s
D
30
15
mV
-100
-50
50
-15
-30
pA
-45

Ringer's containing 22mM chloride (chloride replaced by gluconate: solution C22, Table 2.1). For these experiments the bath electrode used was a 4M NaCl agar bridge instead of a AgCl pellet, in order to avoid changes in electrode potential when changing $[Cl^-]_o$.

Figure 4.4A shows the currents evoked by glutamate in a cone bathed in Ringer's containing 126mM chloride at voltages indicated next to each current trace. In Figure 4.4B are the currents evoked by glutamate in the same cell but in a superfusion solution containing 22mM chloride. For each external solution the peak currents are plotted against voltage in Figure 4.4C. This shows that the reversal potential of the response is shifted to a more depolarized potential (from -43 to -10mV), when the external chloride concentration is reduced from 126 to 22mM. In another cone a shift from -40 to -12mV was observed. These results confirm that chloride ions pass through the glutamate-activated channel.

4.3.4 Dependence of the glutamate-induced current on other anions

The results of the experiments in sections 4.3.2 and 4.3.3 indicate that at least part of the glutamate-induced current in cones is carried by chloride ions. However, the dependence of the reversal potential on internal and external chloride was weaker than what would be predicted for a chloride-specific channel. In Figure 4.5A the average reversal potentials (±s.d.) of the glutamate-induced current (ordinate) from experiments described in section 4.3.2, are plotted as a function of pipette chloride concentration (abcissa). In Figure 4.5B the average reversal potentials from experiments in section 4.3.3 are plotted as a function of external chloride concentration. In both figures the reversal potentials do not fit the Nernst prediction ($E_{Cl} = -(RT/F).\ln([Cl^-]_o/[Cl^-]_i)$ for a chloride specific channel (dashed lines).

For the experiments of Figures 4.5A, acetate was the other major anion in the intracellular solution. The smooth curve in Figures 4.5A and B is the Goldman-Hodgkin-Katz equation for a channel with a permeability ratio $P_{acetate}/P_{chloride} = 0.1$. $E_{rev} = -(RT/F).\ln\{([Cl^-]_o+0.1[acetate^-]_o)/([Cl^-]_i+0.1[acetate^-]_i)\}$. (Use of this equation assumes that extracellular gluconate (the large anion used to replace extracellular chloride for the experiments of

Figure 4.4 Dependence of the glutamate-induced current on external chloride concentration.

A and B. Glutamate-induced currents in a double cone voltage-clamped to the potential shown beside each current trace. Timing of iontophoresis is shown by the bottom trace. The patch pipette solution contained 9 mM chloride (solution C9, Table 2.3). The external solution in **A** was Ringer's containing 6mM barium and 126mM chloride (solution RB, Table 2.1), and in **B** barium Ringer's containing 22mM chloride (chloride replaced by gluconate: solution C22, Table 2.1).

C. Peak glutamate-induced currents (ordinate) as a function of membrane potential (abscissa) for the experiments in: A (126mM $[Cl^-]_o$), the reversal potential of the response is -43mV; and B (22mM $[Cl^-]_o$), reversal potential of the response is -10mV.

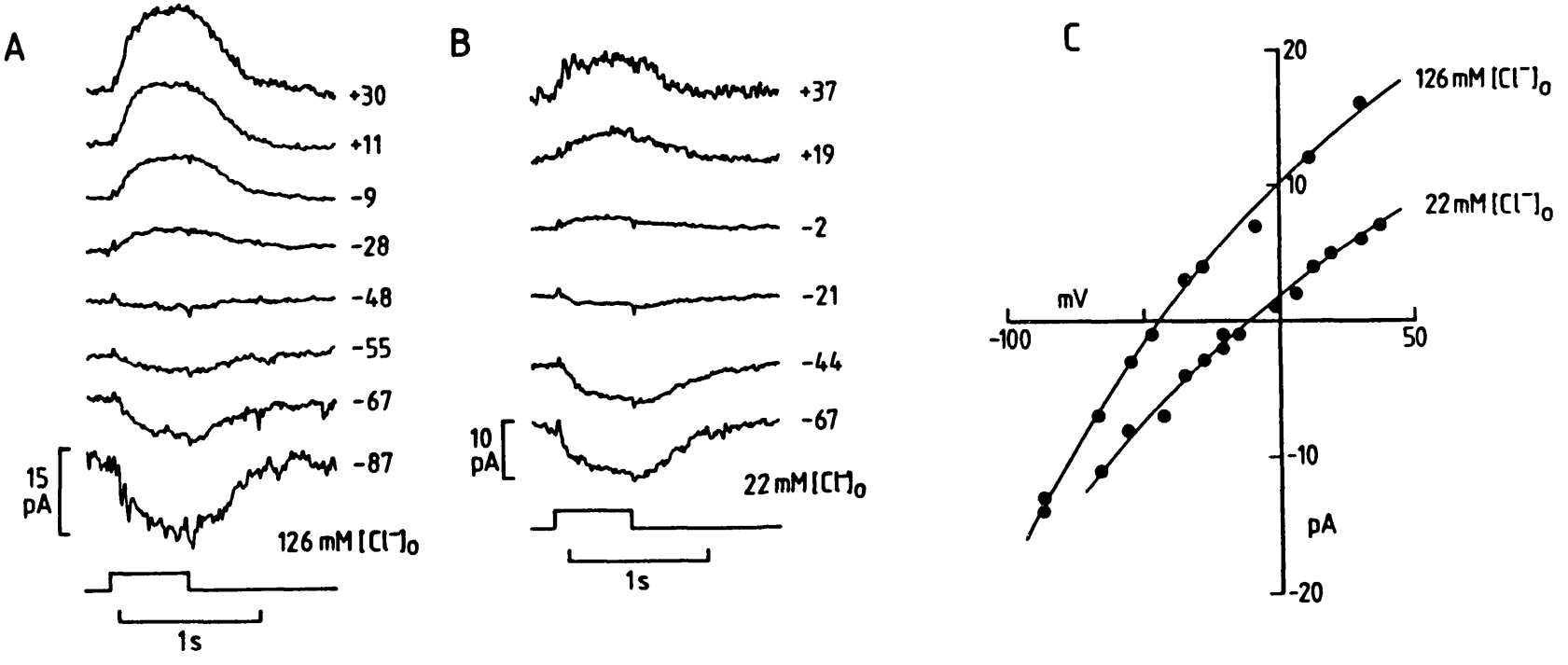
A
+30
+11
-9
-28
-48
-55
-67
-87
15 pA
126 mM [Cl⁻]o
1s
B
+37
+19
-2
-21
-44
-67
10 pA
22 mM [Cl⁻]o
1s
C
20
10
-10
-20
mV
-100
50
pA
126 mM [Cl⁻]o
22 mM [Cl⁻]o

Figure 4.5 Reversal potential of the current induced by glutamate as a function of chloride concentration.

A. Reversal of the glutamate-induced current (ordinate) as a function of the chloride concentration in the patch pipette (abscissa). Filled circles are the mean reversal potentials (bars indicate standard deviation) from experiments on isolated cones. Values were (in mV): -47 ±1.7 (s.d.) (n=4), -27.7 ±2.1 (n=6), and -3.1 ±5.7 (n=10) for 9, 30 and 101mM internal chloride respectively. The dashed line is the Nernst prediction ($E_{rev} = -(RT/F).\ln([Cl^-]_o/[Cl^-]_i)$) for a chloride-specific channel. The smooth curve is the Goldman-Hodgkin-Katz equation for a channel with permeability ratio $P_{acetate}/P_{chloride}=0.1$.

B. Reversal potential of the current induced by glutamate (ordinate) as a function of chloride concentration in the superfusion solution. Filled circles are the mean reversal potentials (±s.d.) from experiments on isolated cones. Values were (in mV): -41.5 ±1.5 (s.d.) (n=2) and -11.0 ±1.0 (n=2) for 126 and 22mM external chloride respectively. The dashed line is the Nernst prediction for a chloride-specific channel. The smooth curve is the Goldman-Hodgkin-Katz equation for a permeability ratio $P_{acetate}/P_{chloride} = 0.1$, and $P_{gluconate}/P_{chloride}=0$. The dashed curve is the Goldman-Hodgkin-Katz equation for permeability ratios $P_{acetate}/P_{chloride}=0.1$ and $P_{gluconate}/P_{chloride}=0.1$.

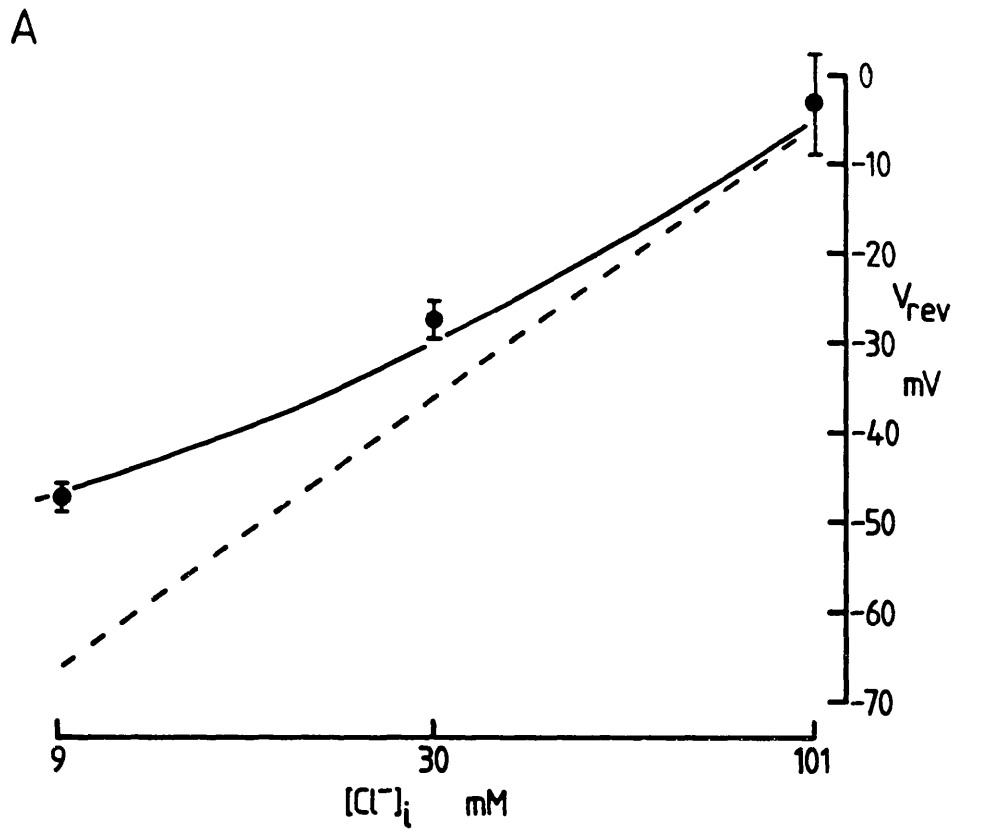
A
0
-10
-20
V_{rev}
-30
mV
-40
-50
-60
-70
9
30
101
$[Cl^-]_i$ mM

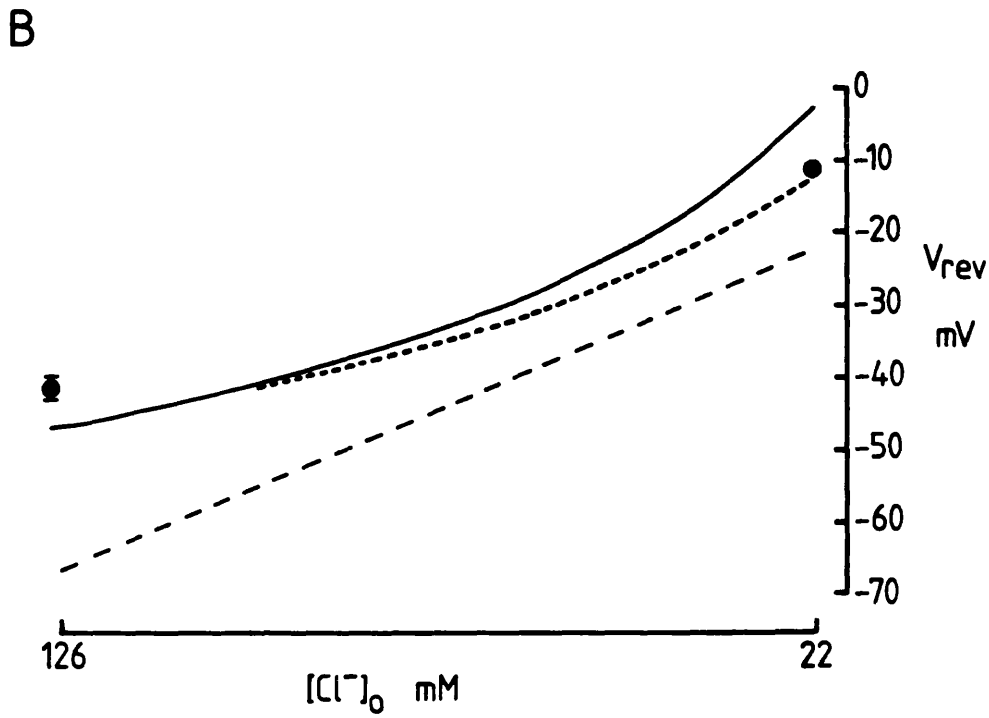
B
0
-10
-20
V_{rev}
-30
mV
-40
-50
-60
-70
126
22
$[Cl^-]_o$ mM

Figure 4.5B is not permeant through the channel). In Figure 4.5A this curve fits the data points (obtained from experiments in which internal chloride was replaced by acetate) quite well but the fit in Figure 4.5B is poor. In Figure 4.5B, the data points from experiments in which external chloride was replaced by gluconate (closed circles) are better fitted by a Goldman-Hodgkin-Katz equation: $E_{rev} = -(RT/F) \cdot \ln\{([Cl^-]_o+(0.1[acetate^-]_o)+(0.1[gluconate^-]_o))/([Cl^-]_i+(0.1[acetate^-]_i)+(0.1[gluconate^-]_i))\}$ with permeability ratios $P_{acetate}/P_{chloride}=0.1$ and $P_{gluconate}/P_{chloride}=0.1$ (dashed curve).

4.3.5. The glutamate-induced increase in chloride conductance in cones is different from that evoked by gamma-aminobyturic acid

I considered the possibility that the glutamate-induced anion current in cones could in fact be an indirect effect due to GABA acting on the cone membrane. This could happen for the following reason: theoretically, it might be possible for a piece of horizontal cell to stay attached to the cone synaptic pedicle during the cell isolation procedure, since horizontal cell dendrites invaginate the cone synapse (Chapter 6, Figure 6.2). In vivo, glutamate released from cones depolarizes horizontal cells. If a piece of horizontal cell stayed attached to the isolated cone, glutamate applied during experiments could depolarize the piece of horizontal cell, which in turn could lead to GABA being released from this piece of cell (Ayoub and Lam, 1984) and activating chloride channels in the cone membrane. GABA has been shown to gate chloride channels in turtle cones (Kaneko and Tachibana, 1986).

To check that GABA itself did not affect the size of the glutamate-induced current in cones, 200μM GABA in Ringer's was perfused onto isolated cones while they were responding to glutamate applied by iontophoresis. Application of GABA had no effect on the magnitude of the glutamate-induced current in 5 cells (Figure 4.6A). Interestingly, GABA evoked no current itself, possibly because the GABA receptors believed to exist on the cone synaptic terminal were somehow lost during the cell isolation procedure.

Receptors for GABA which gate chloride channels in the cone have been shown to be $GABA_A$-type receptors (Kaneko and Tachibana,

Figure 4.6 GABA does not affect the glutamate-induced current in isolated cones.

A. Glutamate was repeatedly applied by iontophoresis (bottom trace) to an isolated single cone voltage-clamped at -55mV. The patch pipette contained solution C101 (Table 2.3). 200μM GABA was added to the superfusion solution (solution RB, Table 2.1). GABA did not affect the glutamate-induced current.

B. Glutamate was repeatedly applied by iontophoresis (bottom trace) to an isolated single cone voltage-clamped at -53mV. The patch pipette contained solution C101 (Table 2.3). 100μM bicuculline and 10μM strychnine were added to the superfusion solution (solution RB, Table 2.3) and did not affect the glutamate-induced current.

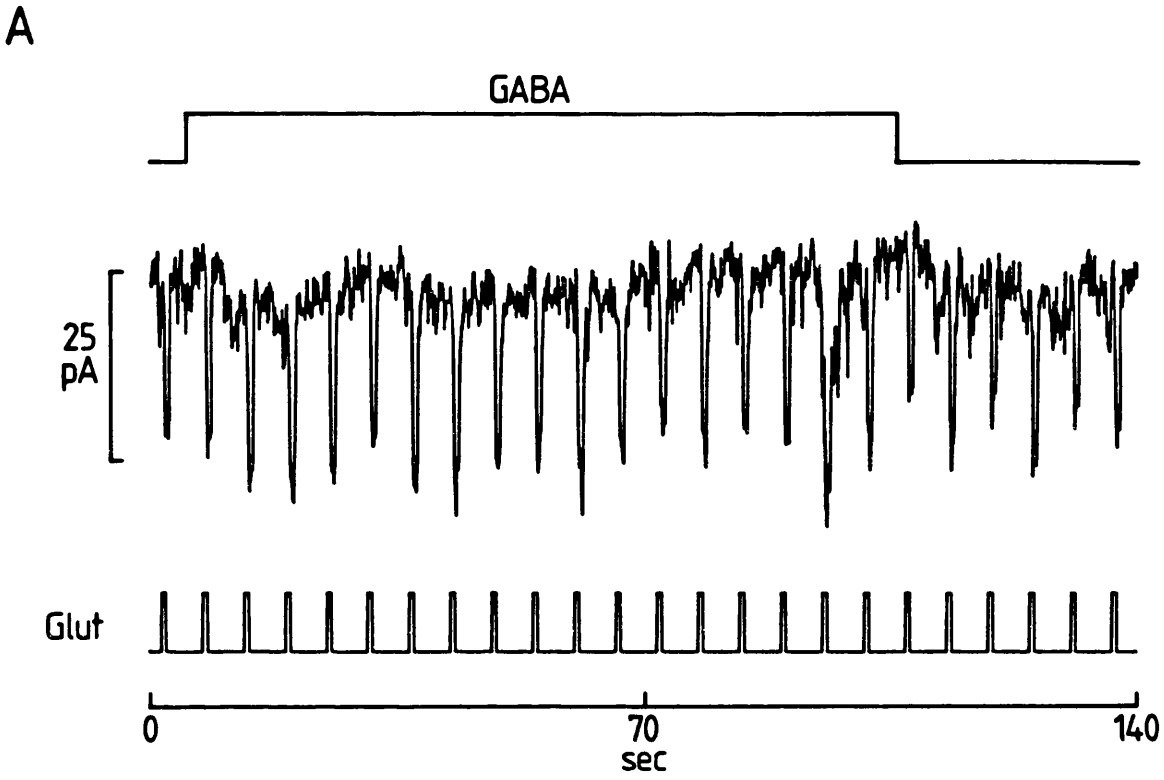
A
GABA
25
pA
Glut
0
70
140
sec

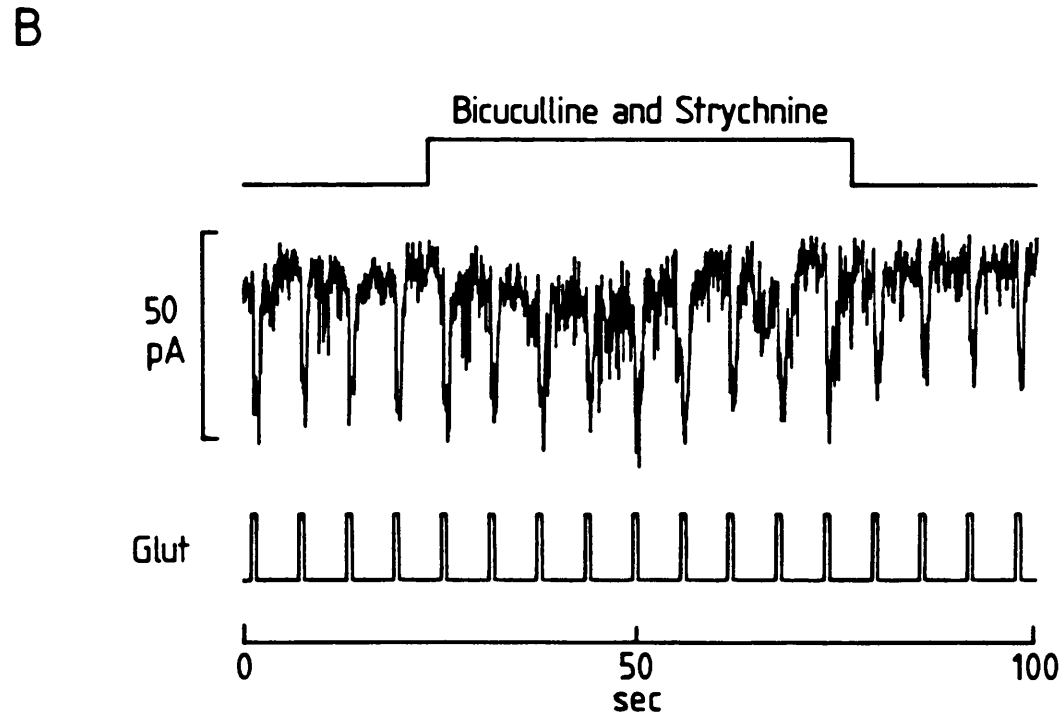
B
Bicuculline and Strychnine
50
pA
Glut
0
50
100
sec

1986). Figure 4.6B shows an experiment in which, during application of glutamate to an isolated cone, the $GABA_A$ antagonist bicuculline (100μM) and the glycine antagonist strychnine (10μM, to block any possible glycinergic input) were applied. Application of these antagonists did not significantly affect the magnitude of the glutamate-induced current (n=10 cells).

To check that the antagonists bicuculline and strychnine were effective at blocking GABA and glycine-induced currents at the concentrations used, these agents effects were tested on other retinal neurones. 100μM bicuculline blocked the GABA-induced current in isolated retinal ganglion cells (Figure 4.7A) (n=4 cells), and 10μM strychnine blocked the glycine-induced current in isolated retinal bipolar cells (Figure 4.7B) (n=4 cells).

The results described above show that the glutamate-induced current in isolated cones is not a result of GABA-gated chloride channels being opened by glutamate-induced release of GABA from a hypothetical piece of horizontal cell left attached to the cone synaptic terminal.

4.3.6 The effect of sodium removal on the glutamate-induced current when the external calcium concentration is low

A possible explanation for the sodium-dependence of the glutamate response in cones is that removal of external sodium ions may inhibit sodium-calcium exchange in the membrane, resulting in the accumulation of calcium inside the cell. This increase in intracellular calcium may inhibit the glutamate-evoked current. An elevation of intracellular calcium has been shown to accelerate a run down of GABA responses in hippocampal neurones, by stimulating a calcium-dependent phosphatase (Chen et al., 1990). To investigate this possibility I carried out experiments in which the external sodium concentration was reduced (sodium replaced by choline) in the presence of a very low concentration of external calcium (to prevent a build-up of internal calcium). If sodium removal does abolish the glutamate-evoked current by inhibiting sodium-calcium exchange, one would expect sodium removal to have no effect on the glutamate-evoked current in this situation.

In Figure 4.8 are the responses of a cone voltage-clamped at -50mV to which glutamate was repeatedly applied by iontophoresis,

Figure 4.7 Bicuculline and strychnine block the currents in retinal neurones evoked by GABA and glycine respectively.
A. GABA was applied by iontophoresis (bottom trace) to an isolated ganglion cell voltage-clamped at -36mV. The patch pipette contained solution Cl01 (Table 2.2). 100μM bicuculline was added to the superfusion solution (solution RA, Table 2.1) and blocked the GABA-induced current.
B. Glycine was applied by iontophoresis (bottom trace) to an isolated bipolar cell voltage-clamped at -42mV. The patch pipette contained solution Cl01 (Table 2.3). 10μM strychnine was added to the superfusion solution (solution RA, Table 2.1) and blocked the glycine-induced current.

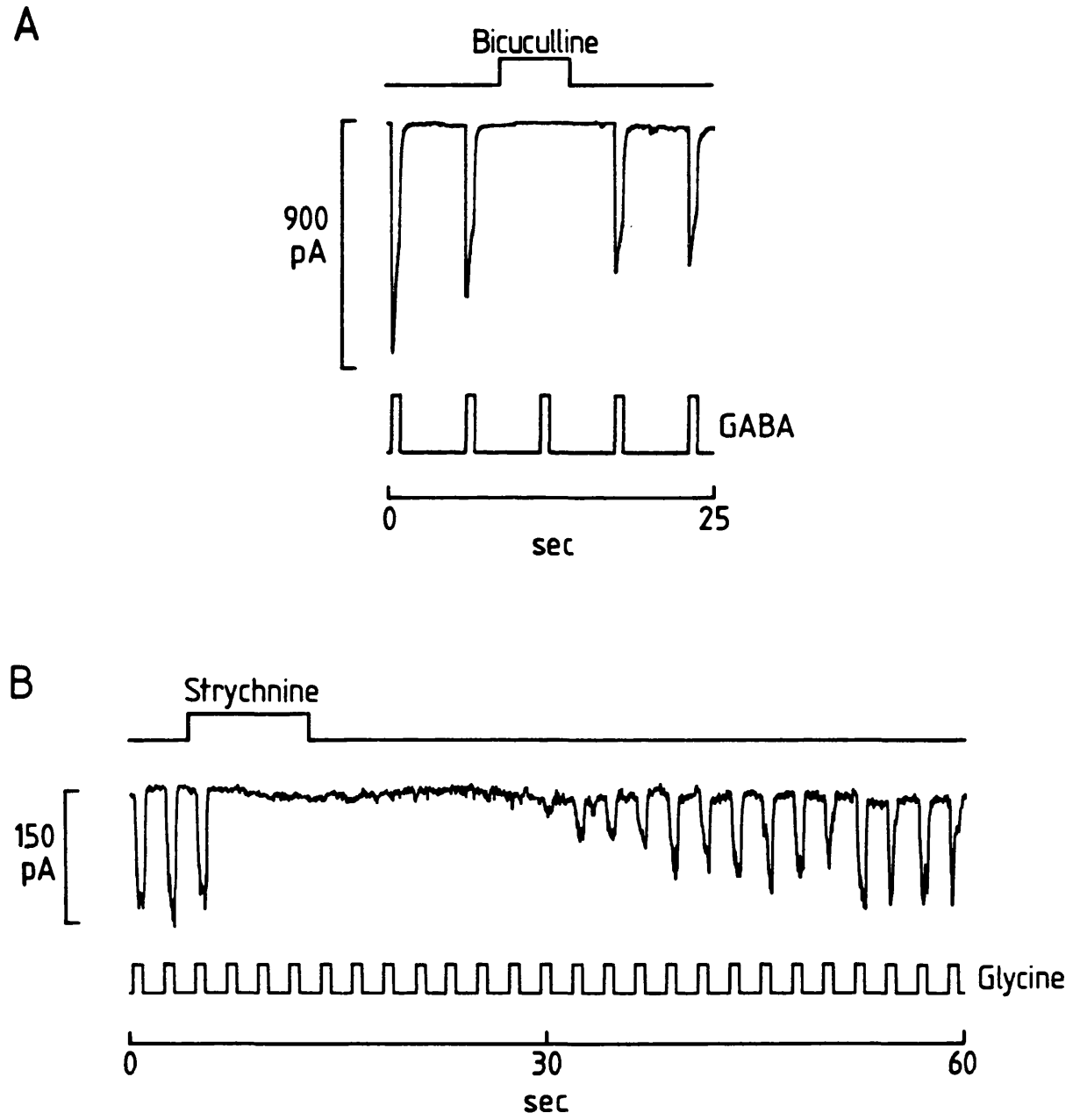
A
Bicuculline
900
pA
GABA
0
25
sec
B
Strychnine
150
pA
Glycine
0
30
60
sec

Figure 4.8 Removal of external sodium abolished the glutamate-evoked current even when $[Ca^{2+}]_o$ is low.
Glutamate was applied by iontophoresis (bottom trace) to half of an isolated double cone voltage-clamped at -50mV. The patch pipette contained solution Cl01 (Table 2.3). The top two traces give the concentrations of sodium and calcium in the superfusion solutions. Normal Ringer's contained 107 or 108mM sodium and 3mM calcium (solution RA, Table 2.3). The first part of the figure shows a reduction in the glutamate-induced current when the extracellular sodium concentration is reduced (sodium replaced by choline) in the presence of 3mM extracellular calcium. In the second part of the figure, Ringer's solution contains 3×10^{-8}M calcium (1×10^{-4}M $[Ca^{2+}]$ buffered by EGTA: solution LCa, Table 2.2). Reducing extracellular calcium had no effect on the glutamate-induced current. When sodium is reduced in low calcium Ringer's (i.e. in solution Na2/LCa, Table 2.2), the glutamate-induced current is still reduced.

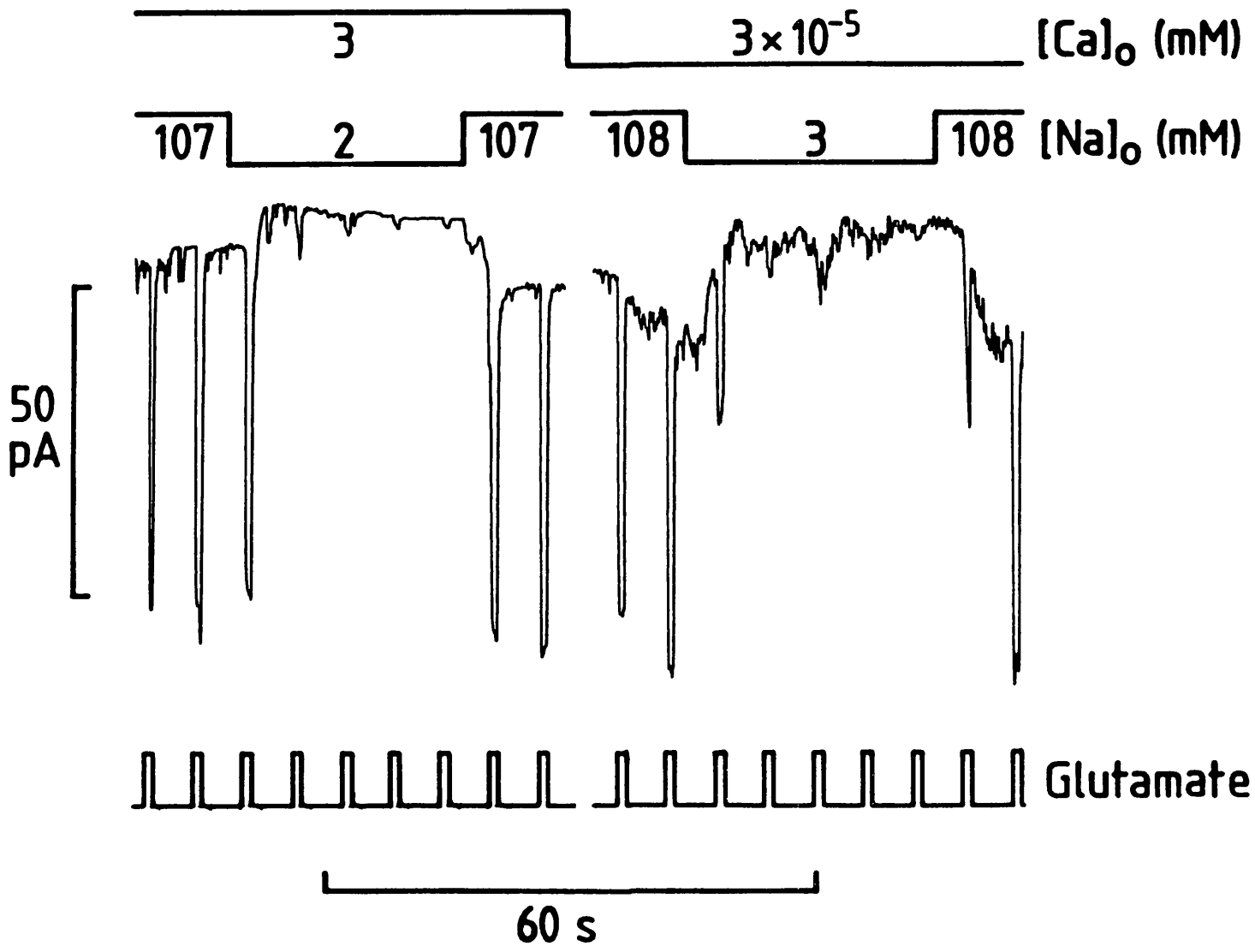
3
3×10⁻⁵
[Ca]o (mM)
107
2
107
108
3
108
[Na]o (mM)
50
pA
Glutamate
60 s

evoking an inward current of around 55pA. For the first part of the figure, normal barium-free Ringer's (containing 107mM sodium and 3mM calcium; solution RA, Table 2.1) was replaced by Ringer's containing 2mM sodium (and 3mM calcium; solution Na2, n=0, without barium chloride, Table 2.2). Lowering external sodium virtually abolished the glutamate-induced current as in Figure 4.1. For the second part of the figure the experiment was repeated but now the Ringer's solutions contained 0.1mM $CaCl_2$ and 0.5mM EGTA to reduce the free calcium concentration to a calculated 3×10^{-8}M, while sodium was reduced from 108 to 3mM (solutions LCa and Na2/LCa, Table 2.2).

Under these conditions the glutamate-induced current was still reduced in external solutions containing low sodium concentrations (n=4 cells). This suggests that the reduction in glutamate-induced current in external solutions containing 2mM sodium is not due to a build-up of intracellular calcium following inhibition of sodium-calcium exchange. It may be that the suppressive effect of sodium removal results from sodium being required in some way for glutamate to be able to bind to its receptor in the membrane of the cone synaptic terminal. Further work is needed to resolve this point.

Chapter 5

Electrogenic uptake of glutamate into retinal glial (Müller) cells

5.1 Introduction

This chapter describes experiments showing that application of glutamate evoked an inward current in isolated glial (Müller) cells of the rabbit retina. This current is different from the glutamate-induced current in cone photoreceptors as described in Chapters 3 and 4: in this chapter I describe experiments which indicate that in Müller cells glutamate does not increase the conductance by opening ion channels, but that a current is generated by the uptake of glutamate via an electrogenic carrier mechanism. The use of the whole-cell variant of the patch-clamp technique enabled me to study the uptake mechanism in single cells, while controlling the membrane potential and the composition of intra- and extracellular solutions. Experiments to study the glutamate-evoked current in rabbit Müller cells are dealt with under the following headings:

(1) Pharmacological profile of the glutamate-induced current. (2) Voltage-dependence of the glutamate-induced current. (3) Dependence of the glutamate-induced current on external glutamate concentration. (4) The effect of a blocker of glutamate uptake. (5) Dependence of the glutamate-induced current on external sodium concentration. (6) Dependence of the glutamate-induced current on internal potassium concentration. (7) Dependence of the glutamate-induced current on external potassium concentration. (8) Prediction of the inhibition of Müller cell glutamate uptake during ischaemia or anoxia.

The main purpose of these experiments was to test whether, as in the Müller cells of lower vertebrates, glutamate uptake into mammalian Müller cells is electrogenic and can be studied by patch-clamping. As will be seen below, these experiments on mammalian cells are much harder than those on lower vertebrates, because the glutamate-evoked current is much smaller. Nevertheless, useful information on the properties of mammalian glutamate uptake was obtained.

5.2 Methods

The experiments described in this chapter were performed on retinal glial (Müller) cells from the rabbit. The cells were isolated by enzymatic dissociation of the retina (Chapter 2, section 2.1.1.3). Pipettes to whole-cell patch-clamp the cells contained solution Q (Table 2.5) except for experiments in which the effect of changes in internal potassium ion concentration was studied (section 5.3.6), in which case the patch pipette contained solutions K140-K0 (Table 2.5). Pharmacological agents were added to Ringer's and applied by bath-perfusion. Glutamate was often applied by iontophoresis, evoking an inward current typically of about 12pA at -40mV.

The external solution in almost all experiments contained 6mM barium. The membrane current is less noisy in barium Ringer's (noise decrease measured in 3 cells), because barium blocks most of the cells' potassium conductance (Newman, 1985). This lower current noise facilitated accurate measurement of the size of the glutamate-induced current. Adding barium to the Ringer's had little effect on the size of the glutamate-induced current when cells were held at voltages ranging from -43 to -90mV. For example in Figure 5.1 the responses of a rabbit Müller cell to glutamate (applied by iontophoresis at-43mV), are similar in normal Ringer's (solution RC, Table 2.4), and in Ringer's containing 6mM barium (solution RD, Table 2.4).

5.3 Results

5.3.1 Pharmacological profile of the glutamate-induced current

In order to determine whether the pharmacological properties of the mechanism responsible for the glutamate-induced current in rabbit Müller cells were similar to those of glutamate-activated channels or those of a glutamate transporter, various analogues of glutamate were applied to cells.

Figure 5.2 shows that an inward current of 13pA is activated by bath-perfusion of 20μM glutamate in a cell voltage-clamped at -43mV. When D- (D-ASP) and L-aspartate (L-ASP) (20μM), which are known to be tranported on the glutamate uptake carrier (Balcar and Johnston, 1972; Brew and Attwell, 1987; Barbour, Brew and Attwell, 1991), were applied to the same cell, a current similar to that evoked by

Figure 5.1 Barium has little effect on the glutamate-induced current in isolated rabbit Müller cells.
Glutamate was applied by iontophoresis (timing shown by the top trace) to a Müller cell, isolated by enzymatic dissociation (section 2.1.1.3) and voltage-clamped at -43mV. The patch pipette contained solution Q (Table 2.5). In **A** the external solution was Ringer's (solution RC, Table 2.4), and in **B** the external solution was Ringer's containing 6mM barium (solution RD, Table 2.4). Adding barium reduces the current noise fluctuations without greatly affecting the size of the glutamate-induced current.

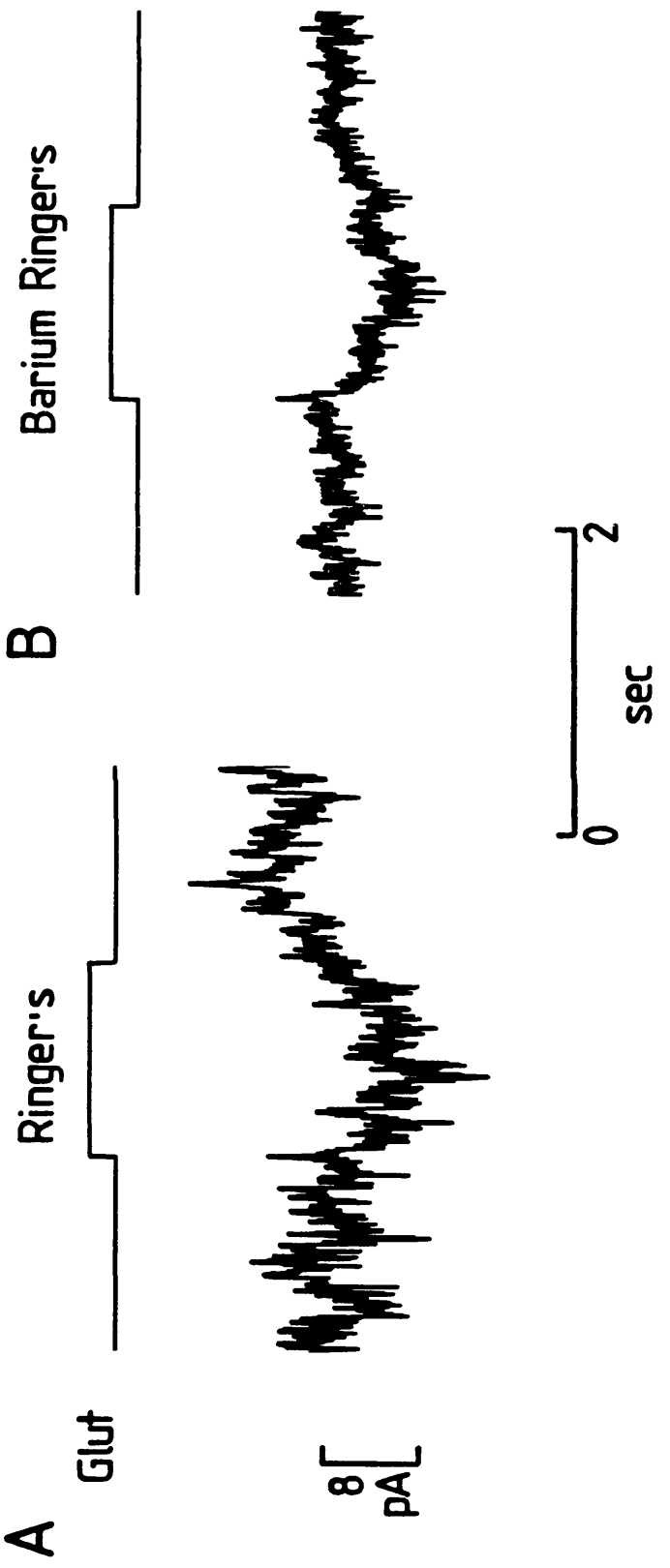
A
Glut
Ringer's
8
pA
B
Barium Ringer's
0
2
sec

Figure 5.2 Pharmacology of the glutamate-induced current in Müller cells.

The current induced by 20μM concentrations of L-glutamate (L-GLU), N-methyl-D-aspartate (NMDA), kainate (KA), quisqualate (QUIS), D-aspartate (D-ASP) and L-aspartate (L-ASP) by bath-perfusion (as indicated by the bar above each current trace), in a Müller cell voltage-clamped at -43mV. The patch pipette contained solution Q (Table 2.5) and the superfusion solution was Ringer's containing 6mM barium (solution RD, Table 2.4).

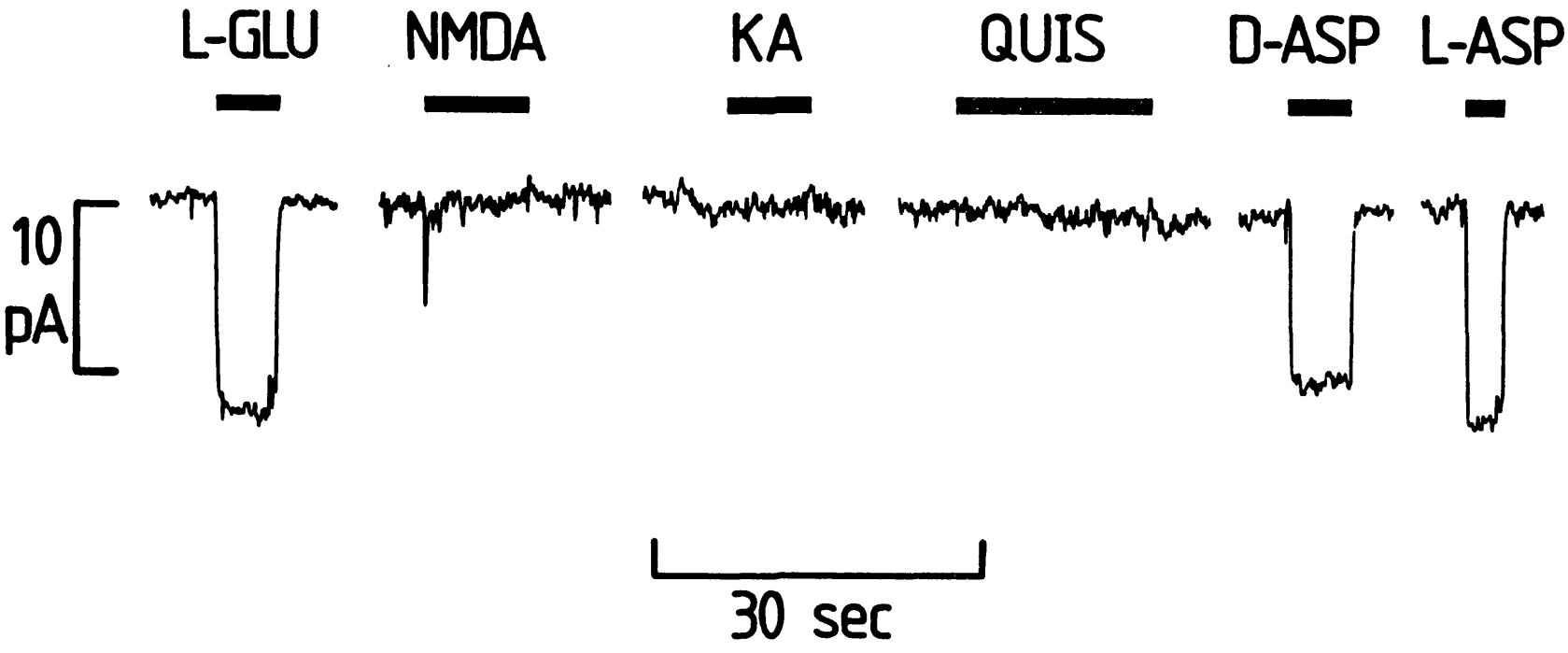
L-GLU
NMDA
KA
QUIS
D-ASP
L-ASP
10
pA
30 sec

glutamate was recorded. However, the analogues that relatively selectively activate different types of glutamate-gated ion channel, i.e. N-methyl-D-aspartate (NMDA), kainate (KA) and quisqualate (QUIS) produced almost no current (Figure 5.2). In three cells the mean current evoked at -43mV by 20μM L-glutamate, L-aspartate, D-aspartate, kainate, NMDA and quisqualate had relative magnitudes 1 : 0.99 : 0.79 : 0.02 : 0.02 : 0. This pharmacological profile is as expected for glutamate uptake, since kainate, NMDA and quisqualate are not usually taken up (Stallcup, Bulloch and Baetge, 1979; Watkins and Evans, 1981).

5.3.2 Voltage-dependence of the glutamate-induced current in Müller cells

The current evoked by glutamate in isolated Müller cells was strongly voltage-dependent. Figure 5.3A shows the currents induced in a cell by iontophoretically applied glutamate at voltages as indicated next to each current trace. At -43mV, which is around the resting potential of the cell in Ringer's containing 6mM barium, the inward current evoked by glutamate in this cell was -37pA. The average current evoked in Müller cells by glutamate applied iontophoretically in cells held at -43mV was -12.3 ±8.7 (s.d.) pA (n=16 cells).

The inward current was larger at more hyperpolarized potentials and smaller at potentials positive to -43mV. However, the current did not reverse, even when the cell was depolarized to +50mV (Figure 5.3B). The reversal potential of most glutamate-gated channels is around 0mV. This current-voltage relation is therefore consistent with glutamate activating an uptake carrier which transports a net positive charge into the cell. The positive charge presumably reflects the co-transport of excess sodium ions into the cell with each glutamate anion (see section 5.3.5 below). Note that although, in principle, the net current generated by the uptake carrier must have a reversal potential, the change of current generated when glutamate is applied to the outside of the cell (forcing the carrier to operate more in the uptake direction) will always be inward (Chapter 7, section 7.2.1): the magnitude of the inward current decreases as the potential is made more positive, simply because it is more difficult to transport positive charge into the cell at more

Figure 5.3 Voltage-dependence of the glutamate-induced current in Müller cells.

A. Changes in membrane current of an isolated, voltage-clamped Müller cell in response to iontophoresis of glutamate (timing indicated by the top trace) at membrane potentials as shown alongside each current trace. The patch pipette contained solution Q (Table 2.5). The extracellular solution was Ringer's containing 6mM barium (solution RD, Table 2.4).

B. Peak glutamate-induced currents (ordinate) as a function of membrane potential (abscissa) for the experiment in A.

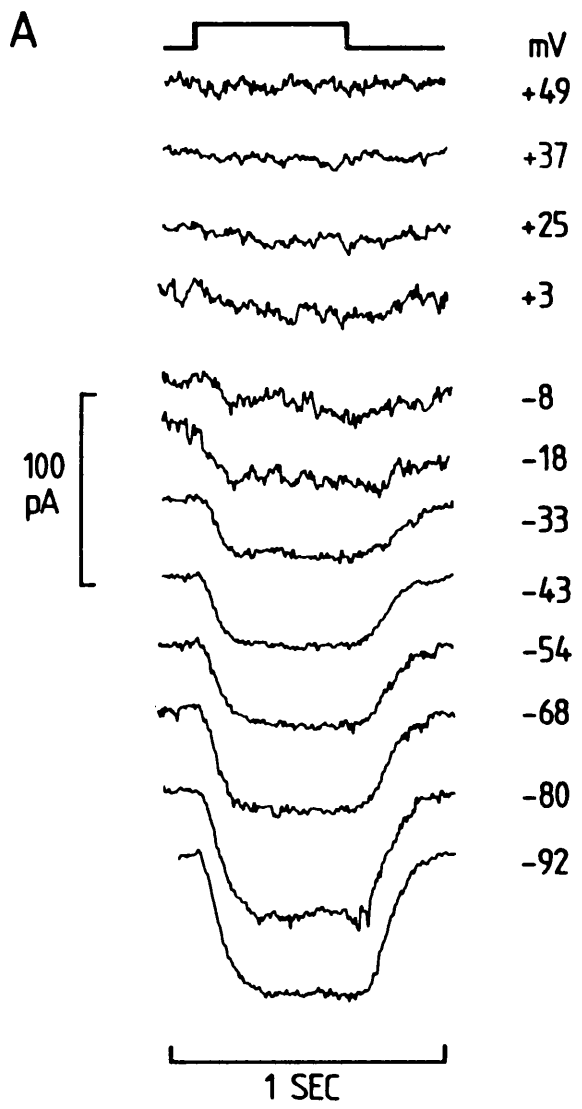
A
mV
+49
+37
+25
+3
-8
-18
-33
-43
-54
-68
-80
-92
100
pA
1 SEC

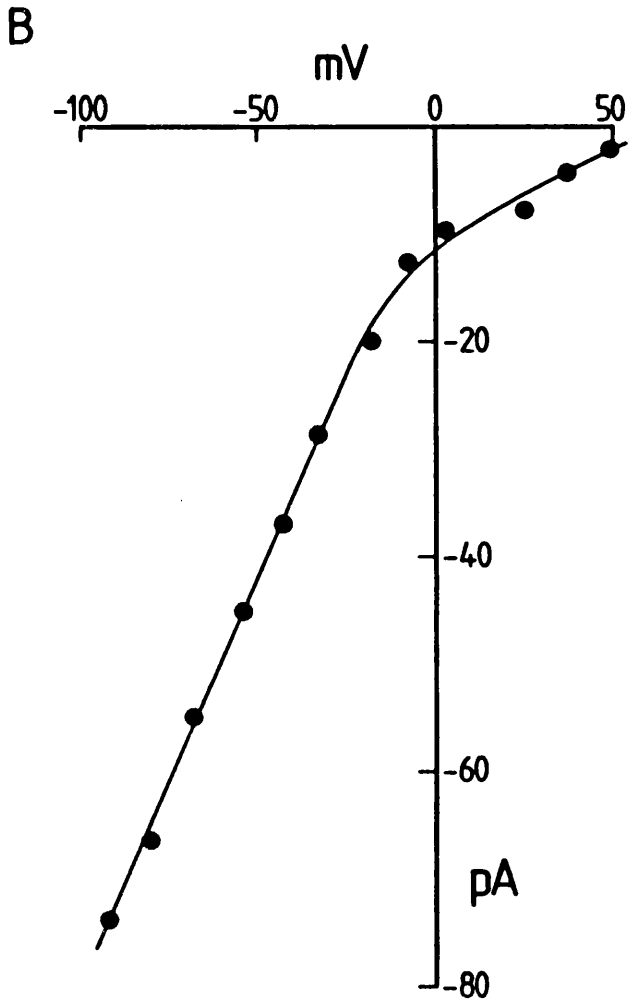
B
mV
-100
-50
0
50
-20
-40
-60
-80
pA

positive potentials.

5.3.3 Dependence of the glutamate-induced current on external glutamate concentration

Part A of Figure 5.4 shows the current flowing across the membrane of a Müller cell held at -43mV, during the sequential application, by bath-perfusion, of solutions containing different concentrations of glutamate. The currents became larger with higher glutamate concentrations up to 1000μM (which gave a maximum current in this cell of 8pA). Part B of Figure 5.4 shows the average dose-response data (±s.d.) from experiments like that in A on 4 cells at -43mV. The curve through the points is a Michaelis-Menten relation (current=[glutamate]/([glutamate]+K_m)). The fact that the activation of the current by glutamate obeys Michaelis-Menten (first order) kinetics suggests that one glutamate anion is transported into the cell for each cycle of the uptake carrier. The K_m for the mean data, obtained from Lineweaver-Burke plots, was 4.7 ±0.6μM. This low value for K_m indicates that the glutamate uptake system present is a high affinity system. Radiotracing data have previously shown the existence of two types of uptake systems: high affinity (with K_m around 25μM) and low affinity (with $K_m \geq 0.2$mM) (Lerner, 1987).

5.3.4 The effect of a blocker of glutamate uptake

A blocker of glutamate uptake, threo-3-hydroxy-DL-aspartate (THDA) (Balcar and Johnston, 1972) was tested, to determine whether the glutamate-induced current was inhibited by this agent. Inhibition of the current would be expected if the current was due to a carrier, while if the current was flowing through glutamate-gated channels one might expect the current to be unaffected or even potentiated (if the glutamate concentration near the channels becomes higher due to the inhibition of uptake).

Figure 5.5 shows the effect of 30μM THDA on the current induced in a Müller cell by iontophoretically applied glutamate. On application of THDA, the glutamate-induced current was greatly reduced. THDA itself produced an inward current (i.e. the baseline current in the absence of glutamate moved inward), suggesting that this analogue of glutamate is transported into the cell on the

Figure 5.4 Dose-response data for the glutamate-induced current in Müller cells.

A. The current induced in an isolated Müller cell voltage-clamped at -43mV, by sequential superfusion with barium Ringer's (solution RD, Table 2.4), containing different concentrations of glutamate (shown by the bar below the current trace). Solution Q (Table 2.5) was used to fill the patch pipette.

B. Averaged dose response data (±s.d.) from experiments like that in A on 4 cells at -43mV. Currents were normalized to the response in 1000μM glutamate. The curve through the points is a Michaelis-Menten relation (current=[glutamate]/([glutamate]+K_m)) with K_m=5μM.

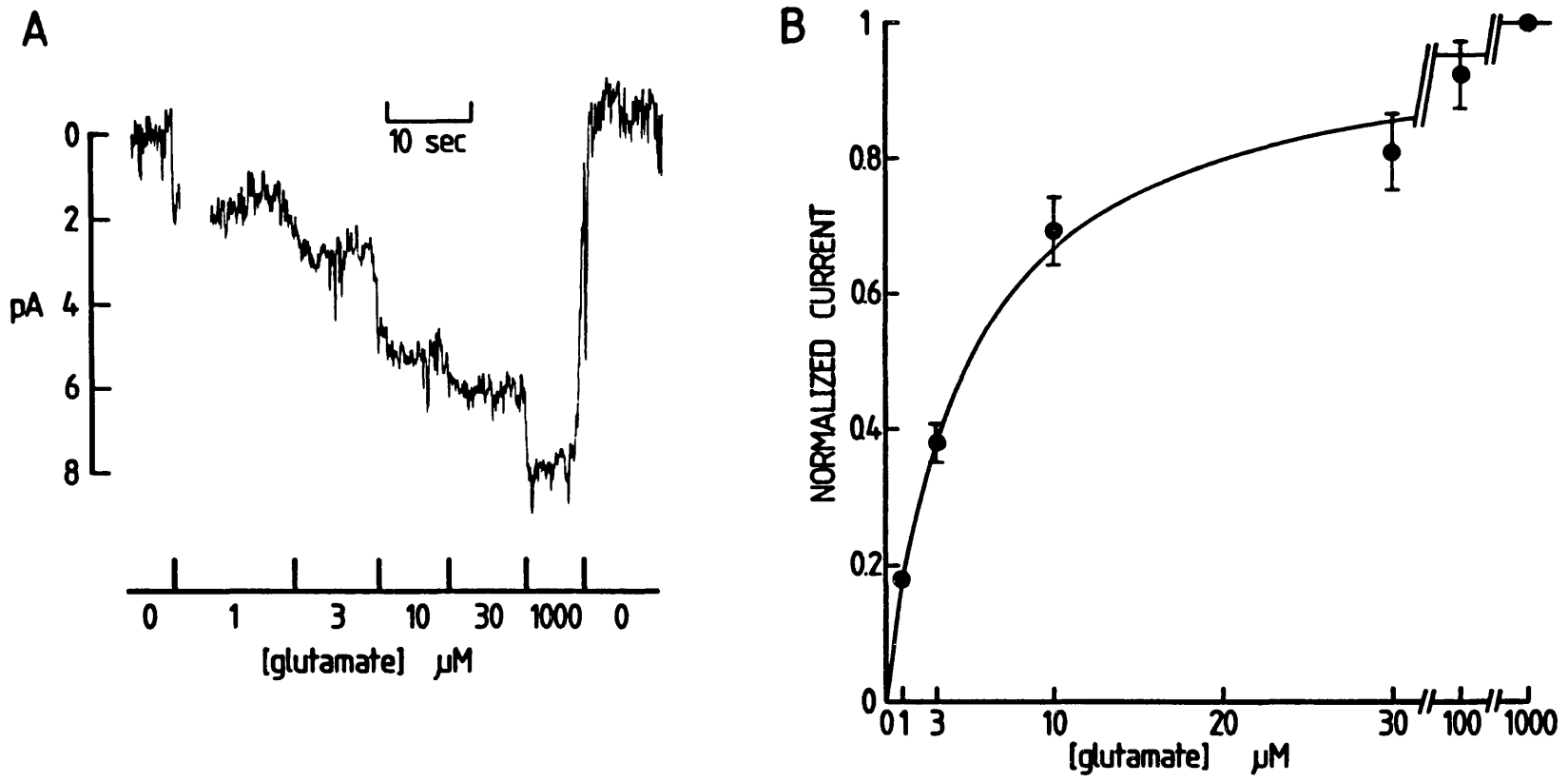
A
10 sec
pA
0
2
4
6
8
0
1
3
10
30
1000
0
[glutamate] µM
B
NORMALIZED CURRENT
1
0.8
0.6
0.4
0.2
0
0 1 3
10
20
30
100
1000
[glutamate] µM

Figure 5.5 The effect of a blocker of glutamate uptake on the glutamate-induced current in Müller cells.
Glutamate was applied by iontophoresis (timing shown by the upward deflections in the bottom trace) to a Müller cell, voltage-clamped at -43mV. Application of 30μM threo-3-hydroxy-DL-aspartate (THDA) by bath-perfusion (shown by the bar at the top), reversibly blocked the glutamate-induced current. The patch-pipette contained solution Q (Table 2.5), and the external solution was barium Ringer's (solution RD, Table 2.4).

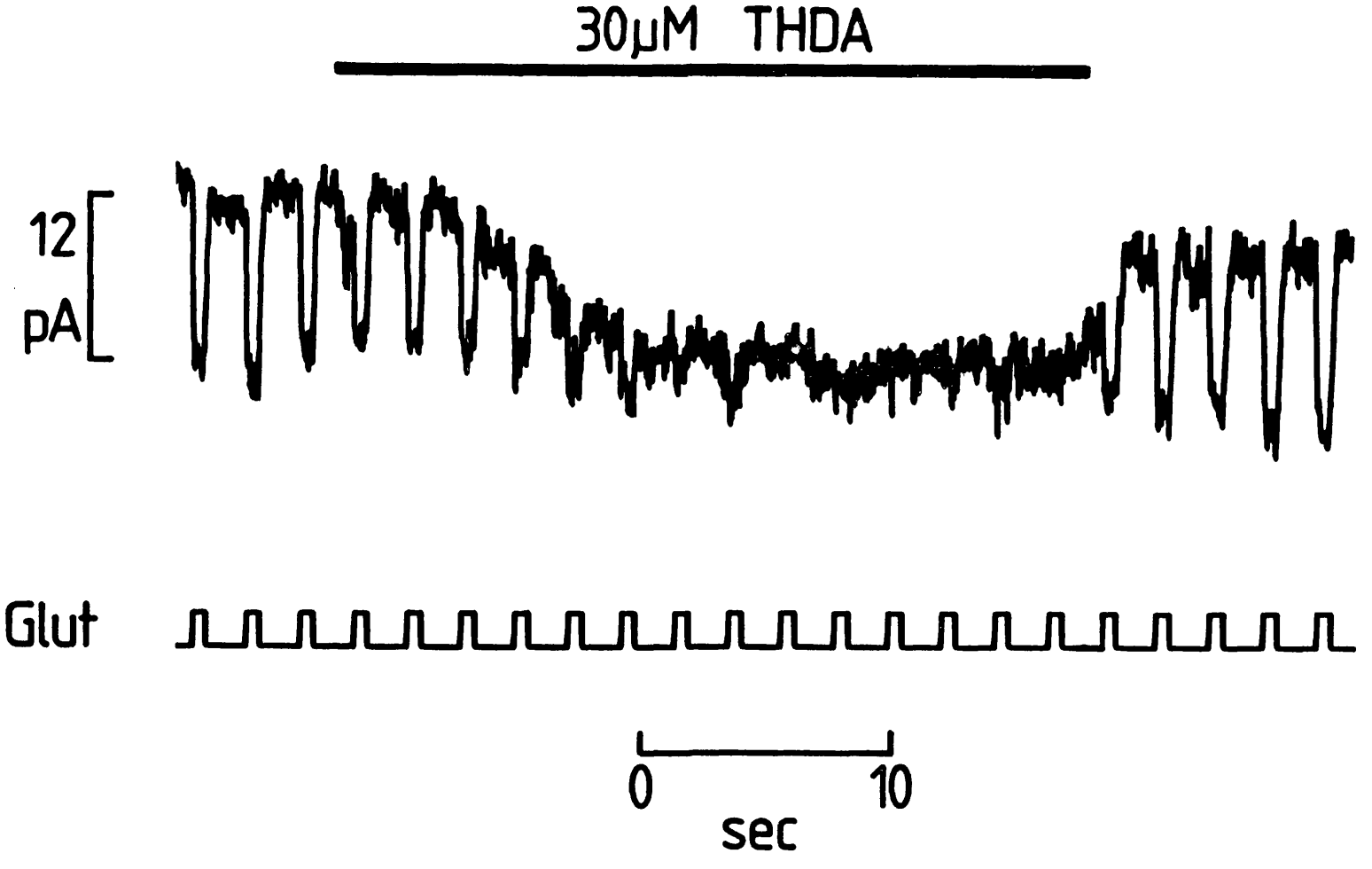
30μM THDA
12
pA
Glut
0
10
sec

glutamate uptake carrier. The inhibition of the glutamate-induced current by THDA (n=2 cells) is consistent with the glutamate-evoked current being due to the activation of a glutamate uptake carrier mechanism. However, since THDA was also shown to block the glutamate-induced conductance increase through channels in the salamander cone synaptic terminal (Chapter 4, section 3.3.5), the blocking action of THDA in Figure 5.5 does not prove that the glutamate-evoked current is due to uptake.

5.3.5 Dependence of the glutamate-induced current on external sodium concentration

Co-transport of sodium ions on the glutamate uptake carrier is thought to provide the energy needed to transport glutamate into the cell. At pH 7.4, more than 99% of glutamate is negatively charged. For glutamate to evoke an inward current in Müller cells, a net positive charge must flow into the cell. Co-transport of more than one sodium ion, with every negatively charged glutamate, could account for the inward current generated when glutamate is applied. To test the dependence of the glutamate-induced current on external sodium concentration, I carried out experiments in which the external sodium was partly replaced by choline.

Figure 5.6A shows the currents evoked when glutamate was applied by iontophoresis to a Müller cell bathed in solutions containing different concentrations of sodium ions. In 143mM external sodium (normal Ringer's), glutamate evoked a 17pA current. The current became smaller as the superfusion solution was replaced by Ringer's containing less sodium, and in 2.5mM external sodium the glutamate-evoked current was abolished.

In Figure 5.6B the normalized glutamate-induced currents from experiments such as in A were plotted against external sodium concentration. The dependence of current on external sodium had a sigmoid onset at low concentrations, suggesting that two or more sodium ions are transported on the uptake carrier. The currents at low $[Na^+]_o$ were too small to determine accurately whether the current is proportional to the 2nd, 3rd or a higher power of $[Na^+]_o$.

5.3.6 Dependence of the glutamate-induced current on internal potassium concentration

It has been suggested, on the basis of radiotracing experiments

Figure 5.6 Sodium-dependence of the glutamate-induced current in Müller cells.

A. Glutamate-induced currents in a Müller cell voltage-clamped at -43mV. Each current trace is an average of 3 responses. Timing of the iontophoretic application of glutamate is shown by the bar at the top. The patch pipette contained solution Q (Table 2.5). The external solutions were barium Ringer's with sodium concentrations as indicated next to each current trace (sodium replaced by choline) (solutions RD and Na70-Na2.5, Table 2.4).

B. Normalized sodium dose-response curve from data such as in A. The number of cells is indicated next to each point and the bars indicate s.e.. The currents at each sodium concentration were normalized to the current in Ringer's containing 143mM sodium (ordinate), and plotted against sodium concentration (abscissa).

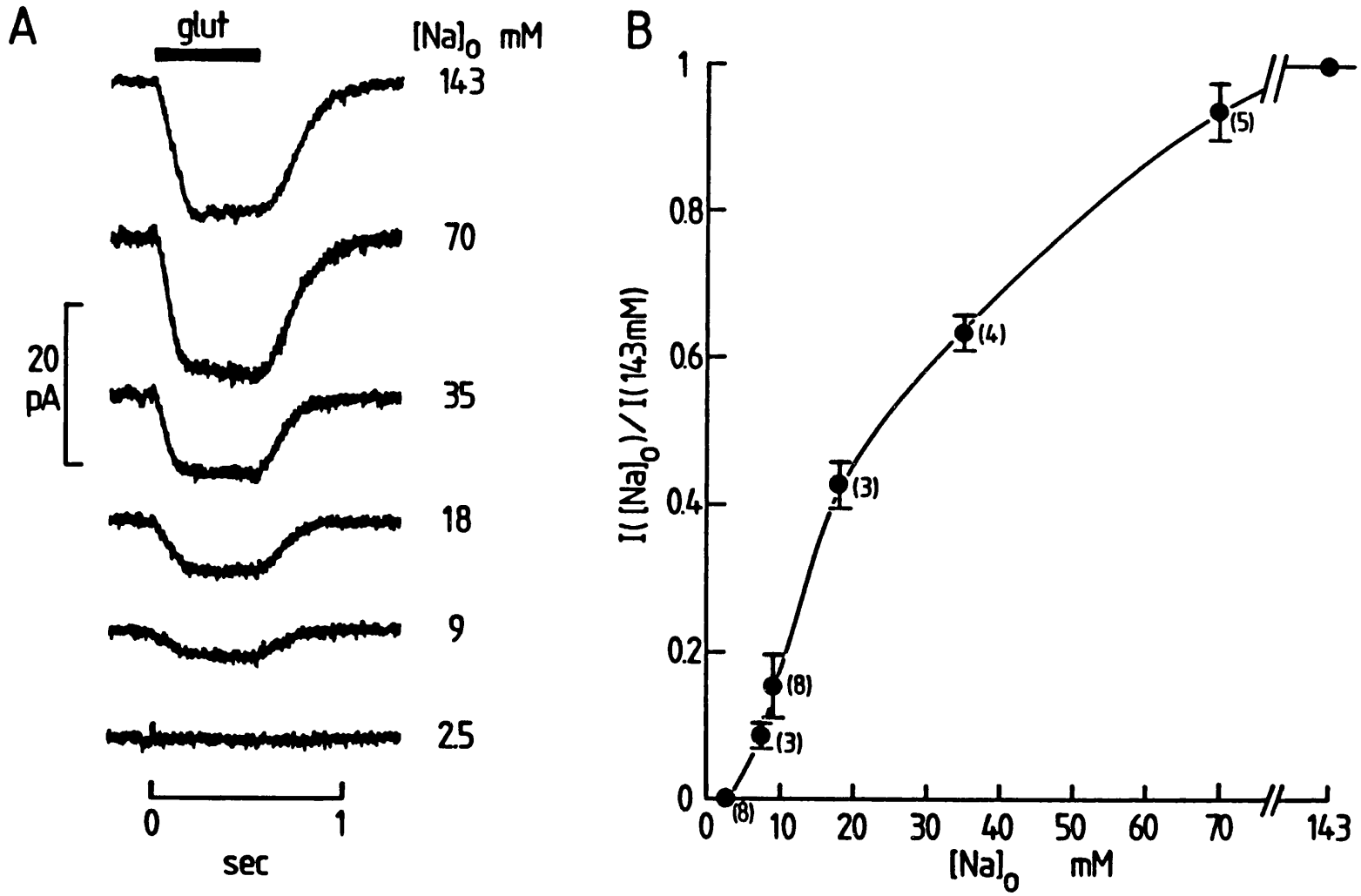
A
glut
[Na]o mM
143
70
35
18
9
2.5
20 pA
0
1
sec
B
I([Na]o)/I(143mM)
1
0.8
0.6
0.4
0.2
0
(5)
(4)
(3)
(8)
(3)
(8)
0
10
20
30
40
50
60
70
143
[Na]o mM

and patch-clamp experiments on glial cells of lower vertebrates, that the uptake of glutamate is activated by internal potassium ions (Kanner and Sharon, 1978; Barbour, Brew and Attwell, 1988). I investigated whether this could be the case in rabbit Müller cells, by changing the concentration of potassium ions in the patch pipette and hence in the intracellular solution (potassium was replaced by choline). In these experiments KCl was ommitted from the external medium to prevent potassium ions leaking into the cell through any potassium channels that were not blocked by barium, and thus raising $[K^+]_i$ when $[K^+]_{pipette}$ was zero. Removing external potassium ions has a negligible effect on the glutamate-evoked current when $[K^+]_i$ is high (section 5.3.7, Figure 5.8).

In Figure 5.7A are the responses evoked in three different cells by bath-perfusion of 30μM glutamate when the patch pipette used to record from each cell contained a different potassium concentration. The intracellular solution equilibrated with that in the patch pipette within 2-3 minutes (assessed from a change in glutamate-evoked current). To compare data from different cells studied with different values of $[K^+]_{pipette}$, the current data were normalized by the capacitance of each cell (typically 70pF) to reduce scatter resulting from variation in cell size.

When the potassium concentration in the patch pipette was high (140mM), the current at -43mV was relatively large (173 ±55 (s.d.) pA/nF (n=10 cells)). With 15mM potassium in the patch pipette the glutamate-induced current was reduced to 90 ±50 pA/nF (n=3 cells). When $[K^+]_{pipette}$ was zero, the glutamate-induced current decreased to zero in the first few minutes after going to whole-cell mode (n=8 cells).

In these experiments recordings were made from pairs of cells from the same dissociation, one cell with the patch pipette containing 140mM potassium (control cell) and one cell with either 15 or 0mM potassium in the patch pipette. For Figure 5.7B the currents with 15 and 0mM $[K^+]_{pipette}$ were normalized to the current in the control cell and plotted against potassium concentration in the patch pipette. If the curve through the points were a Michaelis-Menten (more experiments will have to be carried out to establish this), this would imply that the uptake of glutamate is activated by the binding of one potassium ion at the inner surface of the cell

Figure 5.7 The glutamate-induced current in Müller cells is activated by internal potassium.

A. Currents evoked by bath-perfusion (indicated by the bar above each current trace) of 30μM glutamate in three Müller cells voltage-clamped at -43mV, with 140, 15 and 0mM potassium in the patch pipette respectively (potassium replaced by choline: solutions KQ140-KQ0, Table 2.5). The currents were normalized by the capacitance of each cell (61pF, 51pF and 55pF respectively for $[K^+]_{pipette}$=140, 15 and 0mM) to compensate for variation in cell size. The external solution was barium Ringer's (solution RD, Table 2.4) without KCl.

B. Dependence of glutamate uptake current on pipette potassium concentration. The currents obtained as in part A of this figure were first divided by the capacitance of each cell. Secondly, these values of current/capacitance for cells with 0 and 15mM potassium in the patch pipette were normalized to the value of current/capacitance in a control cell from the same dissociation, with 140mM potassium in the patch pipette (recorded from just before recording from the cell with low internal potassium).

The currents, normalized as described above were then plotted against the potassium concentration in the patch pipette (abscissa). The 15mM $[K^+]_i$ point is an average of three cells (bar indicates standard error), the 0mM $[K^+]_i$ point is an average of 8 cells.

A

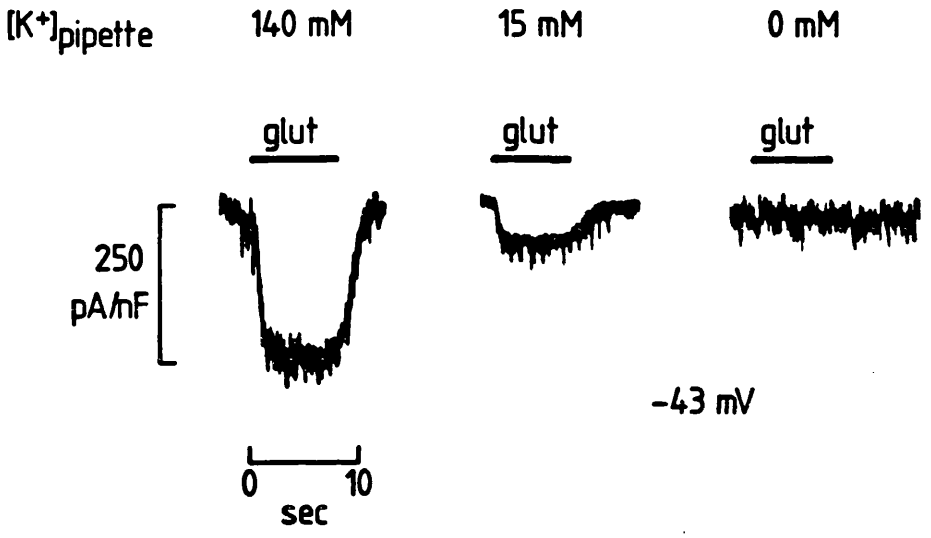
[K+]pipette
140 mM
15 mM
0 mM
glut
glut
glut
250
pA/nF
-43 mV
0
10
sec

B

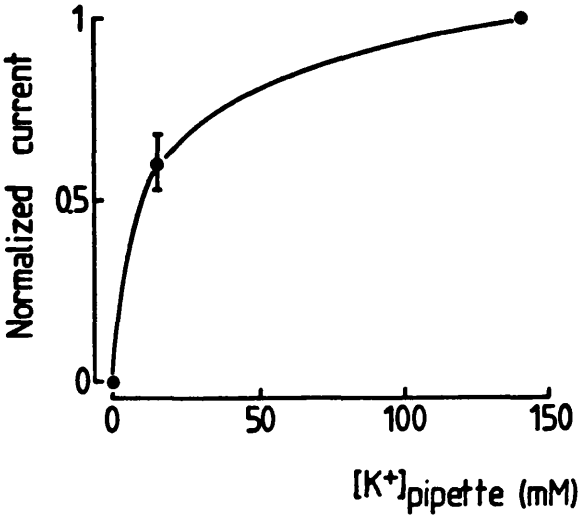
Normalized current
1
0.5
0
0
50
100
150
[K+]pipette (mM)

membrane. From a Lineweaver-Burke plot with the limited data points available, the estimated K_m value was 12mM.

5.3.7 Dependence of the glutamate-induced current on external potassium concentration

The dependence of the glutamate uptake current on $[K^+]_{pipette}$ in Figure 5.7 could be due to internal potassium simply activating the uptake carrier in some way (i.e. acting as a catalyst or co-factor), or it could be due to K^+ ions being transported out of the cell on the uptake carrier. If potassium is actually transported out of the cell by the carrier, the glutamate-activated current would be expected to be reduced when the extracellular potassium concentration is high, because it will then be more difficult for the carrier to lose K^+ ions at the outer surface of the membrane.

Figure 5.8A shows the glutamate-evoked currents in a Müller cell produced by repeated iontophoresis of glutamate during the sequential application by bath-perfusion of Ringer's solution containing different concentrations of potassium ions. For these experiments potassium was replacing choline and (to allow this substitution) $[Na^+]_o$ was set at only 70mM, a value which allows $[K^+]_o$ to be raised to 70mM, but which is not low enough to greatly inhibit glutamate uptake (Figure 5.6). Raising $[K^+]_o$ reduced the glutamate-evoked current (n=3 cells). In Figure 5.8B the current, normalized to its value with 0mM $[K^+]_o$, is plotted against external potassium concentration. The current is halved in 28mM $[K^+]_o$. These results are consistent with potassium ions being transported out of the cell on the glutamate uptake carrier.

5.3.8 Prediction of the inhibition of Müller cell glutamate uptake during ischaemia or anoxia

Experiments described in section 5.3.7 show that the glutamate-induced current in Müller cells is inhibited by external potassium. In those experiments the cell was voltage-clamped. In vivo, a raised extracellular potassium concentration would depolarize the cell, and depolarization also inhibits the glutamate-induced current (section 5.3.2). Thus, in pathological conditions such as ischaemia and anoxia, where the extracellular potassium rises, possibly up to 60mM (Walz and Hertz, 1983), the uptake of glutamate will be inhibited

Figure 5.8 The glutamate-induced current in Müller cells is inhibited by external potassium.

A. Glutamate-evoked inward currents (average of 3 traces at each $[K^+]_o$) from a Müller cell voltage-clamped at -43mV. Glutamate was applied by iontophoresis, the timing of which is shown by the top trace. The patch pipette contained solution Q (Table 2.5). Externally the cell was superfused with barium Ringer's solutions containing the different concentrations of potassium ions indicated next to each current trace (solutions K0-K70, Table 2.4) and containing only 70mM sodium chloride.

B. Normalized dependence of glutamate-evoked current (ordinate, mean ±s.e.) on $[K^+]_0$ (abscissa) from 3 cells studied as in A. The currents at each potassium concentration were normalized to the current (in the same cell) in 0mM $[K^+]_o$.

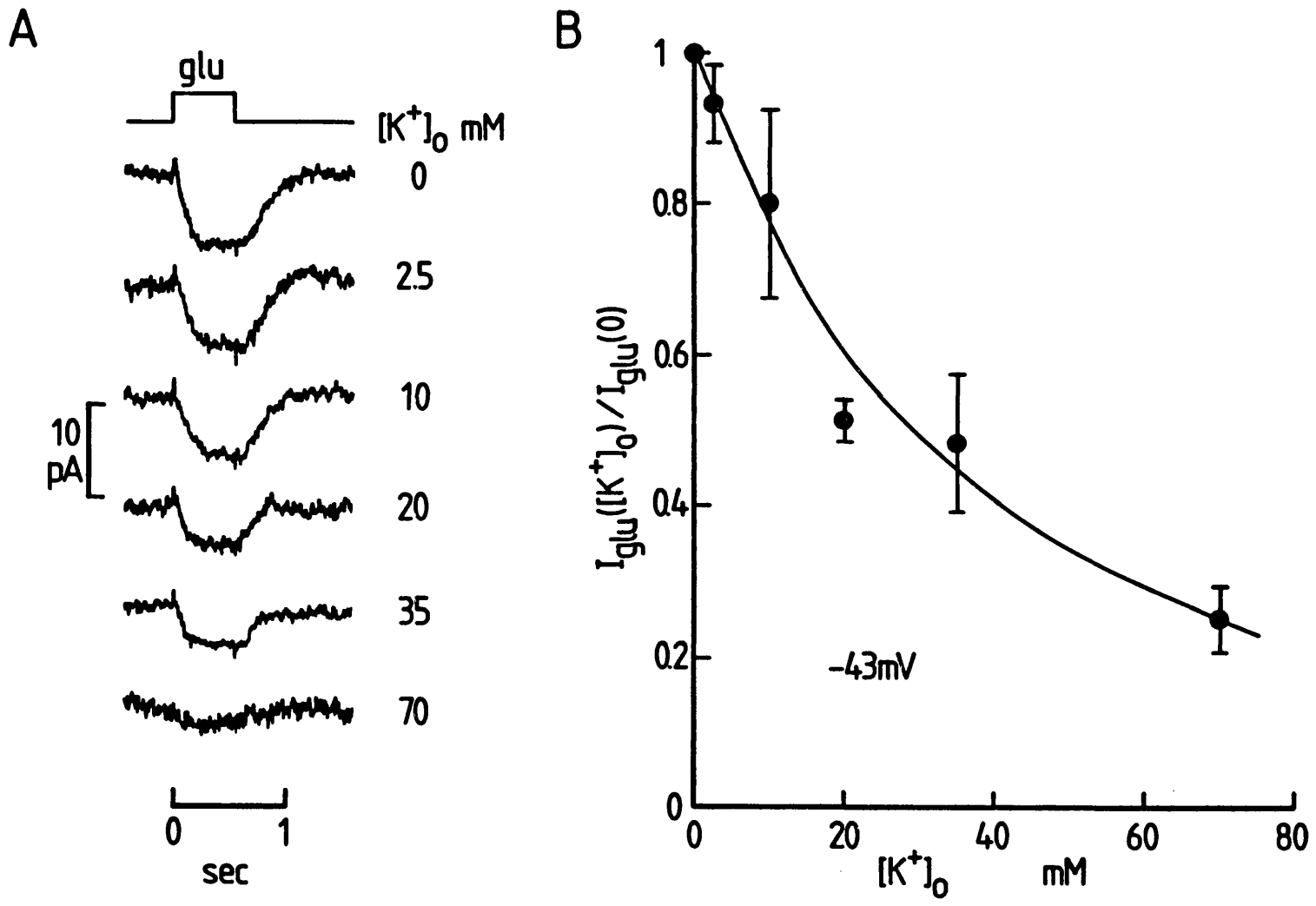
A
glu
$[K^+]_o$ mM
0
2.5
10
20
35
70
10 pA
0
1
sec
B
1
0.8
0.6
0.4
0.2
0
$I_{glu}([K^+]_o)/I_{glu}(0)$
-43mV
0
20
40
60
80
$[K^+]_o$ mM

for 3 reasons:

(1) due to the raised $[K^+]_o$ because this makes it more difficult for the carrier to lose K^+ ions at the outer membrane surface;

(2) due to a reduced $[Na^+]_o$ occurring when $[K^+]_o$ is raised (Siesjö, 1990);

(3) due to the depolarization caused by the raised $[K^+]_o$.

I have calculated the combined inhibitory effect of a rise in $[K^+]_o$ on the uptake of glutamate, taking these three factors into account as follows. First, the dependence of uptake current on $[K^+]_o$ in Figure 5.8B was plotted, normalized to its value in 2.5mM $[K^+]_o$. This graph, shown as the dashed curve labelled $[K^+]_o\uparrow$ in Figure 5.9, shows the effect on uptake of a pure rise in $[K^+]_o$, ignoring the fact that a rise in $[K^+]_o$ will also depolarize the cell. Next, a rise in $[K^+]_o$ was converted to a cell depolarization by assuming that the glial cell membrane potential obeys the Nernst potential for K^+ at 37°C i.e. $V_m = 61mV \times \log([K^+]_o/[K^+]_i)$ (with $[K^+]_i$=140mM). The calculated voltage values were converted to values of uptake current using the voltage-dependence of Figure 5.3B. The resulting curve (normalized to its value at 2.5mM $[K^+]_o$ and labelled ΔV_m in Figure 5.9) shows the effect on uptake of the depolarization produced by the rise in $[K^+]_o$. Finally, by assuming that $[Na^+]_o$ falls from its normal value of 143mM by the same amount as $[K^+]_o$ rises, the Na^+-dependence in Figure 5.6B was used to calculate the effect of the fall in $[Na^+]_o$ as a function of $[K^+]_o$ (dashed curve labelled $[Na^+]_o\downarrow$ in Figure 5.9.)

If it is assumed, for simplicity, that the inhibitory effects of a rise in $[K^+]_o$, of the associated membrane depolarization, and of the fall in $[Na^+]_o$, are independent, then multiplying the three dashed curves together in Figure 5.9 gives a prediction for the total inhibition occurring (solid curve in Figure 5.9).

These graphs show that the main factors inhibiting uptake are the rise in $[K^+]_o$ and the resulting membrane depolarization, while the $[Na^+]_o$ decrease is relatively unimportant. For a rise in $[K^+]_o$ to 60mM, the rise of $[K^+]_o$ alone produces a 69% inhibition, the resulting membrane depolarization to -23mV gives a 72% inhibition, and the fall in $[Na^+]_o$ to 63mM produces an 11% inhibition. The combined effect of these three factors is calculated to reduce glutamate uptake to less than 8% of its normal rate.

Figure 5.9 Quantification of failure of glutamate uptake in vivo under anoxic conditions.

The dashed curves show how three factors are predicted to alter the glutamate uptake current (ordinate) when $[K^+]_o$ rises (abscissa). Glutamate uptake is shown normalized to its normal value in 2.5mM $[K^+]_o$. The curve labelled $[K^+]_o\uparrow$ is a plot of the dependence of the uptake current (at -43mV) on $[K^+]_o$ from Figure 5.8B. The curve labelled ΔV_m shows the dependence of uptake current on the membrane potential depolarization produced by a rise in $[K^+]_o$: to obtain this plot, the dependence of uptake on voltage (at constant $[K^+]_o$) in Figure 5.3B was replotted as a function of $[K^+]_o$ by assuming that the glial cell membrane potential depends on $[K^+]_o$ according to the Nernst potential (with $[K^+]_i$=140mM). The curve labelled $[Na^+]_o\downarrow$ shows the inhibition predicted to be produced by a fall in $[Na^+]_o$: to produce this plot as a function of $[K^+]_o$ the dependence on $[Na^+]_o$ in Figure 5.6B was transformed by assuming that $[Na^+]_o$ falls by the same amount as $[K^+]_o$ rises. The continuous curve shows the total inhibition predicted for glutamate uptake by taking the product of the three dashed curves. This procedure assumes that the inhibitions produced by $[K^+]_o$, depolarization and a fall in $[Na^+]_o$ are all independent.

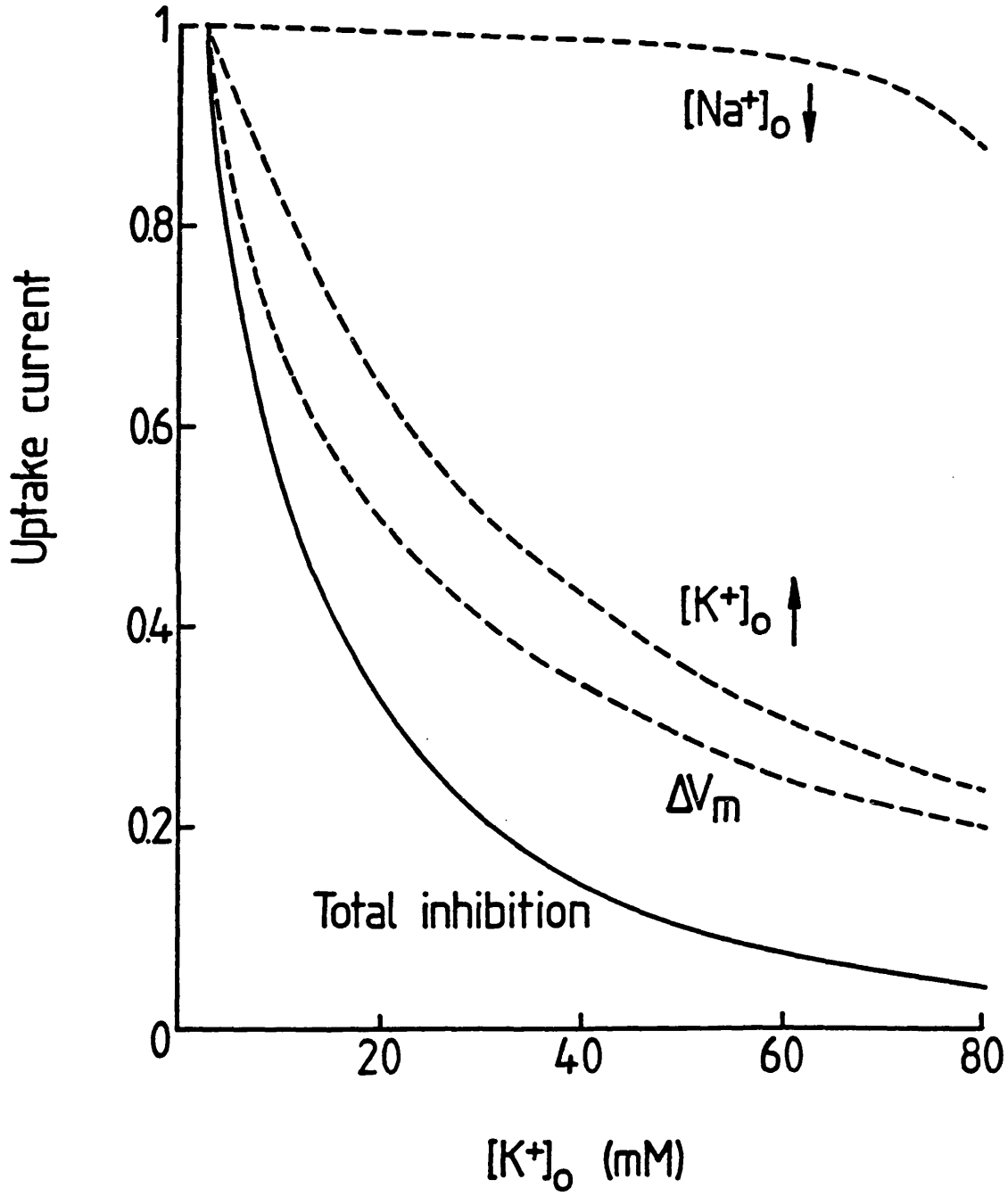
Uptake current
1
0.8
0.6
0.4
0.2
0
20
40
60
80
[Na+]o
[K+]o
ΔVm
Total inhibition
[K+]o (mM)

Chapter 6
The spatial relationship between Müller cell processes and the photoreceptor output synapse

6.1 Introduction

This chapter describes experiments investigating the spatial relationship between the processes of retinal glial (Müller) cells and the photoreceptor output synapse in the tiger salamander retina. Termination of the action of glutamate, the transmitter released from photoreceptors, is thought to be at least partly due to uptake into Müller cells, if only because Müller cell uptake keeps the extracellular glutamate concentration low, allowing glutamate to diffuse out of the synaptic cleft down its concentration gradient. However, it is not known how close Müller cell processes come to the site of glutamate release in the photoreceptor synaptic terminal, and this is the question that is addressed in this chapter. Having such information is important as a basis for understanding the role of Müller cells in glutamatergic transmission in the outer retina, in particular to understand whether the kinetics of synaptic transmission are determined by proximity to Müller cell processes (Chapter 7, section 7.3.2).

6.2 Methods

The experiments described in this chapter were performed on retinae isolated from the tiger salamander, flatmounted ganglion cell layer up (Chapter 2, section 2.2.1). Micropipettes were used to inject Müller cells with HRP. They had resistances ranging from 200 to 300MΩ when filled with HRP solution (Chapter 2, section 2.2.2), backfilled with 3M potassium acetate and immersed in Ringer's (solution RA, Table 2.1). Pipettes with a higher resistance blocked easily while pipettes with larger tips often damaged the cell and resulted in a low resting potential.

Injection of 1-2nA current pulses (50% duty cycle) for 1-3 min was enough to fill the Müller cells with sufficient HRP for observation in the electron microscope. Use of more current often blocked the pipette, while longer injections resulted in HRP leaking out of the cell.

After injection with HRP the tissue was fixed in a mixture of

paraformaldehyde and glutaraldehyde (Karnovsky, 1965; Stell and Lightfoot, 1975). This was followed by deposition of the dark brown HRP reaction product (Chapter 2, section 2.2.3). The tissue was then postfixed in osmium tetroxide (OsO_4) (Chapter2, sections 2.2.3 and 2.2.4). This procedure resulted in adequate preservation of the tissue (although the quality of preservation was limited by the fact that the retina had to be isolated from the eye and remain flatmounted for up to 1 hour prior to fixation). Although paraformaldehyde has been reported to reduce the enzymatic activity of HRP, this effect can be minimized by fixation at 4°C (Straus, 1964).

Better tissue preservation was obtained when the tissue was fixed in a mixture of glutaraldehyde and OsO_4 (Hirsch and Fedorko, 1968; Lasansky, 1973) prior to developing the reaction product. However, after treating the retina with osmium the tissue turns dark brown and it then becomes very difficult to see the HRP reaction product develop. For most experiments involving HRP injections and processing for electron microscopy, therefore, the tissue was fixed in a paraformaldehyde-glutaraldehyde mixture and postfixed in OsO_4 after visualizing the HRP reaction product.

6.3 Results

6.3.1 HRP-injected Müller cell: light microscopy

Figure 6.1 shows a micrograph of a Müller cell injected with HRP in a transverse retinal section embedded in epon. This tissue was not postfixed in OsO_4. The Müller cell spans the whole width of the retina (Ramón y Cajal, 1892) from the outer limiting membrane (OLM) near the photoreceptors (at the top of the figure) to the endfoot (E) near the ganglion cells at the inner limiting membrane (ILM) (at the bottom of the figure). In situ the outer limiting membrane is situated near the back of the eye while the inner limiting membrane borders the vitreous humour. The photoreceptor segments (P) project out towards the back of the eye. Müller cell processes extend laterally from the main trunk (stalk) of the cell into the inner plexiform layer (IPL) and around cell bodies in the inner (INL) and outer nuclear layers (ONL). A single Müller cell sends out processes to partly surround approximately 8 photoreceptor cell bodies in the outer nuclear layer.

Figure 6.1 Light micrograph of an HRP-injected Müller cell.

Light micrograph of a 50μm transverse section through a tiger salamander retina containing an HRP-injected Müller cell. The tissue was fixed in glutaraldehyde (Chapter 2, section 2.2.3) and embedded in epon. The Müller cell spans the whole width of the retina from the endfoot (E) at the inner limiting membrane (ILM) bordering the vitreous humour, to the outer limiting (apical) membrane (OLM). The 5 different layers that make up the retina are indicated: ganglion cell layer (GCL); inner plexiform layer (IPL); inner nuclear layer (INL); outer plexiform layer (OPL); and the outer nuclear layer (ONL). Photoreceptor segments (P) project out from the outer limiting membrane towards the back of the eye. Processes of the injected Müller cell project out laterally from the stalk into the inner plexiform layer and project around the cell bodies in the inner (INL) and outer nuclear layer (ONL). Magnification x450.

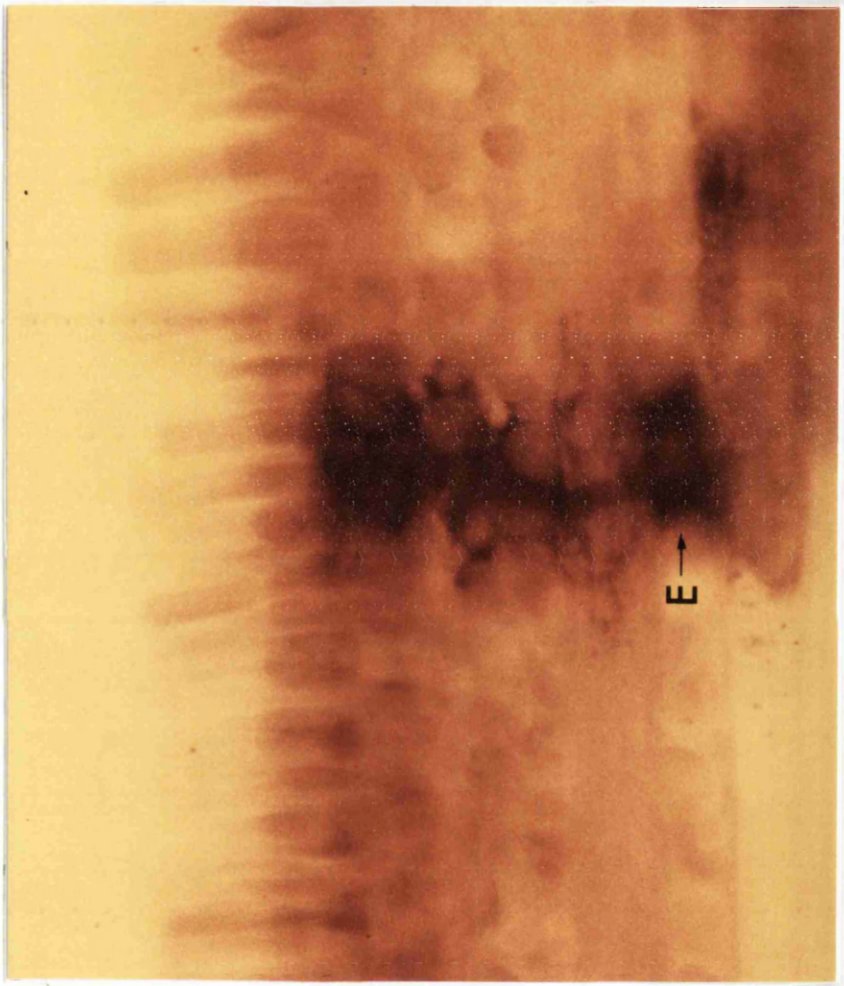
P
OLM
ONL
OPL
INL
IPL
GCL
ILM
E

6.3.2 Chemical synaptic contacts between photoreceptors and postsynaptic cells

Synaptic contacts between photoreceptors (whose cell bodies are in the outer nuclear layer) and bipolar and horizontal cells (with cell bodies in the inner nuclear layer) lie in the outer plexiform layer. The chemical synapses between photoreceptors and postsynaptic cells are marked by the presence of synaptic ribbons in the pedicles of rods and cones (Sjöstrand, 1958), generally releasing transmitter to 2 or 3 nearby postsynaptic cells. Although synaptic contacts without synaptic ribbons exist, the chemical nature of these contacts is not certain (Lasansky, 1973). In this study I used the synaptic ribbons to define sites of glutamate release, and investigate how close Müller cell processes come to these sites.

Figure 6.2 shows several ribbon synapses in a synaptic pedicle, i.e. the output synapse, of a rod photoreceptor (rp). They are readily identified by the presence of an electron dense line surrounded by an array of synaptic vesicles (arrows). Electron dense material, the arciform density, which may serve to anchor the ribbon to the membrane, is associated with the presynaptic membrane (arrow head).

On the postsynaptic side of the synapse, processes from horizontal and bipolar cells invaginate the synaptic pedicle of the photoreceptor resulting in a "dyadic" (d) or "triadic" (t) arrangement where a synaptic ribbon releases transmitter to either 2 or 3 processes of postsynaptic cells (Figure 6.2). However, what looks like a dyad when examined in a single section may prove to be triadic when serial sections are examined. Some of the processes invaginating rod pedicles may arise from cone receptors since rod cell pedicles make ribbon junctions onto processes of cone photoreceptors (Lasansky, 1973).

In the electron micrographs in this chapter, the cell bodies of photoreceptors are identified by the nuclei and labelled cn (cone nucleus) and rn (rod nucleus) respectively. Pedicles from rods and cones can be distinguished because the rod cell nuclei are more externally placed (towards the pigment epithelium) while cone nuclei are located nearer the synaptic region (Lasansky, 1973). As a consequence, cone cell bodies are continuous with their pedicles (cp) (Figure 6.3A) while the rod cell bodies are linked to their

Figure 6.2 Electron micrograph of a synaptic pedicle of a rod photoreceptor.

Electron micrograph of a rod synaptic pedicle (rp) in tissue fixed in a glutaraldehyde/OsO_4 mixture (Chapter 2, section 2.2.3). The pedicle contains several ribbon synapses each surrounded by an array of synaptic vesicles (arrows). Arrow head indicates the arciform density. On the postsynaptic side processes from bipolar and horizontal cells and possibly from cone photoreceptors form dyads (d) and triads (t). These synaptic contacts are situated in the outer plexiform layer (OPL). The rod pedicle sits next to a cone pedicle (cp), cn indicates the nucleus in the cone cell body. Magnification x20750.

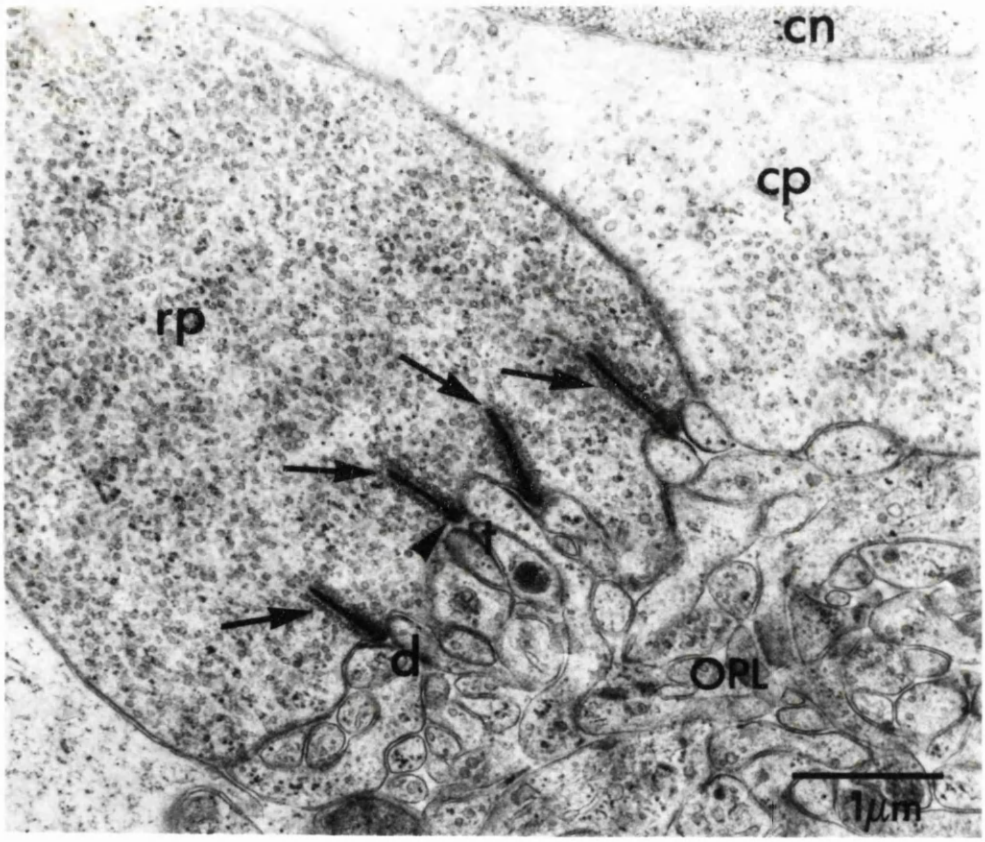
cn
cp
rp
d
ORL
1μm

pedicles (rp) by means of an axon (arrows, Figure 6.3B). Rod and cone pedicles can also be distinguished following fixation in glutaraldehyde-OsO_4 mixtures, because rod pedicles appear more electron opaque than the cone pedicles, as seen in Figure 6.2 (see also Lasansky, 1973). This is less obvious for the tissue fixed in a glutaraldehyde-paraformaldehyde mixture (Figures 6.3 to 6.5).

6.3.3 Müller cell processes in the outer retina: electron microscopy

The HRP reaction product in injected Müller cells can be easily identified as an electron dense precipitate (Mc and arrow heads in Figure 6.3A, Mc in Figures 6.3B, C, 6.4 and 6.5). Figure 6.3C is a low magnification electron micrograph showing HRP-filled Müller cell processes in the outer retina. Very few processes project laterally from the main trunk of the cell into the outer plexiform layer (OPL). However, large processes wrap around the cell bodies of photoreceptors. Serial sectioning of two HRP injected Müller cells revealed that a single Müller cell sends large processes, filling the space between photoreceptor cell bodies, to at least 6 photoreceptors and projects processes to several more photoreceptors surrounding only part of their cell bodies.

Although Müller cell processes surround much of the cell bodies of photoreceptors (Figure 6.3C) and also invade the pedicles (Figure 6.3B, arrow head), processes hardly ever project into the outer plexiform layer near the ribbon synapses of the photoreceptors. Figure 6.4A shows Müller cell processes wrapping around a cone cell body, completely surrounding it. Figure 6.4B is an electron micrograph of another section through the same cone cell body in which the synaptic pedicle is visible. Although Müller cell processes are present all around the cell body, there are no processes in the outer plexiform layer near the ribbon synapses (arrows).

Fourteen pedicles of rod and cone photoreceptors approached by HRP-injected Müller processes were sectioned and examined. On only two occasions were minor Müller cell processes found to be present in the outer plexiform layer close to a synaptic ribbon. As an example of this, Figure 6.4C shows a rod synaptic pedicle (the same pedicle as in Figure 6.3B but in this section ribbon synapses are

Figure 6.3 General organization of Müller cell processes around the synaptic terminals of photoreceptors.
The tissue in these electron micrographs was fixed in a glutaraldehyde-paraformaldehyde mixture followed by postfixation in OsO_4 (Chapter 2, sections 2.2.3 and 2.2.4).
A. Cone nucleus (cn) with synaptic pedicle (cp) containing ribbon synapses (arrows). The pedicle is continuous with its cell body. HRP-filled Müller cell processes are indicated by Mc and arrow heads. The cone cell body borders the outer plexiform layer (OPL). Magnification x10320.
B. Rod nucleus (rn) with a synaptic pedicle (rp) which is connected to the cell body via an axon (arrows). HRP-filled Müller cell processes surround the cell (Mc). Arrow head indicates a Müller cell process invaginating the rod synaptic pedicle. Magnification x5610.
C. HRP-filled processes of a Müller cell (Mc) wrap around rod (rn) and cone (cn) photoreceptor cell bodies and surround one side of a cone synaptic pedicle (cp) containing ribbon synapses (arrow heads). Some small processes of the Müller cell project into the outer plexiform layer (OPL) (arrows). Magnification x2600.

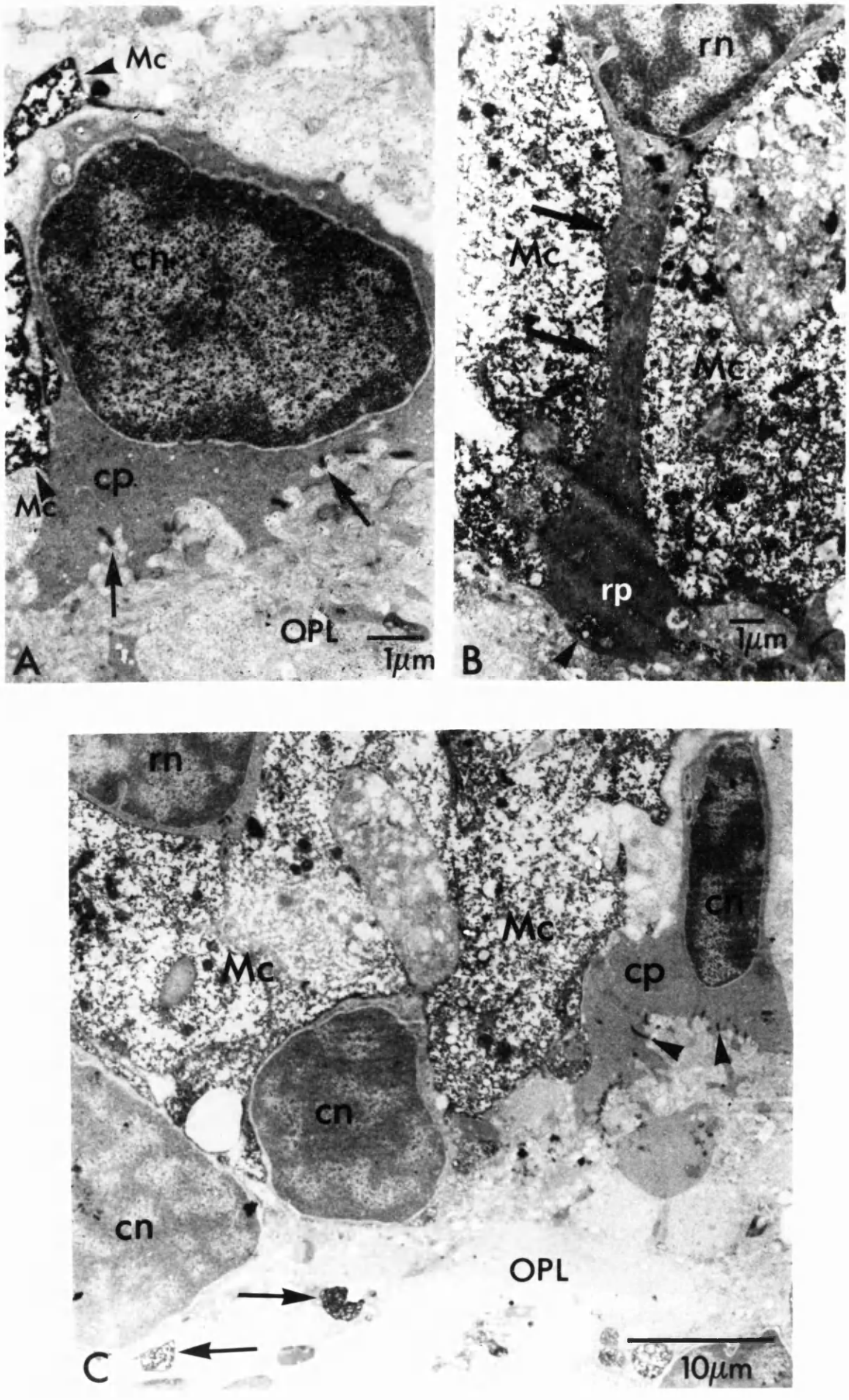
Mc
cn
cp
Mc
OPL
1μm
A
rn
Mc
Mc
rp
1μm
B
rn
Mc
Mc
cp
cn
cn
cn
OPL
10μm
C

Figure 6.4 Müller cell processes only rarely come close to synaptic ribbons.

The tissue in these electron micrographs was fixed as described in the legend to figure 6.3.

A. A cone cell body (cn) surrounded by HRP-filled processes of a Müller cell (Mc). In this section the cell body is surrounded on all sides by Müller cell processes. Magnification x13860.

B. Another section through the cone photoreceptor shown in A, but now the synaptic pedicle (cp) with ribbon synapses (arrows) is seen. HRP-filled Müller cell processes (Mc) surround the cone cell body (cn) but are not present near the synaptic region in the outer plexiform layer (OPL). Magnification x6500.

C. Section through a rod pedicle (rp) next to a cone cell body (cn), arrow heads indicate the membranes that separate them. HRP-filled Müller cell processes (Mc) wrap around the pedicle (as was seen for all photoreceptors) but in addition (and unusually) a Müller cell process (arrow) projects out into the outer plexiform layer (OPL) close to a ribbon synapse (open arrow). Magnification x16500.

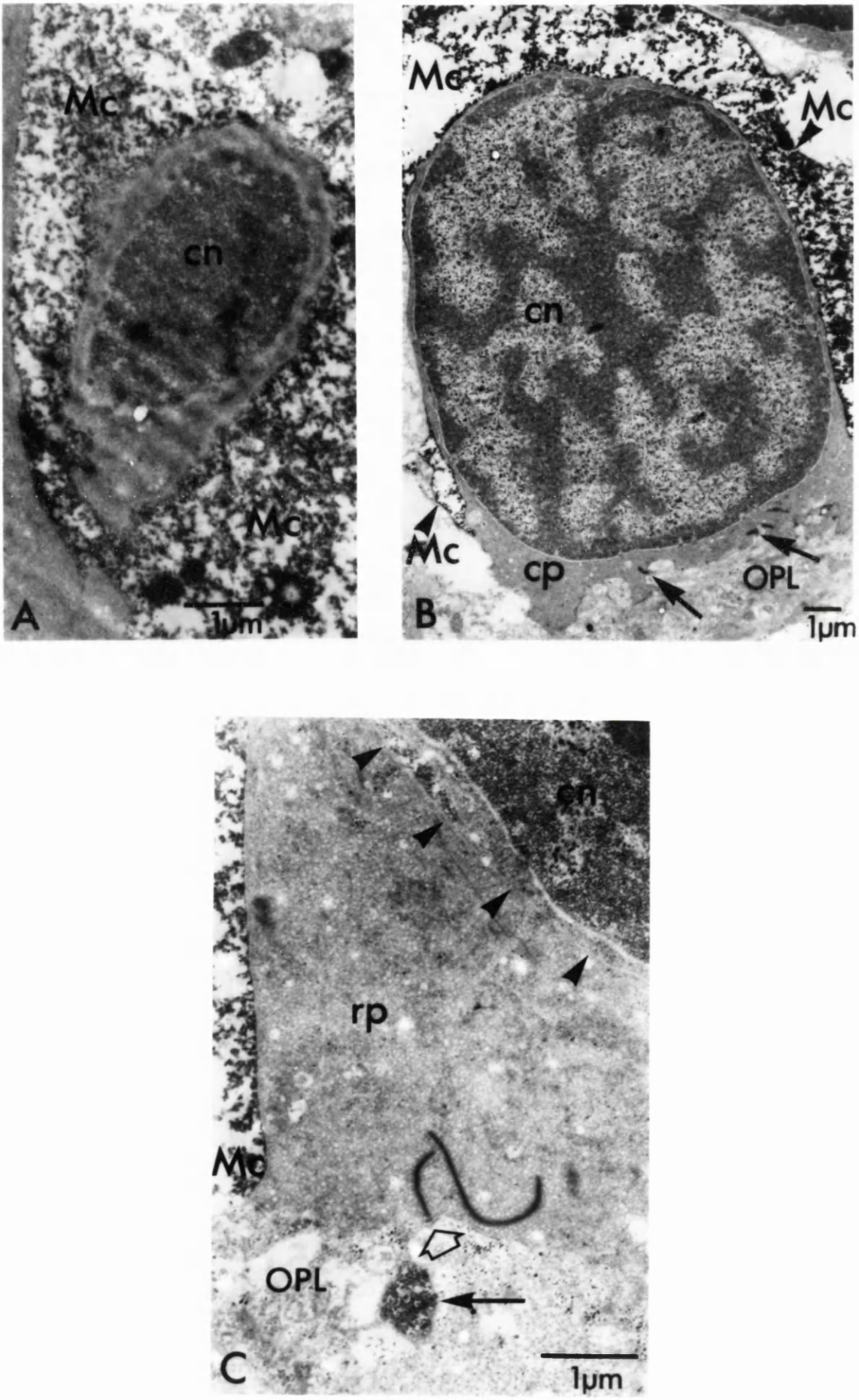
Mc
cn
Mc
A
1µm
Mc
Mc
cn
Mc
cp
OPL
B
1µm
cn
rp
Mc
OPL
C
1µm

present (open arrow head)). A Müller cell process in the outer plexiform layer is shown by an arrow. Further sections through this pedicle showed the presence of many more ribbon synapses (Figure 6.5A, arrows), but no Müller cell processes, other than the one in Figure 6.4C, were observed to project into the postsynaptic region in the outer plexiform layer.

To quantify the closest approach of Müller cell processes to ribbon synapses, for each of the pedicles sectioned I measured the distance between the archiform density end of the synaptic ribbon nearest to a Müller cell process and that process. This process was in the OPL for the pedicle of Figure 6.4C (and the one other pedicle that had a synaptic ribbon closely approached by a Müller cell process in the OPL), but more usually the process was to one side of the pedicle (as for the cone of Figure 6.3A and 6.4B; see also Figure 6.5). The resulting distances (measured in a straight line) were 1.05 $\pm$0.51 (s.d.) μm for the 6 rod pedicles, 3.04 $\pm$1.37μm for the 4 cone pedicles, and 0.92 $\pm$0.63μm for 4 pedicles that could not be identified as belonging to a rod or a cone.

6.3.4 Clustering of synaptic pedicles

Figure 6.5A shows a cone cell body with a synaptic pedicle. The cone pedicle (cp) abuts 2 rod pedicles (rp) (arrow heads indicate the cell membranes that separate them). This arrangement of pedicles is often observed: a cone pedicle can be surrounded by up to 4 rod pedicles (Lasansky, 1973). This corresponds to the idea that the photoreceptors are roughly arranged in a lattice in which 4 rods surround each cone (Attwell, Wilson and Wu, 1984). When the pedicles are clustered like this, Müller cell processes wrap around the whole group of pedicles without projecting between them or into the outer plexiform layer (Figure 6.5A). Figure 6.5B is a section through a cone pedicle without any rod pedicles near it. As seen before, Müller cell processes wrap around the pedicle but again no processes are present in the outer plexiform layer near the synaptic region.

6.3.5 Müller cell processes in the outer retina: schematic diagram

Figure 6.6 is a schematic diagram of the results described in this chapter showing the relation of Müller cell processes and the

Figure 6.5 Clustered and isolated photoreceptor synaptic pedicles.

The tissue in these electron micrographs was fixed as described in the legend to figure 6.3.

A. Section through a cone cell body (cn) with a synaptic pedicle (cp). The pedicle is surrounded by two rod pedicles (rp), arrow heads indicate the membranes that separate them. The rod pedicle containing synaptic ribbons (arrows) is a section through the same pedicle as shown in Figure 6.4C. In contrast to that figure, no Müller cell processes are present in the outer plexiform layer (OPL). HRP-filled processes (Mc) are seen wrapping around the cone cell body and the group of pedicles without projecting between the pedicles. Magnification x12540.

B. Section through a cone cell body (cn) with a synaptic pedicle (cp) containing synaptic ribbons (arrows). In this section the cone pedicle is not surrounded by rod pedicles. HRP-filled Müller cell processes (Mc) wrap around the cone pedicle but again are not present in the outer plexiform layer (OPL) near the synaptic region. Magnification x26000.

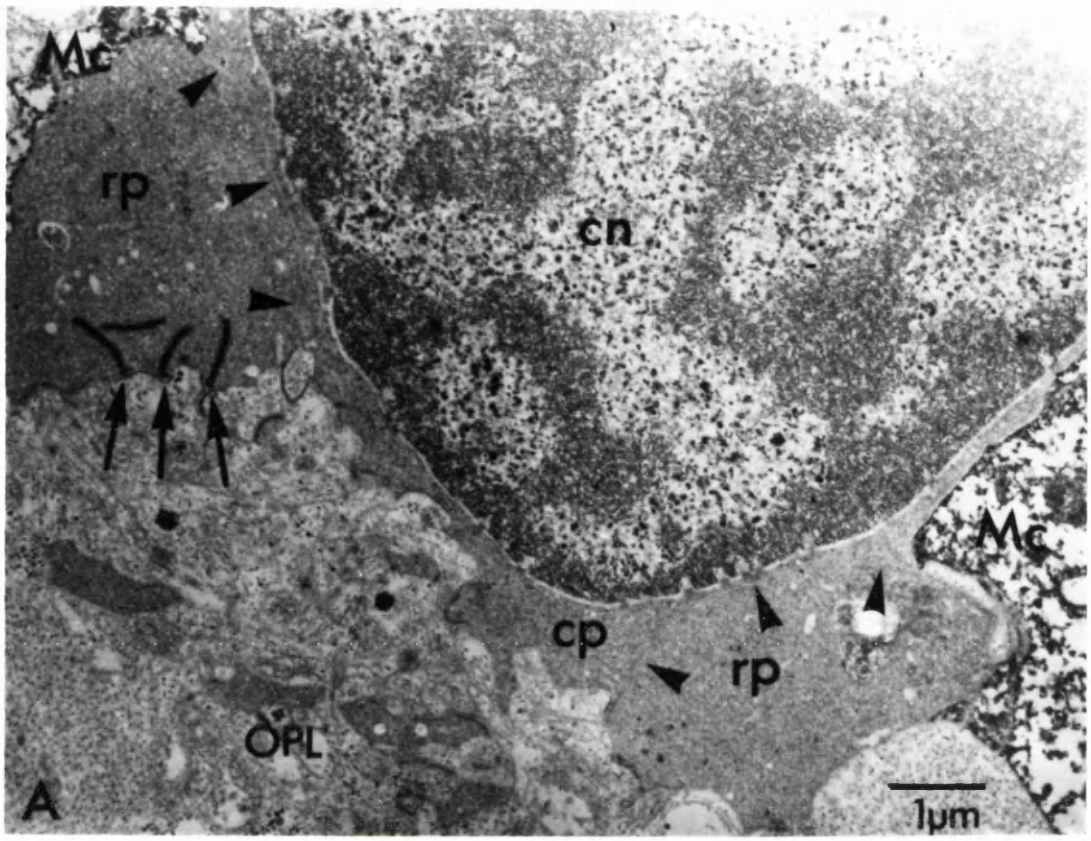
Mc
rp
cn
Mc
cp
rp
OPL
A
1μm

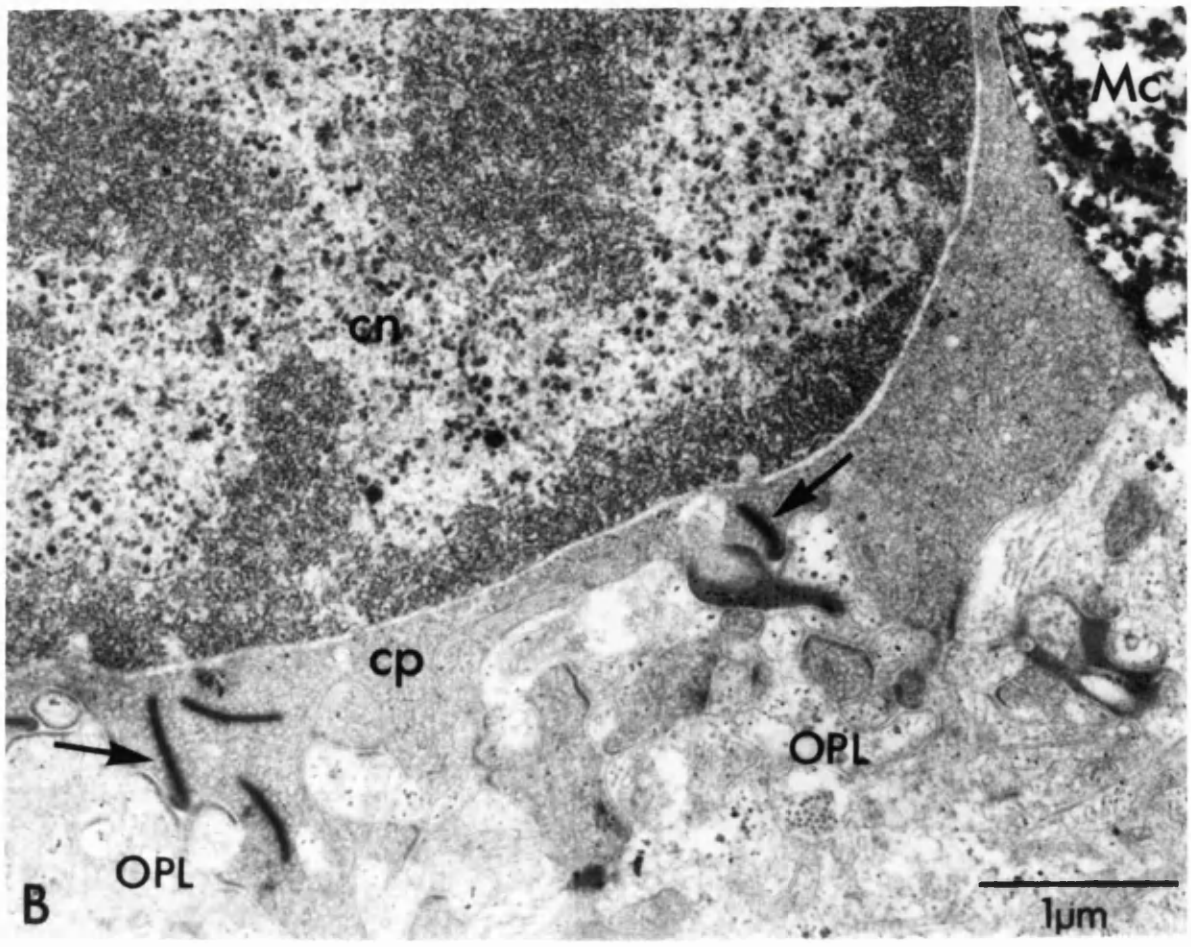
Mc
cn
cp
OPL
OPL
B
1μm

Figure 6.6 Schematic diagram of Müller cell processes in the outer layers and in the inner nuclear layer of the salamander retina.

Rod and cone synaptic pedicles (whose cell bodies are in the outer nuclear layer (ONL)) make ribbon synapses with postsynaptic bipolar and horizontal cells (whose cell bodies are in the inner nuclear layer (INL). These synaptic contacts take place in the outer plexiform layer (OPL). Cone pedicles are continuous with the cone cell body while rod pedicles are linked to the cell body by means of an axon. Müller cell processes (shaded areas) project out from the main trunk (stalk) of the Müller cell and wrap around cell bodies and synaptic pedicles of photoreceptors in the outer nuclear layer. Only occasionally does a Müller cell process project out into the outer plexiform layer near the synaptic region of the photoreceptor output synapse. Müller cell processes wrap around cell bodies in the inner nuclear layer. The stalk of the Müller cell extends to the inner limiting membrane ending in an endfoot in the ganglion cell layer (not shown, below the bottom of this diagram).

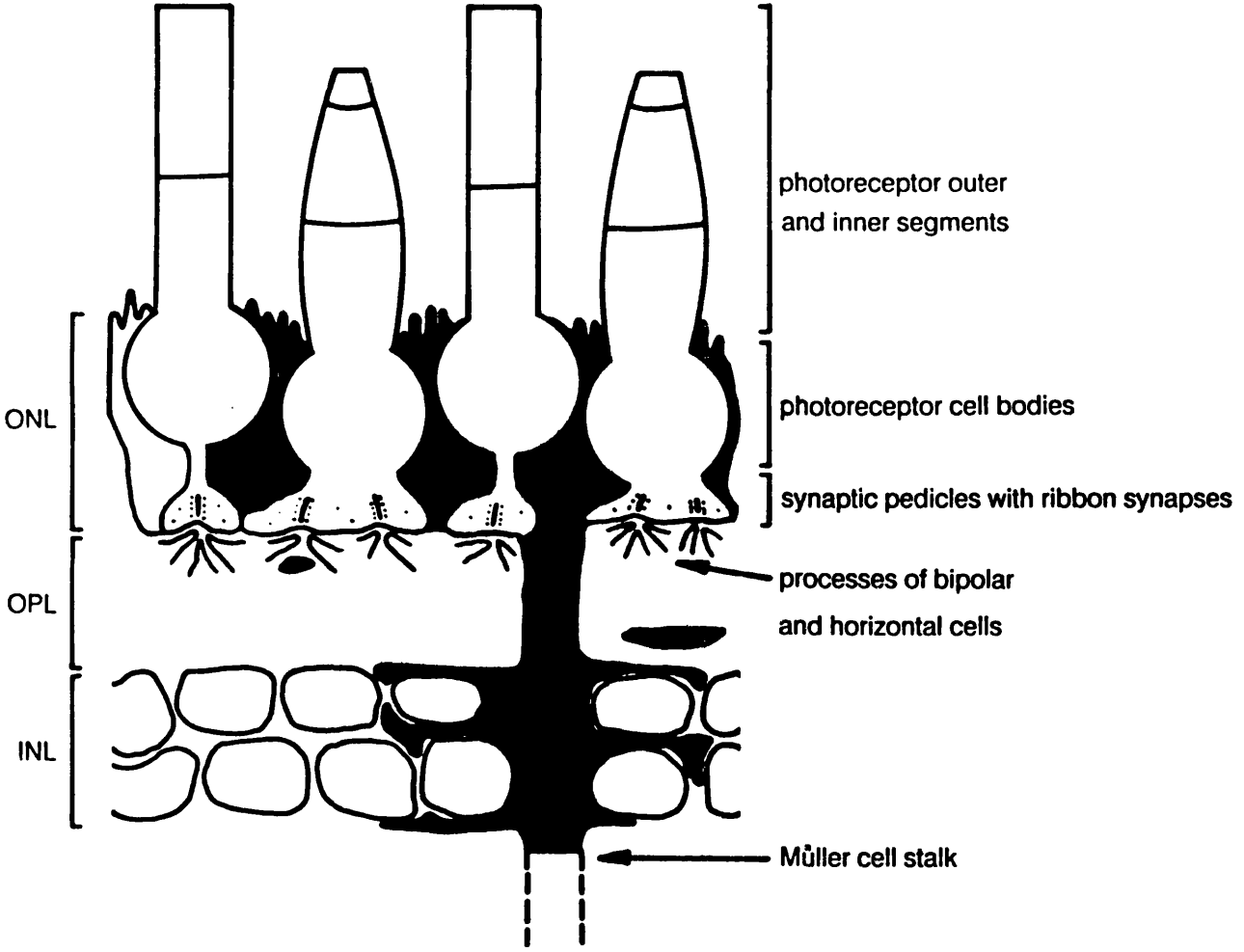

the shaded areas represent HRP-filled Müller cell processes

photoreceptor output synapse. It shows rod and cone photoreceptors with their synaptic pedicles. The Müller cell in the diagram is indicated by the shaded area. The cell bodies in the outer plexiform layer are surrounded by Müller cell processes. Processes also wrap around the synaptic pedicles that contain the synaptic ribbons. However, Müller cell processes are only occasionally present in the outer plexiform layer on the side of the pedicle where the synaptic ribbons are and even then the Müller cell processes do not invade in between the processes of horizontal and bipolar cells to border the synaptic cleft. Müller cell processes also surround the cell bodies of the horizontal and bipolar cells in the inner plexiform layer.

Chapter 7
Discussion

This chapter is divided into three sections. The first section (7.1) discusses the results in Chapters 3 and 4, of experiments studying the effect of glutamate on cone photoreceptors. Sections 7.2 and 7.3 discuss the results of experiments to study glutamate uptake in rabbit Müller cells (Chapter 5) and the anatomical arrangement of Müller cell processes near the photoreceptor output synapse in the salamander retina (Chapter 6) respectively.

7.1. Discussion of the results in Chapters 3 and 4

In these Chapters it was shown that glutamate evokes a current in cone photoreceptors isolated from the salamander retina. The voltage-dependence, pharmacological profile, dose dependence, ionic basis, increase in current noise, and spatial localization of the response were described. It was also shown that glutamate increases the conductance of cones in the isolated intact retina.

7.1.1 Glutamate evokes a current in cone photoreceptors

Application of glutamate changes the conductance of voltage-clamped cones isolated from the salamander retina. This effect was seen when recording from a single or from half of a double cone. Glutamate has the same effect on cones in the isolated, intact retina. Glutamate is believed to be the neurotransmitter released from photoreceptors conveying the visual signal to postsynaptic bipolar and horizontal cells (Chapter 1, section 1.3.2). Previously it has been reported that glutamate has no effect on rods in the intact gecko retina (Murakami, Ohtsu and Ohtsuka, 1972). However, a glutamate-evoked current has been shown in isolated photoreceptors of the turtle retina (Kaneko and Tachibana, 1987; Tachibana and Kaneko, 1988).

7.1.2 Does glutamate act via opening channels or does it activate a carrier-mechanism in the cone membrane?

The glutamate-induced current reverses around 0mV with 101mM chloride in the patch pipette (Chapter 3, Figure 3.2). The fact that the current reverses, together with the pharmacological profile

(Chapter 3, Figure 3.5) and the observed noise change (Chapter 3, section 3.3.4), suggest that at least part of the current must be due to glutamate acting on ion channels. The dependence of the glutamate-gated current on voltage show s inward rectification above the reversal potential. This is surprising: glutamate-gated channels usually have ohmic or outwardly rectifying current-voltage relations (Attwell et al., 1987; Cull-Candy and Usowicz, 1987).

In principle, two mechanisms may contribute to the glutamate-evoked current. In addition to opening ion channels, uptake of glutamate via an electrogenic carrier mechanism may generate an inward current as has been shown in a variety of glial cells (Chapter 5, rabbit Müller cells; Brew and Attwell, 1987, salamander Müller cells; Cull-Candy, Howe and Ogden, 1988, rat cerebellar astrocytes). Radiotracing experiments have shown that glutamate is taken up into photoreceptors (Marc and Lam, 1981; White and Neal, 1976), presumably to enable the cell to re-use the transmitter. In turtle photoreceptors (Tachibana and Kaneko, 1988) the glutamate-evoked current is not suppressed by the channel blocker kynurenic acid (Ganong, Lanthorn and Cotman, 1983) at a concentration of 1mM, but was partially blocked by 200μM p-chloromercuriphenylsulfonate, a glutamate uptake inhibitor (Balcar and Johnston, 1972).

The combination of the current-voltage relation for uptake (the glutamate-evoked current is smaller as the cell is depolarized but does not reverse; Chapter 5, Figure 5.3), and the currents produced by ion channels might account for the unusual inward rectification seen for the glutamate-gated current in cones. The glutamate analogue threo-3-hydroxy-DL-aspartate (THDA), which is supposed to be a blocker of glutamate uptake, was applied to investigate whether part of the glutamate-induced current could be due to uptake. However, THDA blocked virtually the whole current, indicating only that it is not specific for uptake, since we know that a large part of the current is carried by chloride ions moving through ion channels (Chapter 4, sections 4.3.2 and 4.3.3). A strong indication that there is no significant contribution of current generated by electrogenic uptake comes from the properties of kainate-induced currents in cones. Kainate, a glutamate channel analogue which is not usually taken up (Chapter 5, Figure 5.2; Brew and Attwell, 1987; Johnston, Kennedy and Twitchin, 1979), produces a current-voltage

relation with a similar shape to that produced by glutamate (Chapter 3, Figure 3.6). In the remainder of this discussion therefore, I will assume that glutamate acts solely on ion channels in the cone membrane.

7.1.3 Which glutamate receptor is present in the cone membrane?

It has been suggested that there are at least three pharmacologically distinguishable types of glutamate receptor linked to ion channels, relatively selectively activated by NMDA, kainate and quisqualate. When these agonists were applied to voltage-clamped, isolated cone photoreceptors of the salamander, only kainate evoked a response and this was larger than the glutamate-evoked current (Chapter 3, Figure 3.5). This indicates that the glutamate receptor in the cone membrane is a kainate receptor. Kaneko and Tachibana (1987) reported a similar result in turtle photoreceptors, although in a later report (Tachibana and Kaneko, 1988) they stated that no current was evoked with NMDA, kainate or quisqualate.

It has been suggested that kainate and quisqualate act on the same receptor in spinal neurones (Honore et al., 1988)). However, quisqualate did not evoke a response in cones, suggesting that the receptor only binds kainate. Thus, the cone kainate receptors are unlike those controlling glutamate-operated channels in retinal horizontal cells, which are sensitive to kainate and quisqualate (Lasater, 1982). A pure kainate receptor has also been identified on mammalian C-fibres (Foster and Fagg, 1984). No current was evoked in cones when NMDA was applied. The presence of Mg^{2+} in the superfusion solutions would reduce the effective conductance of the NMDA channel (Novak et al., 1984), but about 35% of the current should still flow at the potentials used (-43 to -53mV) and it is unlikely that the presence of Mg^{2+} prevented the detection of an NMDA response.

7.1.4 How many glutamate anions bind to the receptor?

The dose-response data for glutamate show that a significant proportion of the current was activated by 1μM glutamate (external glutamate concentration in the intact brain may be around 2μM (Benveniste, et al., 1984)). The dose-response data were fitted by a Michaelis-Menten relation with K_m values ranging from 1.0-5.5μM. This indicates high affinity binding of one glutamate molecule to

the receptors in the cone membrane. The Hill coefficient for the data in Chapter 3, Figure 3.3 is 0.78, again indicating binding of one glutamate anion. Tachibana and Kaneko (1988) find a Hill coefficient of 1 for the glutamate-induced current in turtle photoreceptors (but a much larger K_m of 40μM).

In other preparations Hill coefficients for the binding of glutamate to receptors are 2 or larger for channels in horizontal cells in the dogfish retina (Shiells, Falk and Naghshineh, 1986), in chick spinal neurones (Trussell and Fischbach, 1989) and in crayfish muscle (Dudel, Franke and Hatt, 1990), indicating the binding of two or more glutamate molecules to the receptor. This apparent difference may lie in the fact that in the experiments to determine the dose response curve (Chapter 3, section 3.3.2) the lowest dose of glutamate used (1μM) produced one half of the maximal current. It is quite possible that at lower doses the dose-response has a sigmoid onset. More experiments will have to be carried out to resolve this question. Another reason for the discrepancy may be that there is fast desensitization of the response. This was never observed in any of the experiments in Chapters 3 and 4, and kainate-type responses do not usually desensitize (Kiskin, Krishtal and Tsyndrenko, 1986). However, glutamate-activated channels have shown desensitization within several milliseconds in central neurones (Trussell and Fischbach, 1989) and in muscle (Dudel, Franke and Hatt, 1990), which is within the timescale of drug application in our experiments.

7.1.5 Which ions carry the current?

(1) Cations

Glutamate usually gates non-specific cation channels, mainly permeable to sodium and potassium ions, in vertebrate neurones (Mayer and Westbrook, 1985; Hablitz and Langmoen, 1982). The glutamate-induced current in cone photoreceptors was abolished in superfusion solutions from which nearly all the sodium was removed (Chapter 4, Figure 4.1), but was not converted into the outward current expected for a channel permeable to both sodium and potassium. Furthermore, when the external concentration of sodium was reduced by partly replacing it by choline, the currents were reduced but there was no change in the reversal potential of the

response (Chapter 4, Figure 4.2). These data imply that Na^+ is not a major carrier of the glutamate-evoked current (although it clearly modulates the current). Experiments discussed below suggest that chloride ions carry the bulk of the glutamate-evoked current. In principle however, sodium ions may still carry part of the current, although it is unusual for a channel to be permeable to both cations and anions. If the permeability ratio, chloride:sodium, was (say) 10:1, the reversal potential of the response would be expected to shift by only 2mV (according to the Goldman-Hodgkin-Katz equation) when the external sodium is reduced from 107 to 25mM as in the experiments in Figure 4.2.

There are, in principle, several possible causes of the glutamate-gated current being totally abolished when the external sodium concentration is virtually zero. Removal of external sodium inhibits sodium-calcium exchange in the membrane, resulting in accumulation of calcium inside the cell. The increase in intracellular calcium may reduce the conductance of the glutamate-gated channel via a calcium-dependent phosphorylation mechanism (Chen et al., 1990). Increasing the intracellular calcium concentration has also been shown to decrease the affinity of receptors for GABA in sensory neurones from the bullfrog (Inoue et al., 1986) and for acetylcholine in pond snail neurones (Chemeris et al., 1982). However, as shown in Chapter 4 (Figure 4.8), the glutamate-evoked current is still abolished by removing extracellular sodium in low calcium containing solutions (which will prevent a rise in $[Ca^{2+}]_i$). It may be, therefore, that sodium is in some way required externally for glutamate to bind to its receptor in the cone membrane. In the turtle photoreceptor Tachibana and Kaneko (1988) found a hyperpolarizing shift in the reversal potential when external sodium was reduced, and suggested that glutamate acts via two mechanisms (as discussed in section 7.1.3) i.e. by opening channels and by activating a sodium-dependent carrier mechanism. Their data are difficult to reconcile with mine (see below).

(2) Anions

Changing the internal or external chloride concentration changed the reversal potential of the glutamate-induced current

in cone photoreceptors (Chapter 4, Figures 4.3 and 4.4), indicating that at least part of the current is carried by chloride ions. Glutamate-gated chloride channels have previously been shown to exist in locust muscle fibres (Cull-Candy, 1976) and in snail neurones (Szczepaniak and Cottrell, 1973). It is puzzling that Tachibana and Kaneko (1988) reported that the glutamate-induced current in turtle photoreceptors did not change when chloride was removed from the superfusate (replaced by methanesulfonate).

The reversal potentials of the cone response to glutamate were slightly more depolarized than what would have been predicted for a chloride-specific channel but the reversal potentials fitted the Goldman-Hodgkin-Katz equation with permeability ratios $P_{acetate}/P_{chloride} = 0.1$ and $P_{gluconate}/P_{chloride} = 0.1$ reasonably well (Chapter 4, Figure 4.5). This suggests that acetate and gluconate may pass through the glutamate-activated channels in the cone membrane. Acetate has been shown to pass through GABA- and glycine-gated chloride channels (Bormann, Hamill and Sakmann, 1987).

The glutamate-gated chloride conductance in salamander cone photoreceptors is different from GABA- and glycine-gated chloride channels. The glutamate-induced current was unaffected by bicuculline and strychnine at doses which reduced the GABA-induced current in ganglion cells (Chapter 4, Figure 4.7A) and the glycine-induced current in bipolar cells (Chapter 4, Figure 4.7B) respectively. The chloride current evoked by glutamate in cones shows inward rectification around the reversal potential, unlike the slight outward rectification observed for GABA-gated chloride currents in turtle cones (Kaneko and Tachibana, 1986). Furthermore, glutamate-gated channels in the cone membrane were less chloride-specific than those activated by GABA and glycine in retinal bipolar cells (Attwell et al., 1987).

7.1.6 Conductance of the glutamate-activated channel

The glutamate- and kainate-induced currents in cone photoreceptors were associated with a noise increase, consistent with these currents resulting from the opening of ion channels. (Current fluctuations are not usually detected in carrier-mediated responses (like glutamate uptake) since the charge translocated by a single "cycle" of the carrier is small.) The single channel

conductance calculated from the current noise increase during the kainate response in cones was 3.8 ±0.6 (s.d.) pS (n=3). Kainate predominantly activates the small conductance state of channels in hippocampal neurones (less than 5pS) (Jahr and Stevens, 1987), in cerebellar neurones (1-2pS) (Cull-Candy and Usowicz, 1987) and in retinal horizontal cells (2-3pS) (Ishida and Neyton, 1985). The single channel conductance calculated from the noise in the glutamate response was 1.4 ±1 (s.d.) pS (n=3). The conductance of the glutamate-activated channel in turtle cones is 0.5pS (Tachibana and Kaneko, 1988). In other central neurones the values reported are 140fS in rat cerebellar granule neurones (Cull-Candy, Howe and Ogden, 1988) and 5.4pS for axolotl retinal hyperpolarizing bipolar cells (Attwell et al., 1987).

Usually higher additional conductance levels are observed in channels gated by glutamate and its analogues. The various conductance levels produced are believed to be subconductance states of a single channel type with the predominant conductance level depending on the receptor type that is activated (Cull-Candy and Usowicz, 1987) and agonist concentration (Jahr and Stevens, 1987). Single channel recordings from membrane patches are necessary to test whether multiple conductance states occur for the glutamate-gated channels in the cone membrane.

From a spectral analysis of whole-cell noise, an estimate of the channel characteristics was made. The power spectra of the glutamate- and kainate-induced current fluctuations could be fitted by the sum of two Lorentzians. This implies a 3-state channel model (with for example 2 closed states and 1 open state; Chapter 3, section 3.3.4) assuming that there is only one type of glutamate-gated channel present in the cell membrane. It could be that there are two types of glutamate- (kainate-) gated channel in the membrane, each with two kinetically distinct states, contributing 2 Lorentzian components with different half power frequencies. Similar conclusions have been reached for glutamate-induced currents in cerebellar granule cells (Cull-Candy and Ogden, 1985) and retinal bipolar cells (Attwell et al., 1987)

7.1.7 Functional significance of the glutamate-induced current in cones

Glutamate evokes a current in cells that also release it. The magnitude of the current generated by this "autoreceptor" effect will depend (among other things) on how close the glutamate receptors are to the site of glutamate release. The response has been localized to the synaptic terminal of the cone (Chapter 3, Figure 3.10). Glutamate released from neighbouring rods or cones could also activate the cone glutamate receptors. These receptors are presynaptic with respect to transmission of information from photoreceptors to second order neurones. Glutamate receptors on presynaptic terminals have also been suggested to exist in the vertebrate cerebellum (Ferkany, Zaczek and Coyle, 1982), hippocampus (Errington, Lynch and Bliss, 1987), olfactory cortex (Collins, Anson and Surtees, 1983) and at the crayfish neuromuscular junction (Thieffry and Bruner, 1978). Usually, the autoreceptor systems for various neurotransmitters characterized to date have been found to operate in a negative feedback way (Starke, 1981).

Whether glutamate mediates a positive or negative feedback loop in cone photoreceptors depends on the chloride concentration in salamander cones. The chloride concentration in turtle cones has been estimated (Kaneko and Tachibana, 1986) to be between 12 and 24mM, suggesting a reversal potential for the glutamate-evoked current in vivo between -34 and -43mV (from Chapter 4, Figure 4.5A). Thus, over most or all of the cone light-response range (Attwell, Werblin and Wilson, 1982) (-40 to -65mV), glutamate will evoke an inward current in the cone and, when a stimulus (removal of light) depolarizes a cone, the feedback action of glutamate released will further depolarize the cone. As a result, the gain for the conversion of changes in light intensity into changes of glutamate release will be increased. This can be seen as follows. If a change of light intensity generates a current change, ΔI_{light}, in the cone outer segment, the resulting change of cone voltage, ΔV, will be determined by the cone resistance, R, and by the change in the current, ΔI_{glu}, evoked by glutamate binding to autoreceptors in the cone synaptic terminal:

$$\Delta V = R(\Delta I_{light} + \Delta I_{glu}) \qquad (13)$$

Assuming, for simplicity, that for small changes of light intensity the change in glutamate-evoked current is proportional to the local change in glutamate concentration, which in turn is assumed to be proportional to the membrane potential change (so that $\Delta I_{glu} = k\Delta V$ with k a constant), equation 13 becomes:

$$\Delta V = R(\Delta I_{light} + k\Delta V)$$

or

$$\Delta V = R\Delta I_{light} / (1-kR) \qquad (14)$$

Thus, the changes in cone voltage and glutamate release are increased by a factor of 1 / (1-kR) relative to the situation with no autoreceptors (k=0). This gain increase could be significant, because the glutamate-gated currents are comparable in size to the current changes produced by light (Chapter 3, Figure 3.12).

It might be expected that such a positive feedback loop could lead to a runaway depolarization in the cone. In theory, this will not occur as long as the strength of the feedback loop is low enough, i.e. $kR<1$ in equation 14. The strength of the feedback mechanism depends on several factors, including the fully-activated magnitude of the glutamate-induced current, the voltage-dependence of glutamate release, the reduction of glutamate concentration near the cone by diffusion away and by uptake into glial cells (all of which affect k), and the cone membrane resistance (R). In addition, cone depolarization is probably counteracted by the action of inhibitory transmitters released from horizontal cells onto cones (Attwell, et al., 1983). In practice, the cone potential is stable under normal conditions, showing graded voltage changes in response to illumination changes (Chapter 3, Figure 3.12).

It has been reported previously that when glutamate is perfused onto the intact retina photoreceptors are not polarized (Murakami, Ohtsuka and Ohtsuka, 1972). This may be accounted for as follows. In the dark the reversal potential for the glutamate-gated current is close to the cone dark potential, and so activating the current will generate little voltage change. In the light the glutamate applied to the whole retina will depolarize horizontal cells, causing a release of inhibitory neurotransmitter (e.g. GABA) which

hyperpolarizes the cones (Wu, 1986; Kaneko and Tachibana, 1986). For bulk perfusion of glutamate, there will be a large change in the voltage of the horizontal cells, and the inhibitory action on cones which results may outweigh the direct depolarizing action of glutamate seen here in isolated cells. However, for spatially restricted changes in illumination, there will be little voltage change in the horizontal cells as a result of changes in transmitter release from one or a few cones (i.e. only a small fraction of the cones projecting to each horizontal cell (Werblin and Dowling, 1969), and the positive feedback loop for glutamate will not be outweighed by inhibitory inputs from horizontal cells.

7.2. Discussion of the results in Chapter 5

Chapter 5 described the results of experiments studying the electrogenic uptake of glutamate into rabbit Müller cells. The pharmacological profile, voltage-dependence, dependence on extracellular glutamate, sodium and potassium, and dependence on intracellular potassium concentration were characterized.

7.2.1. Glutamate activates an electrogenic carrier mechanism in the membrane of rabbit Müller cells

Glutamate has been shown to gate ion channels in some cultured astrocytes (Sontheimer *et al.*, 1988; Usowicz, Gallo and Cull-Candy, 1989) and in isolated glial cells (Barres *et al.*, 1990), and astrocytes *in situ* (Clark and Mobbs, 1990), but in salamander Müller cells glutamate generates a current by activating an electrogenic uptake carrier (Barbour, Brew and Attwell, 1988; Brew and Attwell, 1987). The presence of electrogenic glutamate uptake in some glial cells is presumably related to their funtion of clearing synaptically-released glutamate from the extracellular space. The function of the glutamate-gated channels in other glial cells remains uncertain.

Rabbit retinal glial cells are known, from radiotracing experiments, to posses a glutamate uptake system (Ehinger, 1977). Glutamate generates an inward current in rabbit Müller cells that does not reverse even at very positive potentials (Chapter 5, Figure 5.3), suggesting that the current is due to glutamate acting on a electrogenic carrier mechanism. (Note that if glutamate and

sodium are present inside the cell, the uptake carrier must, at sufficiently positive potentials, reverse and produce an outward current. However, applying glutamate to the outside of a cell, as in the experiments described, will always result in an inward current being recorded, although this may be the result of suppressing an outward current produced by an efflux of glutamate with an excess of sodium ions.) The pharmacological profile of the response is another indication that glutamate acts on an uptake carrier rather than on ion channels. The compounds that produce an inward current, L-aspartate, D-aspartate and THDA, are all inhibitors of uptake of radiolabelled glutamate and have been shown (except THDA) to be taken up into cells (Balcar and Johnston, 1973; Erecinska et al., 1986). In addition, the glutamate analogues which activate different types of glutamate-gated ion channels, NMDA, quisqualate and kainate, produced almost no current.

In Müller cells of the rabbit retina glutamate evokes currents that are much smaller than those evoked in Müller cells of the salamander retina. However, when current data from both species are normalized by the capacitance of each cell (typically 300pF in salamander, 70pF in rabbit), to take into account the difference in cell size, values for uptake per unit area are more similar (0.4pA/pF at -40mV in salamander, 0.2pA/pF in rabbit). A glutamate-evoked current with a similar voltage-dependence, possibly reflecting electrogenic glutamate uptake, has been found in rat cerebellar type-1 astrocytes (Cull-Candy, Howe and Ogden, 1988).

7.2.2 Stochiometry of glutamate uptake

Glutamate

The fact that the activation of the current by glutamate obeys Michaelis-Menten kinetics (Chapter 5, Figure 5.4) suggests that one glutamate is transported into the cell for each cycle of the uptake carrier. If uptake of glutamate into glial cells is important for terminating the synaptic action of glutamate, uptake has to operate at micromolar concentrations. The uptake carrier in rabbit Müller cells has an apparent K_m for glutamate binding of 4.7μM. Glutamate is negatively charged at physiological pH. Other positively charged ions must be co-transported on the uptake carrier to generate an inward current.

Sodium

The dependence of the current on external sodium is sigmoid at low concentrations (Chapter 5, Figure 5.6), suggesting that two or more sodium ions bind to the carrier to activate uptake. This result disagrees with earlier radiotracing data from glial cells. Drejer, Larsson and Schousboe (1982) show a sigmoid sodium-dependence for uptake in cultured granule cells, but a Michaelis-Menten sodium-dependence for cultured astrocytes. However, direct measurement of sodium and glutamate fluxes found a sodium:glutamate transport ratio of 2 in both neuronal and glial cultures (Stallcup, Bulloch and Baetge, 1979; Baetge, Bulloch and Stallcup, 1979) or of 2-3 in cultured astrocytes (Kimelberg, Pang and Treble, 1989). Co-transport of sodium ions on the glutamate uptake carrier is thought to provide the energy needed to transport glutamate into the cell (Baetge, Bullock and Stallcup, 1979; Roskoski, 1978). It could be postulated that sodium activates the glutamate-evoked current in Müller cells but is not actually transported into the cell. However, raising internal sodium ion concentration suppresses the glutamate-activated uptake current in salamander Müller cells, an observation it is difficult to account for without postulating sodium transport.

Potassium

Radiotracing experiments have suggested that potassium ions are counter-transported on the glutamate uptake carrier (Kanner and Sharon, 1978); Burckhardt et al., 1980; Kanner and Marva, 1982). However, in this type of experiment where the cell is not voltage-clamped, it is difficult to separate a direct effect of changing the concentration of potassium on glutamate uptake from an effect on uptake of changing the membrane potential (as a result of changing the potassium concentration).

In voltage-clamp experiments internal potassium activates the uptake of glutamate into rabbit Müller cells (Chapter 5, Figure 5.7). The $[K^+]_i$-dependence of the uptake current is, for the limited data available, consistent with Michaelis-Menten kinetics, suggesting that one intracellular potassium ion binds to the carrier and is presumably transported out of the cell for each cycle of the carrier. Raising external potassium ion concentration inhibits glutamate uptake (Chapter 5, Figure 5.8). One explanation for this

result could be that potassium competes with sodium for the binding site. However, Barbour, Brew and Attwell (1988) have shown that in salamander Müller cells the apparent affinity for sodium is not changed when external potassium is raised from 2.5 to 57mM. The inhibition by external potassium supports the idea that potassium is transported out of the cell on the glutamate uptake carrier. Szatkowski, Barbour and Attwell (1990) have recently shown that external potassium stimulates reversed uptake (release) of glutamate in salamander Müller cells: another indication that potassium is transported by the carrier.

It has been suggested that some potassium-independent uptake may occur in salamander Müller cells (Barbour, Brew and Attwell, 1991), although most of the glutamate-evoked current is abolished in zero internal potassium concentration. Potassium-independent uptake takes place in the kidney (Burckhardt et al., 1980; Nelson et al., 1983). Recently Schwartz and Tachibana (1990) have shown that removing potassium from the patch pipette solution does not reduce the D-aspartate-evoked uptake current in salamander Müller cells. This probably results from the fact that they used small diameter (high resistance) patch pipettes and may therefore not have been controlling the intracellular solution adequately. This is especially important when looking at the effect of reducing internal potassium ion concentration on the uptake of D-aspartate since the K_m for binding of intracellular potassium is much lower when D-aspartate is being transported than when L-glutamate is being carried (Barbour, Szatkowski and Attwell, in preparation). The advantage to the uptake carrier of transporting K^+ is not clear since the resting potential of glial cells is close to the potassium reversal potential and therefore little energy is provided by carrying potassium out of the cell.

The first-order dependence of the current on the external glutamate concentration, the dependence on intra- and extracellular potassium concentration and the sigmoid dependence on the external sodium concentration suggest that the simplest stochiometry possible for the carrier is one in which three sodium ions are transported into the cell with every negatively charged glutamate, and one potassium ion is transported out, generating a net inward current.

It has been shown in the salamander that chloride, calcium and magnesium are not involved in generating the glutamate-evoked current (Barbour, Brew and Attwell, 1988). However, it is possible that a hydrogen ion is transported in the place of one sodium ion: transport of hydrogen ions linked to the uptake of glutamate has been shown in the renal brush border (Nelson et al., 1983).

7.2.3. Speed of glutamate uptake by rabbit Müller cells

Whether uptake of glutamate in Müller cells plays an important role in terminating the neurotransmitter action of glutamate will depend on several factors: (1) How close do Müller cell processes come to the synaptic region? (2) How much glutamate is taken up into the presynaptic cell? (3) What is the speed of the uptake mechanism in Müller cells? Chapter 6 describes the results of experiments addressing the question of the anatomical arrangement of Müller cell processes and the photoreceptor output synapse in the retina of the salamander. These results are discussed in section 7.3. It is known from radiotracing experiments that glutamate is taken up into photoreceptors (Marc and Lam,1981; Miller and Schwartz, 1983) but the rate of uptake cannot be determined from those experiments.

From the uptake current described in Chapter 5 it is possible to make an estimate of the time constant for the removal of glutamate from the extracellular space by uptake into rabbit Müller cells, thus addressing question 3 above. To do the calculation the following assumptions have been made: (I) The extracellular glutamate concentration is uniform throughout the retinal extracellular space; (II) The glutamate carriers are evenly distributed in the Müller cell membrane.

The dose-response curve for the glutamate-evoked current shows a Michaelis-Menten dependence on glutamate concentration (Figure 5.4):

$$I = I_{max} \cdot (G / (G + K_m)) \qquad (15)$$

in which: G = extracellular glutamate concentration

I_{max} = 75pA at the Müller cell resting potential

K_m = 4.7μM (Chapter 5, section 5.3.3)

The rate of change of the extracellular glutamate concentration, G (moles/m^3/second, is given by:

$$dG / dt = I / (F \times V) \qquad (16)$$

in which: F = Faraday constant (assuming that one net positive charge moves into the cell for each glutamate taken up

V = the extracellular volume to be cleared of glutamate by each Müller cell is $0.6 \times 10^{-14} m^3$ (Müller cells are spaced 32µm apart (Reichenbach, 1987), the retinal depth is 120µm, and the retinal extracellular volume is 5% (Reichenbach et al., 1988)

Thus, $$dG / dt = -(G / (G + K_m)) \cdot (I_{max} / (F \times V))$$

If $I_{max} / (F \times V)$ is expressed as constant k, this expression can be rearranged as:

$$\int((G + K_m) / G)\, dG = -\int k\, dt$$

solving this equation gives:

$$t_{1/2} = (-(K_m \times \ln 0.5) + G_o/2) / k$$

in which: $t_{1/2}$ is the half clearance time

G_o is the glutamate concentration at t = 0

If G_o is 10µM, $t_{1/2}$ is 7ms and if G_o is 100µM, $t_{1/2}$ is 43ms. For comparison in the turtle retina the time constant of the decay of the postsynaptic event in horizontal cells is 30ms when the presynaptic cell is a cone and 200mS when it is a rod (Copenhagen, Ashmore and Schnapf, 1983). Although the synaptic current time course may be faster in a rabbit, this rough calculation suggests that the removal of glutamate by uptake into Müller cells could be fast enough for the falling phase of the response to reflect the time course of glutamate removal.

The rate of uptake in rabbit Müller cells in vivo may be different to the rate assumed for this calculation. Experiments to study the glutamate uptake carrier in rabbit Müller cells were carried out at room temperature. Stallcup, Bulloch and Baetge (1979) have shown that glutamate transport is temperature dependent in cultured neurones. In these cells the rate of uptake at 37°C was 3-fold higher than at 20°C. The cell isolation procedure may also affect the uptake current since cell processes that probably contain glutamate uptake carriers in the membrane may be pulled of or retracted and enzyme treatment may destroy some carriers. Both of these corrections would imply that glutamate removal in vivo was faster then that calculated above.

7.2.4 Failure of the glutamate-uptake system during pathological conditions

My experiments on rabbit Müller cells suggest that the glutamate uptake carrier in mammalian retinal glia is similar to that in salamander retinal glia (Barbour, Brew and Attwell, 1988) and to that in mammalian neurones (as studied by radiotracing: Kanner and Schuldiner, 1987). In this section I will assume that glutamate uptake in mammalian astrocytes elsewhere in the brain has properties similar to those which I have characterized for mammalian retinal glia, and use my data to analyse why glutamate uptake fails to prevent a rise in extracellular glutamate concentration to neurotoxic levels in pathological conditions like stroke or perinatal asphyxia.

In pathological conditions such as anoxia and ischaemia the intracellular ATP concentration falls, leading to a rise in extracellular potassium concentration (Hansen, 1981). This raised $[K^+]_o$ leads to depolarization of both neurones and glial cells. Consequently, there will be an increase in the release of glutamate from depolarized neurones leading in turn to more neuronal depolarization and thus to more potassium and glutamate release (see Figure 7.1). This chain of events tends to lead to a runaway increase of $[glutamate]_o$ (and $[K^+]_o$). The rise in $[glutamate]_o$ should, in principle, be opposed by the action of glutamate uptake. However, during these events glutamate uptake will be inhibited for three reasons. First, the increased $[K^+]_o$ will prevent transported

Figure 7.1 Schematic diagram of why glutamate uptake fails during anoxia.

Anoxia leads to a decrease of intracellular ATP levels. Consequently, the Na/K pump is unable to maintain the normal transmembrane ion gradients, and $[K^+]_o$ rises and $[Na^+]_o$ falls. ($[Na^+]_o$ will also fall as a result of sodium influx through glutamate-gated channels and through voltage-dependent sodium channels). The rise in $[K^+]_o$ depolarizes neurones and glia. Consequently, neurones release more glutamate and the extracellular glutamate concentration rises. This in turn leads to more depolarization of neurones and more K^+ release, and so the chain of events linked by continuous arrows on the left of the figure is a positive feedback system which tends to generate a runaway increase of $[glutamate]_o$ and $[K^+]_o$. The data in Figures 5.6, 5.8 and 5.3 (Chapter 5) show that the decrease in $[Na^+]_o$, increase in $[K^+]_o$, and membrane depolarization will all inhibit glutamate uptake, making it easier for the extracellular glutamate concentration to rise to neurotoxic levels.

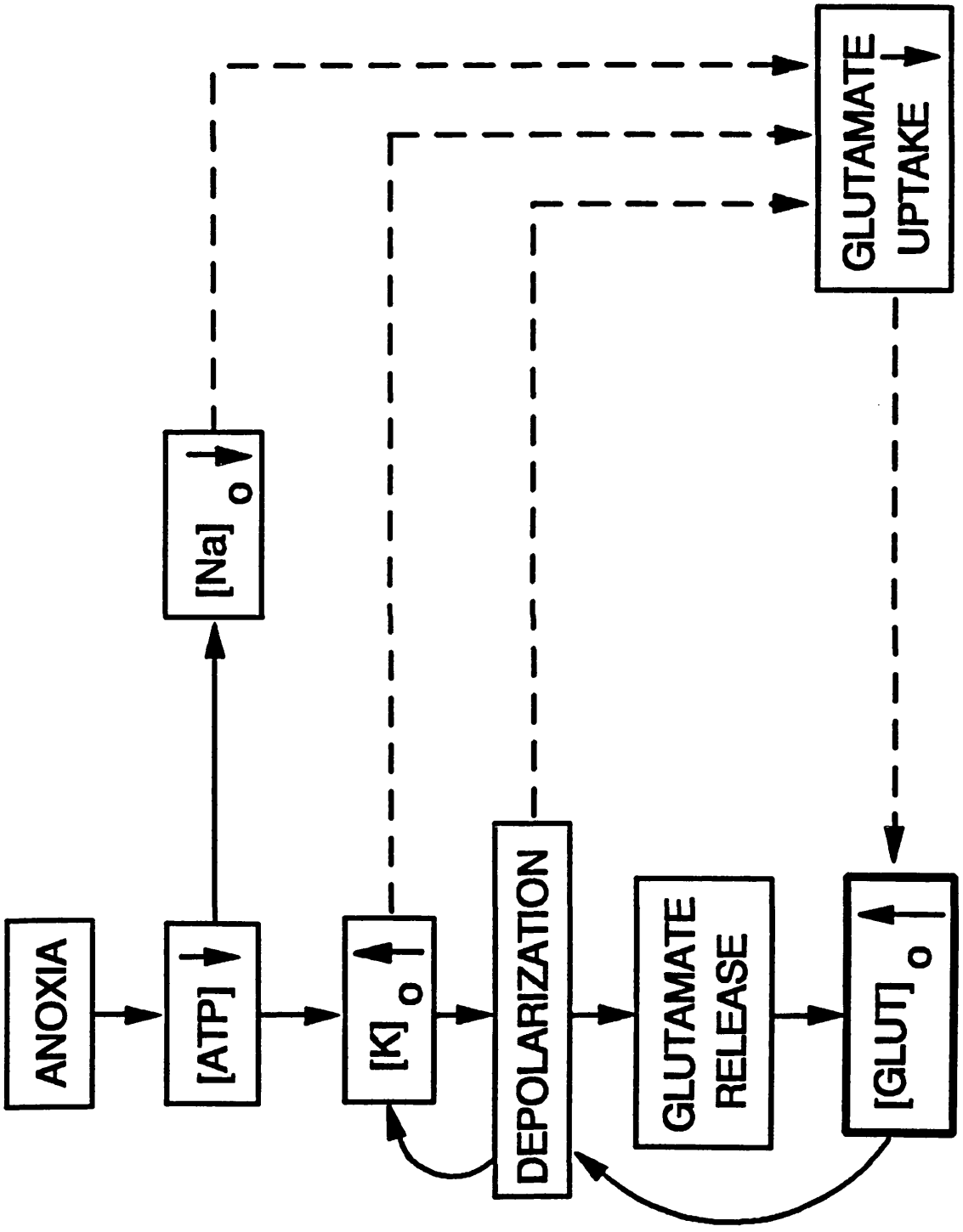
ANOXIA
[ATP]
[Na] o
[K] o
DEPOLARIZATION
GLUTAMATE RELEASE
[GLUT] o
GLUTAMATE UPTAKE

K^+ leaving the carrier at the outer membrane surface (Chapter 5, Figure 5.8). Second, a depolarization of glial cells by the raised $[K^+]_o$ will inhibit glutamate uptake (Chapter 5, Figure 5.3). Third, $[Na^+]_o$ decreases in anoxia because the sodium pump is inhibited and because of Na^+ influx through voltage- and neurotransmitter gated channels, and a $[Na^+]_o$ decrease inhibits uptake. The combination of these effects reduce the uptake rate to less than 8% of the normal rate of uptake (Chapter 5, Figure 5.9).

The rise in extracellular glutamate concentration during anoxia (Rothman and Olney, 1987) may not be solely due to a vesicular release from neurones, since vesicular release is known to be inhibited when ATP levels fall (Sanchez-Prieto and Gonzalez, 1988). It has recently been shown that the changes in voltage and ion gradients described above may lead to a reversal of glutamate uptake, resulting in glutamate being released from glial cells into the extracellular space (Szatkowski, Barbour and Attwell, 1990) thus possibly contributing to the rise in extracellular glutamate concentration.

The combination of the circumstances described above may lead to the extracellular glutamate concentration rising to neurotoxic levels; too much activation of NMDA-type glutamate channels in neurones leads to an excessive influx of calcium which activates lethal proteases in these cells, and neurones may swell due to excessive glutamate-induced ion movement (Rothman and Olney, 1987; Siesjö and Bengtsson, 1989). Choi, Maulucci-Gedde and Kriegstein (1987) showed that 50% of cortical neurones in culture were killed after a 5-minute exposure to 100μM glutamate. It has been shown in animal studies that NMDA antagonists protect against or reduce ischaemic brain damage (Boast *et al.*, 1988; Gill, Foster and Woodruff, 1987; Simon *et al.*, 1984; Steinberg, Saleh and Kunis, 1988). *In vivo*, the extracellular acidification which is known to accompany increased extracellular glutamate levels (Dingledine *et al.*, 1988) might give some limited protection against the neurotoxic effects of raised extracellular glutamate, since protons have been shown to decrease the opening frequency of NMDA channels in cultured neurones (Traynelis and Cull-Candy, 1990).

7.3 Discussion of the results in Chapter 6

In Chapter 6 the anatomical arrangement of Müller cell processes and the photoreceptor output synapse in the outer retina of the salamander is described.

7.3.1 Morphology of Müller cell processes in the outer retina

In morphological studies Müller cell processes are usually identified in between the neural elements by clusters of ribosomes and glycogen particles (Dowling and Boycott, 1966; Reichenbach *et al.*, 1988). However, identification of the processes of these cells can be difficult because: (1) they can be very small, and (2) the above described elements have been reported to be sparser in the processes of the Müller cells in the outer plexiform layer (Reichenbach *et al.*, 1988) which is the layer in which I was most interested. In the experiments described in this thesis (Chapter 6), injecting Müller cells with HRP provided a good marker for even very small processes, as observed in the electron microscope (Chapter 6, Figures 6.3 to 6.5).

The experiments described in Chapter 6 show that Müller cell processes wrap around part of the synaptic pedicles of rod and cone photoreceptors but hardly ever invade the outer plexiform layer where the synaptic contacts with second order neurones are made. Müller cell processes were never seen to be part of the diadic or triadic arrangement of processes on the postsynaptic side of the synaptic cleft.

7.3.2 Müller cells: role in terminating the action of glutamate

Glutamate released from photoreceptors diffuses away from its site of release into the extracellular space. The action of glutamate is thought to be terminated by uptake of the transmitter into Müller cells or neurones since no extracellular enzyme is present to break down glutamate. An approximate formula for the distance (x) glutamate will have diffused at a time (t) after release is:

$$x^2 = 2.D.t \quad \text{(Chapter 3, section 3.3.6)} \qquad (17)$$

in which: D is the diffusion coefficient (about $10^{-9} m^2/s$)

The time course of the decay phase of the postsynaptic event in horizontal cells in the turtle retina is 30ms for glutamate release from cones and 200ms for glutamate release from rods (Copenhagen, Ashmore and Schnapf, 1983). At t=30ms glutamate will have diffused about 7.7μm (according to equation 1.7). For comparison the closest approach of a Müller cell process to the synaptic cleft associated with synaptic ribbons in the pedicles of salamander photoreceptors was measured to be 1.04μm for rods and 3.04μm for cones (Chapter 6, section 6.3.3) (shrinkage of the tissue during processing was not taken into account but is believed to be less than 5% (Glauert, 1975)). It will take 0.6ms for glutamate to diffuse 1.05μm and 4.6ms to diffuse 3.04μm (using equation 17). For most of the ribbon synapses in the photoreceptor terminals of the salamander the distances to a Müller cell processes will be longer than those quoted above. The longest distance that glutamate has to diffuse is 8μm (which will take 32ms according to equation 17) since photoreceptors are spaced on average 16μm apart (Attwell, Wilson and Wu, 1984). Thus, although Müller cell processes do not invade the postsynaptic side of the synapse, processes come close enough to play a role in terminating the action of glutamate.

The time course of the decaying phase of the synaptic current during transmission from rods to postsynaptic horizontal cells is about 7 times longer than for transmission from cones to horizontal cells. This cannot be as a consequence of a longer diffusion distance to a Müller cell which is removing the glutamate: the results described in Chapter 6 show that, typically, the rod output synapse is actually closer to processes of Müller cell than the cone output synapse is: (1) because of the clustering of synaptic terminals in which the rod terminals abut the cone terminals and the Müller cell processes wrap around the outside of the group of terminals and hence are closer to the rod terminals (Chapter 6, Figure 6.5A); (2) even if the Müller cell wraps around single pedicles, the difference in shape between the rod and cone synaptic pedicles (the base of the cone pedicle where the ribbon synapses are situated is much wider) means that the distance between the photoreceptor synaptic ribbon and a Müller cell process is on average shorter in rods.

References

Aizenman, E., Frosch, M. P. and Lipton, S. A. (1988) Responses mediated by excitatory amino acid receptors in solitary retinal ganglion cells from rat, J. Physiol., 396: 75-91.

Ariel, M., Lasater, E. M., Mangel, S. C. and Dowling, J. E. (1984) On the sensitivity of H1 horizontal cells of the carp retina to glutamate, aspartate, and their agonists, Brain Research, 295: 179-183.

Attwell, D., Mobbs, P., Tessier-Lavigne, M. and Wilson, M. (1987) Neurotransmitter-induced currents in retinal bipolar cells of the axolotl, Ambystoma Mexicanum, J. Physiol., 387: 125-161.

Attwell, D., Werblin, F. S. and Wilson, M. (1982) The properties of single cones isolated from the tiger salamander retina, J. Physiol., 328: 259-283.

Attwell, D., Werblin, F. S., Wilson, M. and Wu, S. M. (1983) A sign-reversing pathway from rods to double and single cones in the retina of the tiger salamander, J. Physiol., 336: 313-333.

Attwell, D. and Wilson, M. (1980) Behaviour of the rod network in the tiger salamander retina mediated by membrane properties of individual rods, J. Physiol., 309: 287-315.

Attwell, D., Wilson, M. and Wu, S. M. (1984) A quantitative analysis of interactions between photoreceptors in the salamander (Ambystoma) retina, J. Physiol., 352: 703-737.

Ayoub, G. S. and Lam, D. M. K. (1984) The release of γ-aminobutyric acid from horizontal cells of the goldfish (Carassius Auratus) retina, J. Physiol., 355: 191-214.

Ayoub, G. S., Korenbrot, J. I. and Copenhagen, D. R. (1989) Release of endogenous glutamate from isolated cone photoreceptors of the lizard, Neurosci. Research Suppl., 10: 547-556.

Bader, C. R., Macleish, P. R. and Schwartz, E. A. (1979) A voltage-clamp study of the light response in solitary rods of the tiger salamander, J. Physiol., 296: 1-26.

Baetge, E. E., Bullock, K. and Stallcup, W. B. (1979) A comparison of glutamate transport in cloned cell lines from the central nervous system, Brain Research, 167: 210-214.

Balcar, V. J. and Johnston, G. A. R. (1972) The structural specificity of the high affinity uptake of L-glutamate and L-aspartate by rat brain slices, J. Neurochem., 19: 2657-2666.

Balcar, V. J. and Johnston, G. A. R. (1973) High affinity uptake of transmitters: studies on the uptake of L-aspartate, GABA, L-glutamate and glycine in cat spinal cord, J. Neurochem., 20: 529-539.

Barbour, B., Brew, H. and Attwell, D. (1988) Electrogenic glutamate uptake in glial cells is activated by intracellular potassium, Nature, 335: 433-435.

Barbour, B., Brew, H. and Attwell, D. (1991) Electrogenic uptake of glutamate and aspartate into glial cells isolated from the salamander (Ambystoma) retina, J. Physiol., in press.

Barres, B. A., Koroshetz, W. J., Schwartz, K. J., Chun, L. L. Y. and Corey, D. P. (1990) Ion channel phenotype of white matter glia II. The O2A glial progenitor cell, Neuron, 4: 507-524.

Baylor, D. A., Fuortes, M. G. F. and O'Bryan, P. M. (1971) Receptive fields of cones in the retina of the turtle, J. Physiol., 214: 265-294.

Benveniste, H., Drejer, J., Schousboe, A. and Diemer, N. H. (1984) Elevation of the extracellular concentrations of glutamate and aspartate in rat hippocampus during transient cerebral ischemia monitored by intracerebral microdialysis, J. Neurochem., 43: 1369-1374.

Bloomfield, S. A. and Dowling, J. E. (1985a) Roles of aspartate and glutamate in synaptic transmission in rabbit retina. I. Outer plexiform layer, J. Neurophysiol., 53: 699-713.

Bloomfield, S. A. and Dowling, J. E. (1985b) Roles of aspartate and glutamate in synaptic transmission in rabbit retina. II. Inner plexiform layer, J. Neurophysiol., 53: 714-725.

Boast, C. A., Gerhardt, S. C., Pastor, G., Lehmann, J., Etienne, P. E., and Liebman, J. M. (1988) The N-methyl-D-aspartate antagonists CGS 19755 and CPP reduce ischemic brain damage in gerbils, Brain Research, 442: 345-348.

Bormann, J., Hamill, O. P. and Sakmann, B. (1987) Mechanism of anion permeation through channels gated by glycine and γ-aminobyturic acid in mouse cultured spinal neurones, J. Physiol., 385: 243-286.

Bormann, J. and Kettenmann, H. (1988) Patch-clamp study of γ-aminobutyric acid receptor Cl^- channels in cultured astrocytes, Proc. Natl. Acad. Sci. USA, 85: 9336-9340.

Bowman, C. L. and Kimelberg, H. K. (1984) Excitatory amino acids directly depolarize rat brain astrocytes in primary culture, Nature, 311: 656-659.

Brandon, C and Lam, D. M.-K. (1983) L-Glutamic acid: A neurotransmitter candidate for cone photoreceptors in human and rat retinas, Proc. Natl. Acad. Sci. USA, 80: 5117-5121.

Brew, H. and Attwell, D. (1987) Electrogenic glutamate uptake is a major current carrier in the membrane of axolotl retinal glial cells, Nature, 327: 707-709.

Brightman, M. W. and Reese, T. S. (1969) Junctions between intimately apposed cell membranes in the vertebrate brain, J. Cell Biol., 40: 648-677.

Burckhardt, G., Kinne, R., Stange, G. and Murer, H. (1980) The effects of potassium and membrane potential on sodium-dependent glutamic acid uptake, Biochim. et. Biophys. Acta, 599: 191-201.

Cervetto, L. and Piccolino, M. (1974) Synaptic transmission between photoreceptors and horizontal cells in the turtle retina, Science, 183: 417-419.

Chemeris, N. K., Kazachenko, V. N., Kislov, A. N. and Kurchikov, A. L. (1982) Inhibition of acetylcholine responses by intracellular calcium in Lymnaea stagnalis neurones, J. Physiol., 323: 1-19.

Chen, Q. X., Stelzer, A., Kay, A. R. and Wong, R. K. S. (1990) $GABA_A$ receptor function is regulated by phosphorylation in acutely dissociated guinea-pig hippocampal neurones, J. Physiol., 420: 207-221.

Chin, C.-A. and Lam, D. M. K. (1980) The uptake and release of [^{3}H]-glycine in the goldfish retina, J. Physiol., 308: 185-195.

Choi, D. W., Maulucci-Gedde, M. and Kriegstein, A. R. (1987) Glutamate neurotoxicity in cortical cell culture, J. Neurosci., 7: 357-368.

Clark, B. and Mobbs, P. (1990) Transmitter-gated ion channels in retinal astrocytes in situ studied in the isolated retina of the rabbit, J. Physiol., abstract submitted.

Collins, G. G. S., Anson, J. and Surtees, L. (1983) Presynaptic kainate and N-methyl-D-aspartate receptors regulate excitatory amino acid release in the olfactory cortex, Brain Research, 265: 157-159.

Colquhoun, D. and Hawkes, A. G. (1977) Relaxation and fluctuations of membrane currents that flow through drug-operated channels, Proc. R. Soc. Lond. B., 199: 231-262.

Copenhagen, D. R., Ashmore, J. F. and Schnapf, J. K. (1983) Kinetics of synaptic transmission from photoreceptors to horizontal and bipolar cells in turtle retina, Vision Res., 23: 363-369.

Crank, J. (1976) In: The mathematics of diffusion, Clarendon Press, London.

Cull-Candy, S. G. (1976) Two types of extrajunctional L-glutamate receptors in locust muscle fibres, J. Physiol., 255: 449-464.

Cull-Candy, S. G., Howe, J. R. and Ogden, D. C. (1988) Noise and single channels activated by excitatory amino acids in rat cerebellar granule neurones, J. Physiol., 400: 189-222.

Cull-Candy, S. G. and Ogden, D. C. (1985) Ion channels activated by L-glutamate and GABA in cultured cerebellar neurons of the rat, Proc. R. Soc. Lond. B, 224: 367-373.

Cull-Candy, S. G. and Usowicz, M. M. (1987) Multiple-conductance channels activated by excitatory amino acids in cerebellar neurons, Nature, 325: 525-528.

DeRobertis, E. and Franchi, C. M. (1956) Electron microscope observations on synaptic vesicles in synapses, J. Biophys. Biochem. Cytol., 2: 307-330.

Dingledine, R., Boland, L. M., Chamberlin, N. L., Kawasaki, K., Kleckner, N. W., Traynelis, S. F. and Verdoorn, T. A. (1988) Amino acid receptors and uptake systems in the mammalian central nervous system, CRC Critical Rev. Neurobiol., 4: 1-96.

Dowling, J. E. (1987) The retina: an approachable part of the brain, The Belknap Press of Harvard University Press, London.

not quoted:

Dudel J, Franke C, Hatt H & Usherwood PNR (1989) Chloride channels gated by extrajunctional glutamate receptors (H-receptors) on locust leg muscle. Brain Res. 481: 215-220.

Dowling, J. E. and Boycott, B. B. (1966) Organization of the primate retina: electron microscopy, Proc. R. Soc. Lond. B., 166: 80-111.

Dowling, J. E. and Ehinger, B. (1975) Synaptic organization of the amine-containing interplexiform cells of the goldfish and Cebus monkey retinas, Science, 188: 270-273.

Dowling, J. E. and Ripps, H. (1973) Effect of magnesium on horizontal cell activity in the skate retina, Nature, 242: 101-103.

Dowling, J. E. and Werblin, F. (1969) Organization of the retina of the mudpuppy, Necturus maculosus, I. Synaptic structure, J. Neurophysiol., 32: 315-338.

Drejer, J., Larsson, O. M. and Schousboe, A. (1982) Characterization of L-glutamate uptake into and release from astrocytes and neurons cultured from different brain regions, Exp. Brain Res., 47: 259-269.

Dudel, J., Franke, Ch. and Hatt, H. (1990) Rapid activation, desensitization, and resensitization of synaptic channels of crayfish muscle after glutamate pulses, Biophys. J., 57: 533-545.

Ehinger, B. (1972) Cellular location of the uptake of some amino acids into the rabbit retina, Brain Research, 46: 297-311.

Ehinger, B. (1977) Glial and neuronal uptake of GABA, glutamic acid, glutamine and glutathione in the rabbit retina, Exp. Eye Res., 25: 221-234.

Ehinger, B., Falck, B. and Laties, A. M. (1969) Adrenergic neurons in teleost retina, Z. Zellforsch. Mikrosk. Anat., 97: 285-297.

Erecinska, M., Troeger, M. B., Wilson, D. F. and Silver, I. A. (1986) The role of glial cells in regulation of neurotransmitter amino acids in the external environment. II. Mechanism of aspartate transport, Brain Research, 369: 203-214.

Errington. M. L., Lynch, M. A. and Bliss, T. V. P. (1987) Long-term potentiation in the dentate gyrus: induction and increased glutamate release are blocked by D(-)aminophosphonovalerate, Neurosci., 20: 279-284.

Everett, K., Mobbs, P. and Thompson, R. (1989) The voltage- and transmitter-gated membrane currents of retinal ganglion cells isolated from the salamander retina, J. Physiol., 415: 41P.

Fenwick, E. M., Marty, E. and Neher, E. (1982) A patch-clamp study of bovine chromaffin cells and of their sensitivity to acetylcholine, J. Physiol., 331: 577-597.

Ferkany, J. W., Zaczek, R. and Coyle, J. T. (1982) Kainic acid stimulates excitatory amino acid neurotransmitter release at presynaptic receptors, Nature, 298: 757-759.

Fesenko, E. E., Kolesnikov, S. S. and Lyubarsky, A. L. (1985) Induction by cyclic GMP of cationic conductance in plasma membrane of retinal rod outer segments, Nature, 313: 310-313.

Foster, A. C. and Fagg, G. E. (1984) Acidic amino acid binding sites in mammalian neuronal membranes: their characteristics and relationship to synaptic receptors, Brain Res. Rev., 7: 103-164.

Ganong, A. H., Lanthorn, T. H. and Cotman, C. W. (1983) Kynurenic acid inhibits synaptic and acidic amino acid-induced responses in the rat hippocampus and spinal cord, Brain Research, 273: 170-174.

Gill, R., Foster, A. C. and Woodruff, G. N. (1987) Systemic administration of MK-801 protects against ischemia-induced hippocampal neurodegeneration in the gerbil, J. Neurosci., 7: 3343-3349.

Glauert, A. M. (1975) Fixation, dehydration and embedding of biological specimens, North-Holland Publishing Company, Amsterdam.

Hablitz, J. J. and Langmoen, I. A. (1982) Excitation of hippocampal pyramidal cells by glutamate in the guinea-pig and rat, J. Physiol., 325: 317-331.

Hamill, O. P., Marty, A., Neher, E., Sakmann, B. and Sigworth, F. J. (1981) Improved patch-clamp techniques for high-resolution current recording from cells and cell-free membrane patches, Pflügers Arch., 391: 85-100.

Hansen, A. J. (1981) Extracellular ion concentrations in cerebral ischemia. In: The application of ion-selective microelectrodes, Ed. Zeuthen, T., Elsevier, Amsterdam.

Hirsch, J. G. and Fedorko, M. E. (1968) Ultrastructure of human leucocytes after simultaneous fixation with glutaraldehyde and osmium tetroxide and "postfixation" in uranyl acetate, J. Cell Biol., 38: 616-627.

Honore, T., Davies, S. N., Drejer, J., Fletcher, E. J., Jacobsen, P., Lodge, D. and Nielsen, F. E. (1988) Quinoxalinediones: potent competitive non-NMDA glutamate receptor antagonists, Science, 241: 701-703.

Inoue, M., Oomura, Y., Yakushiji, T. and Akaike, M. (1986) Intracellular calcium ions decrease the affinity of the GABA receptor, Nature, 324: 156-158.

Ishida, A. T. and Cohen, B. N. (1988) GABA-activated whole-cell currents in isolated retinal ganglion cells, J. Neurophysiol., 60: 381-396.

Ishida, A. T., Kaneko, A. and Tachibana, M. (1984) Responses of solitary retinal horizontal cells from Carassius auratus to L-glutamate and related amino acids, J. Physiol., 348: 255-278.

Ishida, A. T. and Neyton, J. (1985) Quisqualate and L-glutamate inhibit retinal horizontal-cell responses to kainate, Proc. Natl. Acad. Sci. USA, 82: 1837-1841.

Jahr, C. E. and Stevens, C. F. (1987) Glutamate activates multiple single channel conductances in hippocampal neurons, Nature, 325: 522-525.

Johnston, G. A. R., Kennedy, S. M. E. and Twitchin, B. (1979) Action of the neurotoxin kainic acid on high affinity uptake of L-glutamic acid in rat brain slices, J. Neurochem., 32: 121-127.

Kaneko, A. and Tachibana, M. (1986) Effects of γ-aminobutyric acid on isolated cone photoreceptors of the turtle retina, J. Physiol., 373: 443-461.

Kaneko, A. and Tachibana, M. (1987) Effects of L-glutamate on isolated turtle photoreceptors, Invest. Ophthalmol. (Suppl.), 28:50.

Kanner, B. I. and Marva, E. (1982) Efflux of L-glutamate by synaptic plasma membrane vesicles isolated from rat brain, Biochemistry, 21: 3143-3147.

Kanner, B. I. and Sharon, I. (1978) Active transport of L-glutamate by membrane vesicles isolated from rat brain, Biochemistry, 17: 3949-3953.

Kanner, B. I. and Schuldiner, S. (1987) Mechanism of transport and storage of neurotransmitters, CRC Critical Reviews in Biochemistry, 22: 1-38.

Karnovsky, M. J. (1965) A formaldehyde-glutaraldehyde fixative of high osmolarity for use in electron microscopy, J. Cell Biol., 27: 137A.

Katz, B. and Miledi, R. (1967) A study of synaptic transmission in the absence of nerve impulses, J. Physiol., 192: 407-436.

Kennedy, A. J., Voaden, M. J. and Marshall, J. (1974) Glutamate metabolism in the frog retina, Nature, 252: 50-51.

Kettenmann, H. and Schachner, M. (1985) Pharmacological properties of γ-aminobutyric acid-, glutamate-, and aspartate-induced depolarizations in cultured astrocytes, J. Neurosci., 5: 3295-3301.

Kimelberg, H. K., Pang, S. and Treble, D. H. (1989) Excitatory amino acid-stimulated uptake of $^{22}Na^{+}$ in primary astrocyte cultures, J. Neurosci., 9: 1141-1149.

Kiskin, N. I., Krishtal, O. A. and Tsyndrenko, A. Y. (1986) Excitatory amino acid receptors in hippocampal neurons: Kainate fails to desensitize them, Neurosci. Lett., 63: 225-230.

Kolb, H. (1970) Organization of the outer plexiform layer of the primate retina: electron microscopy of Golgi-impregnated cells, Phil. Trans. R. Soc. B, 258: 261-283.

Kvamme, E., Schousboe, A., Hertz, L., Torgner, I. A. and Svenneby, G. (1985), Developmental change of endogenous glutamate and gamma-glutamyl transferase in cultured cerebral cortical interneurons and cerebellar granule cells and in mouse cerebral cortex and cerebellum in vivo, Neurochem. Research, 10: 993-1008.

Lasansky, A. (1971) Synaptic organization of cone cells in the turtle retina, Phil. Trans. R. Soc. B, 262: 365-381.

Lasansky, A. (1973) Organization of the outer synaptic layer in the retina of the larval tiger salamander, Proc. R. Soc. Lond. B, 265: 471-489.

Lasater, E. M. and Dowling, J. E. (1982) Carp horizontal cells in culture respond selectively to L-glutamate and its agonists, Proc. Natl. Acad. Sci., USA, 79: 936-940.

Lasater, E. M. and Dowling, J. E. (1985) Dopamine decreases conductance of the electrical junctions between cultured retinal horizontal cells, Proc. Natl. Acad. Sci. USA, 82: 3025-3029.

Lasater, E. M., Dowling, J. E. and Ripps, H. (1984) Pharmacological properties of isolated horizontal and bipolar cells from the skate retina, J. Neurosci., 4: 1966-1975.

Lerner, J. (1987) Acidic amino acid transport in animal cells and tissues, Comp. Biochem. Physiol., 87B: 443-457.

Malchow, R. P., Qian, H. and Ripps, H. (1989) γ-Aminobutyric acid (GABA)-induced currents of skate Müller (glial) cells are mediated by neuronal-like $GABA_A$ receptors, Proc. Natl. Acad. Sci. USA, 86: 4326-4330.

Marc, R. E. and Lam, D. M. K. (1981) Uptake of aspartic and glutamic acid by photoreceptors in goldfish retina, Proc. Natl. Acad. Sci. USA, 78: 7185-7189.

Marc, R. E. and Liu, W.-L. S. (1984) Horizontal cell synapses onto glycine-accumulating interplexiform cells, Nature, 312: 266-268.

Marc, R. E., Stell, W. K., Bok, D. and Lam, D. M. K. (1978) GABA-ergic pathways in the goldfish retina, J. Comp. Neurol., 182: 221-246.

Martell, A. E. and Smith, R. M. (1974) Critical stability constants volume 1: amino acids, London, Plenum Press.

Mayer, M. L. and Westbrook, G. L. (1985) The action of N-methyl-D-aspartic acid on mouse spinal neurones in culture, J. Physiol., 361: 65-90.

McMahon, H. T. and Nicholls, D. G. (1990) Glutamine and aspartate loading of synaptosomes: A reevaluation of effects on calcium-dependent excitatory amino acid release, J. Neurochem., 54: 373-380.

Miller, R. F. and Dacheux, R. F. (1976) Synaptic organization and ionic basis of on and off channels in mudpuppy retina. III A model of ganglion cell receptive field organization based on chloride-free experiments, J. Gen. Physiol., 67: 679-690.

Miller, R. F. and Dacheux, R. F. (1983) Intracellular chloride in retinal neurons: measurement and meaning, Vision Research, 23: 399-411.

Miller, R. F., Frumkes, T. E., Slaughter, M. and Dacheux, R. F. (1981) Physiological and pharmacological basis of GABA and glycine action on neurons of mudpuppy retina. II. Amacrine and ganglion cells, J. Neurophysiol., 45: 764-782.

Miller, A. M. and Schwartz, E. A. (1983) Evidence for the identification of synaptic transmitters released by photoreceptors in the toad retina, J. Physiol., 334: 325-349.

Miller, R. F. and Slaughter, M. M. (1986) Excitatory amino acid receptors of the retina: diversity of subtypes and conductance mechanisms, Trends in Neurosci., 9: 211-218.

Monaghan, D. T., Bridges, R. J. and Cotman, C. W. (1989) The excitatory amino acid receptors: their classes, pharmacology, and distinct properties in the function of the central nervous system, Annu. Rev. Pharmacol. Toxicol., 29: 365-402.

Murakami, M., Ohtsu, K. and Ohtsuka, T. (1972) Effects of chemicals on receptors and horizontal cells in the retina, J. Physiol., 227:899-913.

Murakami, M. T., Ohtsuka, T. and Shimazaki, H. (1975) Effects of aspartate and glutamate on the bipolar cells in the carp retina, Vision Research, 15: 456-458.

Nawy, S. and Jahr, C. E. (1990) Suppression by glutamate of cGMP-activated conductance in retinal bipolar cells, Nature, 346: 269-271.

Nelson, P. J., Dean, G. E., Aronson, P. S. and Rudnick, G. (1983) Hydrogen ion cotransport by the renal brush border glutamate transporter, Biochemistry, 22: 5459-5463.

Newman, E. A. (1984) Regional specialization of retinal glial cell membrane, Nature, 309: 155-157.

Newman, E. A. (1985) Voltage-dependent calcium and potassium channels in retinal glial cells, Nature, 317: 809-811.

Nowak, L., Bregestovski, P., Ascher, P., Herbet, A. and Prochiantz, A. (1984) Magnesium gates glutamate-activated channels in mouse central neurones, Nature, 307: 462-465.

Polyak, S. L. (1941) The retina, University of Chicago Press, Chicago.

Ramón y Cajal, S. (1983) Translation in: Rodieck, R. W. and Maguire, D., The vertebrate Retina (1973), W. H. Freeman and Company, San Francisco.

Reichenbach, A. (1987) Quantitative and qualitative morphology of rabbit retinal glia. A light microscopical study on cells both in situ and isolated by papain, J. Hirnforsch., 28: 213-220.

Reichenbach, A., Hagen, E., Schippel, K. and Eberhardt, W. (1988) Quantitative electron microscopy of rabbit Müller (glial) cells in dependence on retinal topography, Z. mikrosk. anat. Forsch., 102: 721-755.

Riepe, R. E. and Norenburg, M. D. (1977) Müller cell localisation of glutamine synthetase in rat retina, Nature, 268: 654-655.

Rodieck, R. W. (1973) The vertebrate retina, W. H. Freeman, San Francisco.

Roskoski, R. (1978) Net uptake of L-glutamate and GABA by high affinity synaptosomal transport systems, J. Neurochem., 31: 493-498.

Rothman, S. M. and Olney, J. W. (1987) Excitotoxicity and the NMDA receptor, Trends in Neurosci., 10: 299-302.

Sanchez-Prieto, J. and Gonzalez, P. (1988) Occurrence of a large Ca^{2+}-independent release of glutamate during anoxia in isolated nerve terminals (synaptosomes), J. Neurochem., 50: 1322-1324.

Schousboe, A. and Fosmark, H. and Hertz, L. (1975) High content of glutamate and of ATP in astrocytes cultured from rat brain hemispheres: effect of serum-withdrawal and of cyclic AMP, J. Neurochem., 25: 909-911.

Schwartz, E. A. (1986) Synaptic transmission in amphibian retinae during conditions unfavourable for calcium entry into presynaptic terminals, J. Physiol., 376: 411-428.

Schwartz, E. A. and Tachibana, M. (1990) Electrophysiology of glutamate and sodium co-transport in a glial cell of the salamander retina, J. Physiol., 426: 43-80.

Shiells, R. A., Falk, G. and Naghshineh, S. (1981) Action of glutamate and aspartate analogues on rod horizontal and bipolar cells, Nature, 294: 592-594.

Shiells, R. A., Falk, G. and Naghshineh, S. (1986) Iontophoretic study of the action of excitatory amino acids on rod horizontal cells of the dogfish retina, Proc. R. Soc. London, B, 227: 121-135.

Siesjö, B. K. (1990) Calcium, excitotoxins and brain damage, News in Physiol. Sci., 5: 120-125.

Siesjö, B. K. and Bengtsson, F. (1989) Calcium fluxes, calcium antagonists, and calcium-related pathology in brain ischemia, hypoglycemia, and spreading depression: A unifying hypothesis, J Cerebr. Blood Flow Metabol., 9: 127-140.

Simon, R. P., Swan, J. H., Griffiths, T. and Meldrum, B. S. (1984) Blockade of N-methyl-D-aspartate receptors may protect against ischemic damage in the brain, Science, 226: 850-852.

Sjöstrand, F. S. (1958) Ultrastructure of retinal rod synapses of the guinea pig eye as revealed by three-dimensional reconstruction from serial sections, J. Ultrastruct. Res., 2: 122-170.

Slaughter, M. M. and Miller, R. F. (1981) 2-Amino-4-phosphonobyturic acid: a new pharmacological tool for retina research, Science, 211: 182-185.

Slaughter, M. M. and Miller, R. F. (1983a) The role of excitatory amino acid transmitters in the mudpuppy retina: An analysis with kainic acid and N-methylaspartate, J. Neurosci., 3: 1701-1711.

Slaughter, M. M. and Miller, R. F. (1983b) An excitatory amino acid antagonist blocks cone input to sign-conserving second order retinal neurones, Science, 219: 1230-1232.

Slaughter, M. M. and Miller, R. F. (1983c) Bipolar cells in the mudpuppy retina use an excitatory amino acid neurotransmitter, Nature, 303: 537-538.

Slaughter, M. M. and Miller, R. F. (1985) Characterization of an extended glutamate receptor of the on bipolar neuron in the vertebrate retina, J. Neurosci., 5: 224-233.

Snow, P. J., Rose, P. K. and Brown, A. G. (1976) Tracing axons and axon collaterals of spinal neurons using intracellular injection of horseradish peroxidase, Science, 191: 312-313.

Sontheimer, H., Kettenmann, H., Backus, K. H. and Schachner, M. (1988) Glutamate opens Na^+/K^+ channels in cultured astrocytes, Glia, 1: 328-336.

Stallcup, W. B., Bulloch, K. and Baetge, E. (1979) Coupled transport of glutamate and sodium in a cerebellar nerve cell line, J. Neurochem., 32: 57-65.

Starke, K. (1981) Presynaptic receptors, Ann. Rev. Pharmacol. Toxicol., 21: 7-30.

Steinberg, G. K., Saleh, J. and Kunis, D. (1988) Delayed treatment with dextromethorphan and dextrorphan reduces cerebral damage after transient focal ischemia, Neurosci. Lett., 89: 193-197.

Stell, W. K. and Lightfoot, D. O. (1975) Color-specific interconnections of cones and horizontal cells in the retina of the goldfish, J. Comp. Neurol., 159: 473-502.

Straus, W. (1964) Factors affecting the state of injected horseradish peroxidase in animal tissues and procedures for the study of phagosomes and phago-lysosomes, J. Histochem. Cytochem., 12: 470-480.

Sugiyama, H., Ito, I. and Hirono, C. (1987) A new type of glutamate receptor linked to inositol phospholipid metabolism, Nature, 325: 531-533.

Szatkowski, M., Barbour, B. and Attwell, D. (1990) Non-vesicular release of glutamate from glial cells by reversed electrogenic glutamate uptake, Nature, in press.

Szczepaniak, A. C. and Cottrell, G. A. (1973) Biphasic action of glutamic acid and synaptic inhibition in an identified serotonin-containing neurone, Nature, new Biol., 241: 62-64.

Tachibana, M. (1985) Permeability changes induced by L-glutamate in solitary retinal horizontal cells isolated from Carassius auratus, J. Physiol., 358: 153-167.

Tachibana, M. and Kaneko, A. (1988) L-Glutamate-induced depolarization in solitary photoreceptors: A process that may contribute to the interaction between photoreceptors in situ, Proc. Natl. Acad. Sci. USA, 85: 5315-5319.

Tessier-Lavigne, M., Attwell, D., Mobbs, P. and Wilson, M. (1988) Membrane currents in retinal bipolar cells of the axolotl, J. Gen. Physiol., 91: 49-72.

Thieffry, M. and Bruner, J. (1978) Direct evidence for a presynaptic action of glutamate at a crayfish neuromuscular junction, Brain Research, 156: 402-406.

Traynelis, S. F. and Cull-Candy, S. G. (1990) Proton inhibition of N-methyl-D-aspartate receptors in cerebellar neurons, Nature, 345: 347-350.

Trussell, L. O. and Fischbach, G. D. (1989) Glutamate receptor desensitization and its role in synaptic transmission, Neuron, 3: 209-218.

Usowicz, M. M., Gallo, V. and Cull-Candy, S. G. (1989) Multiple conductance channels in type-2 cerebellar astrocytes activated by excitatory amino acids, Nature, 339: 380-383.

Van Buskirk, R. and Dowling, J. E. (1981) Isolated horizontal cells from carp retina demonstrate dopamine-dependent accumulation of cyclic AMP, Proc. Natl. Acad. Sci. USA, 78: 7825-7829.

Vaney, D. I., Peichl, L. and Boycott, B. B. (1981) Matching populations of amacrine cells in the inner nuclear and ganglion cell layers of the rabbit retina, J. Comp. Neurol., 199: 373-391.

Voaden, M. J., Marshall, J. and Murani, N. (1974) The uptake of [^{3}H] γ-amino butyric acid and [^{3}H]glycine by the isolated retina of the frog, Brain Research, 67: 115-132.

Walz, W. and Hertz, L. (1983) Functional interactions between neurons and astrocytes. II. Potassium homeostasis at the cellular level, Prog. Neurobiol., 20: 133-183.

Watkins, J. C. and Evans, R. H. (1981) Excitatory amino acid transmitters, Annu. Rev. Toxicol., 21: 165-204.

Werblin, F. S. (1972) Lateral interactions at the inner plexiform layer of a vertebrate retina: antagonistic response to change, Science, 175: 1008-1010.

Werblin, F. S. and Dowling, J. E. (1969) Organization of the retina of the mudpuppy, Necturus maculosus. II. Intracellular recording, J. Neurophysiol., 32: 339-355.

White, R. D. and Neal, M. J. (1976) The uptake of L-glutamate by the retina, Brain Research, 111: 79-93.

Wong, E. H. F., Kemp, J. A., Priestley, T., Knight, A. R., Woodruff, G. N. and Iversen, L. L. (1986) The anticonvulsant MK-801 is a potent N-methyl-D-aspartate antagonist, Proc. Natl. Acad. Sci. USA, 83: 7104-7108.

Wu, S. M. (1986) Effects of gamma-aminobutyric acid on cones and bipolar cells of the tiger salamander retina, Brain Research, 365: 70-7.

Yazulla, S., Studholme, K. M., Vitorica, J. and DeBlas, A. L. (1987) Localization of GABA receptors on photoreceptor synaptic terminals in goldfish and chicken retinas by immunocytochemistry, Soc. Neurosci. Abs., 13: 1054.